8905-1-F

THEORETICAL AND EXPERIMENTAL INVESTIGATION OF PARASITIC LOOP COUNTERPOISE ANTENNAS

Final Report
(16 June 1967 - 16 June 1968)
Scientific Report No. 3

September 1968

Contract No. FA67WA-1753
Project 330-004-05N
SRDS Report No. RD-68-50

This report has been prepared by The University of Michigan Radiation Laboratory of the Department of Electrical Engineering for the Systems Research and Development Service, Federal Aviation Administration, under Contract FA67WA-1753. The contents of this report reflect the views of the contractor, who is responsible for the facts and the accuracy of the data presented herein, and do not necessarily reflect the official views or policy of the FAA

Prepared by

D. L. Sengupta, J. E. Ferris and V. H. Weston
The University of Michigan Radiation Laboratory
Department of Electrical Engineering
Ann Arbor, Michigan 48108

For

Systems Research and Development Service
Federal Aviation Administration, Washington, DC 20590

ABSTRACT

The radiation field produced by a single parasitic loop counterpoise antenna has been investigated both theoretically and experimentally . Geometrical theory of diffraction is applied to obtain theoretical expressions for the far field produced by such an antenna. Within the range of approximation the agreement between theory and experiment has been found to be very good. In the absence of mutual coupling between the parasitic elements, the present theory can be applied to double- and multiple-parasitic loop counterpoise antennas.

The parasitic loops in general reduce the counterpoise edge diffraction effects on the far field patterns. The behavior of the parasitic loop counterpoise antenna pattern near the principal maximum is not appreciably different than the Alford loop counterpoise pattern near its maximum. Parasitic loops increase the response of the antenna in regions of space near the zenith $\theta = 0^{o}$.

Detailed results of numerical and experimental investigations of various aspects of the parasitic loop counterpoise antenna have been given. These results bring out the effects of the different parameters of this new antenna system on the radiation patterns.

The parasitic loop concept has been found to be capable of shaping the pattern produced by an Alford loop counterpoise antenna pattern in regions of space below the plane of the counterpoise .

On the basis of our investigation we conclude that when suitably designed, the parasitic loop counterpoise antenna is potentially capable of minimizing the siting errors associated with existing VOR systems. We have proposed three new antenna systems which may find possible application in a VOR system.

TABLE OF CONTENTS

TABLE OF CONTENTS
(continued)

LIST OF ILLUSTRATIONS

I

INTRODUCTION

1.1 Preliminary Remarks

This is the Final Report on Contract FA67WA-1753, Project 330-004-05N, "VOR Parasitic Loop Counterpoise System" and covers the period 16 June 1967 to 16 June 1968. The primary purpose of the contract has been to investigate the possibility of using parasitic loops to improve the performance of the antennas used in existing VHF Omni Range systems. The concept of using parasitic loops gave rise to a new antenna configuration named the parasitic loop counterpoise antenna. A major part of the investigation has been devoted to the theoretical and experimental study of the radiation properties of such an antenna. The possible application of the antenna to VOR systems is then explored. In the following sections we discuss briefly the genesis of the parasitic loop concept and give a brief outline of the report.

1.2 Simple VOR Antenna

A detailed description of the VOR antenna system has been given by Anderson[1] and will not be repeated here. For the purpose of the present investigation a simple VOR antenna is assumed to consist of a single Alford loop placed above and parallel to a circular and conducting ground plane or counterpoise. It operates in the frequency range 108 - 118 MHz. In most installations the diameter of the counterpoise used is about 5.7λ at the frequency of 108 MHz. The antenna is oriented with the counterpoise lying in the horizontal plane. It is generally elevated above the ground level to a height depending on the site chosen and its environment. The free space radiation pattern of such an antenna is omnidirectional in azimuth. It should be noted that the actual VOR antenna employs two pair of loops and has a figure-of-eight pattern[1] in azimuth. The elevation plane pattern has a maximum around 50^{o}-60^{o} away from the vertical depending on the height of the Alford loop and the size of the counterpoise.

Due to the counterpoise edge diffraction effects the Alford loop counterpoise antenna has considerable response in directions below the plane of the counterpoise. Because of this, scattering objects such as trees, buildings, etc., in the vicinity of the present VOR antenna systems and also the ground reflection effects, produce errors in the VOR indications[1].

To avoid the errors in the bearing indications of the existing VOR systems the ideal requirements on the antenna radiation pattern are such that in the upper half plane of the counterpoise the elevation field pattern should resemble the Alford loop counterpoise radiation pattern and in directions below the counterpoise plane the field should be zero or negligible. Such a pattern is possible only with an infinitely large counterpoise. However, to increase the counterpoise diameters well beyond the values used in the existing systems is impractical.

1.3 Previous Work Done

Weston et al[2] proposed a new VOR system which uses a stacked array of two or more Alford loops above the counterpoise. They have shown that by properly choosing the amplitude and phase of excitation of the loops the field gradient at the horizon (i. e. the rate of decrease of field below the horizon) can be increased considerably. This was achieved by producing a minimum in the elevation pattern in a direction just below the horizon. Successful operation of this antenna system requires proper phasing and feed network for the Alford loops. Although the theoretical value of the field gradient produced by this antenna was large, the average response of the antenna below the horizon was found to be quite high. It can be shown theoretically that both the horn and lens antennas may provide partial solutions to the problems associated with the existing VOR antenna systems. However, because the operating wavelength is of the order of 10 feet, the structures associated with these systems will be immense. Additional difficulties will arise in adapting the present feed (i. e the Alford loop) to a lens or horn antenna. Because of these reasons the idea of using horn or lens antennas in VOR systems has not been pursued.

1.4 The Parasitic Loop Counterpoise Antenna

The basic objective of reducing the field in directions below the plane of the counterpoise may be achieved by using a large parasitic loop placed above and parallel to the Alford loop counterpoise antenna. Such an antenna will be called the parasitic loop counterpoise antenna. The parasitic loop receives its excitation from the Alford loop. It is then conceivable that by proper choice of the physical parameters of the parasitic loop, the field produced by the parasitic current in the presence of the counterpoise may be of such a phase as to reduce the field produced by the Alford loop counterpoise antenna in the directions below the horizon. The current carried by the parasitic loop being small compared to that of the Alford loop, the parasitic loop will not appreciably alter the field near the principal maximum. However, it is expected that fields near the vertical will be altered appreciably. Thus it appears that one or more parasitic loops may be used advantageously to reduce the siting errors caused by the antennas in the existing VOR systems.

1.5 Outline of the Report

The parasitic loop counterpoise configuration is a new antenna. Hence the major portion of our investigation has been devoted to the study of its radiating properties under various conditions. Throughout the report we shall refer to the Alford loop above the bounterpoise as the basic antenna. The entire study is

directed towards shaping the patterns of the basic antenna in certain regions of space with the help of the parasitic loops. The outline of the report is as follows.

The radiation properties of the Alford loop above the counterpoise are discussed in Chapter II. The effects of changing the counterpoise size on the patterns are given.

The radiation field produced by a single parasitic loop counterpoise antenna is investigated theoretically in Chapter III. The theory is then verified by experiment. The general effects of the parasitic loop parameters on the far field pattern are discussed.

Chapter IV presents in detail the results of numerical and experimental investigations of the radiation properties of a single parasitic loop counterpoise antenna as the different parameters of the system are varied.

The radiation characteristics of a double parasitic loop counterpoise antenna are discussed in Chapter V. The properties of an optimum antenna with best field gradient characteristics are discussed. A brief comparison between the single and double parasitic loop counterpoise antenna is also given.

Multiple parasitic loop counterpoise antennas are discussed in Chapter VI.

Three models of parasitic loop counterpoise antennas are proposed in Chapter VII. All of them may have possible application for the purpose of improving the performance of the existing VOR system.

Chapter VIII gives our general conclusions and recommendations for further work.

The Fortran IV Computer Program used for numerical analysis and some numerical results are given in the Appendices.

II

RADIATION CHARACTERISTICS OF AN ALFORD LOOP ABOVE A COUNTERPOISE

2.1 Introduction

In this chapter, properties of an Alford loop located above and oriented parallel to a counterpoise are discussed. The complete expression for the radiation field produced by such an antenna system has been obtained by Weston et al[2]. They also have reported satisfatory agreement between theoretical and measured radiation patterns. The Alford loop above a counterpoise being the basic antenna system, its radiating properties are of fundamental importance for our investigation. The radiation characteristics of the antenna are therefore investigated in more detail both numerically and experimentally. The results are discussed critically and are represented in a form suitable for later use.

2.2 Radiation Field of an Alford Loop Above a Counterpoise

The cross sectional view of the Alford loop above the circular ground plane along with the coordinate system used is shown schematically in Fig. 2-1. For theoretical analysis the Alford loop is approximated by a small circular loop ($ka \ll 1$) carrying a constant amplitude current. In practice the Alford loop used is square in shape with each side approximately of the order $\lambda/5$ so that the above approximation is reasonable. Since the development of the theoretical expression for the radiation field of the antenna has been discussed elsewhere[2], it will not be repeated here. Only the final result is quoted here. Assuming that the loop carries a current of the form

$$\vec{I} = \hat{\phi}\, I_o\, e^{-i\omega t} ,$$

it can be shown that the complete expression for the far field produced at a point $P(R, \theta)$ and in the range $0 < \theta < \pi$ is given by

$$E_{\phi}^{A} = \eta_o I_o \left(\frac{ka}{2}\right)^2 \frac{e^{i(kR - \pi/4)}}{R} S^{A}(\theta) , \tag{2.1}$$

where

$$S^{A}(\theta) = \left\{ \frac{F^{o}(\theta)\sin\theta}{\sqrt{2}}\, e^{-ikA\sin\theta} + \frac{\cos\theta\, \sin\left(\frac{\phi_o}{2}\right)}{\sqrt{\pi k r_o \sin\theta}}\, e^{ikr_o}\, L^{o}(\theta) \right\}, \tag{2.2}$$

$$L^{o}(\theta) = \frac{e^{i\left(\frac{\pi}{2} - kA\sin\theta\right)}}{\sqrt{1-\sin\theta}} \left(\frac{\cos^{3/2}\phi_o - \sin^{3/2}\theta}{\cos\phi_o - \sin\theta} \right) - \frac{e^{ikA\sin\theta}}{\sqrt{1+\sin\theta}} \frac{\cos^{3/2}\theta_o}{\cos\phi_o + \sin\theta} , \tag{2.3}$$

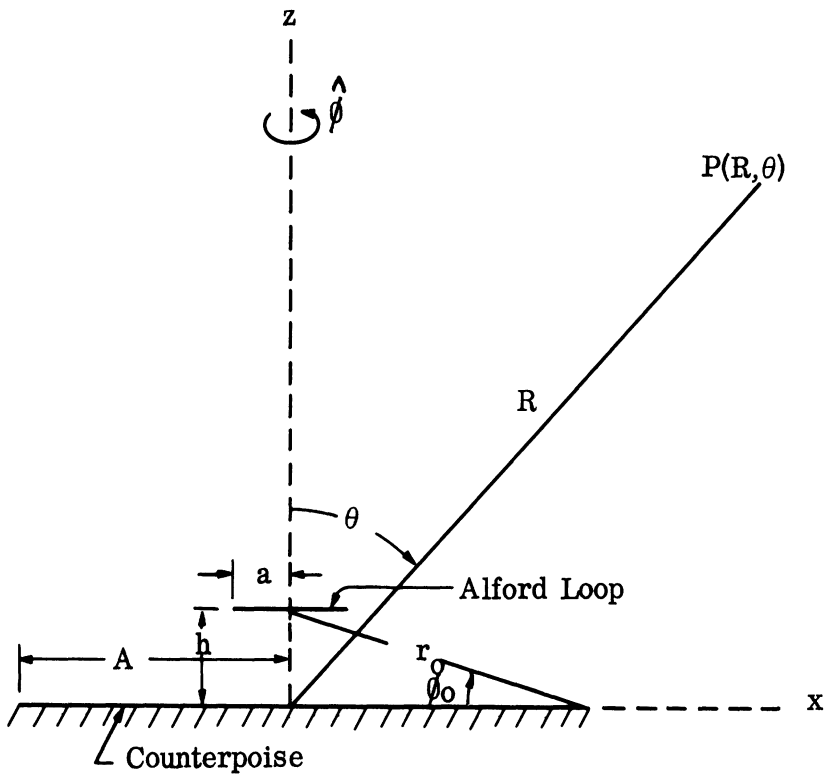

FIG. 2-1: ALFORD LOOP ABOVE COUNTERPOISE SHOWING COORDINATE SYSTEM.

$$F^{o}(\theta)=e^{ikr_o\sin(\theta-\phi_o)}\int_{-\infty}^{p_1} e^{i\pi t^2/2}\,dt-e^{ikr_o\sin(\theta+\phi_o)}\int_{-\infty}^{p_2} e^{i\pi t^2/2}\,dt, \quad (2.4)$$

$$p_1=2\left(\frac{kr_o}{\pi}\right)^{1/2}\cos\left(\frac{\phi_o-\theta-\pi/2}{2}\right), \quad (2.5)$$

$$p_2=2\left(\frac{kr_o}{\pi}\right)^{1/2}\cos\left(\frac{\phi_o+\theta+\pi/2}{2}\right), \quad (2.6)$$

$$r_o^2=A^2+h^2, \quad (2.7)$$

$$\tan\phi_o=\frac{h}{A}, \quad (2.8)$$

$k=\frac{2\pi}{\lambda}$ is the free space propagation constant,

η_o is the intrinsic impedance of free space

and the other parameters are as explained in Fig. 2-1. The implied time dependence in Eq. (2.1) is $e^{-i\omega t}$. The far field produced is polarized in the ϕ-direction and is independent of the azimuthal angle ϕ. The term $S^A(\theta)$ in (2.1) may be looked upon as the complex far field pattern. Thus $|S^A(\theta)|$ is the conventional far field radiation pattern and $\arg|S^A(\theta)|$ gives the variation as a function of θ of the phase of the radiation field at a constant distance R from the origin. To determine the accuracy of Eq. (2.2) the radiation pattern of the antenna has been measured and compared with the theoretical pattern obtained numerically from (2.2). The expression is then studied numerically by varying the different parameters. These are explained in the following sections.

2.3 Description of Experimental Arrangement

Experimental investigations have been carried out at the frequency of 1080 MHz which is about ten times the operating VOR frequency. The Alford loop used is a tenth scale model of a typical loop used in the existing VOR antenna system, the design of which is discussed by Anderson[1]. A photograph of the Alford loop model is shown in Fig. 2-2. The loop is made of brass strips and fed by a coaxial line with the help of a balance-to-unbalance transformer. The loop is square shaped with each side equal to 0.21", which is about $\lambda/5$ at the frequency of 1080 MHz. The counterpoise has been cut from aluminum sheet 0.125" thick and backed with a wooden frame to ensure rigidity. It has a diameter of 5.2'. The loop is mounted 4.8" above the counterpoise with its axis coincident with that of the counterpoise. The experimental Alford loop counterpoise antenna is shown in Fig. 2-3. The present configuration studied corresponds to a full scale simple VOR antenna system consisting of a standard Alford loop above a 52' diameter counterpoise. In all the measurements to be discussed below the above

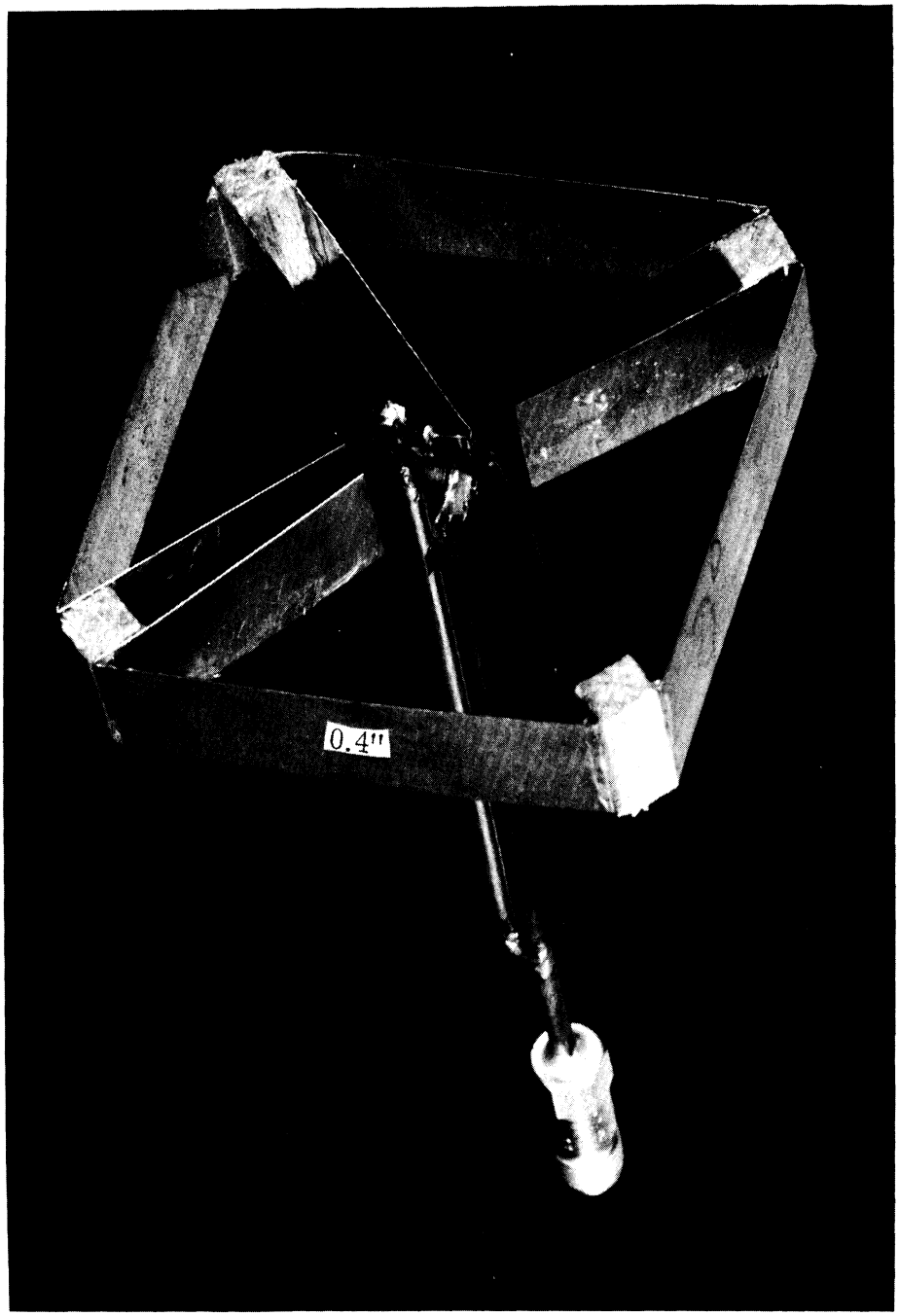

FIG. 2-2: PHOTOGRAPH OF THE ALFORD LOOP MODEL

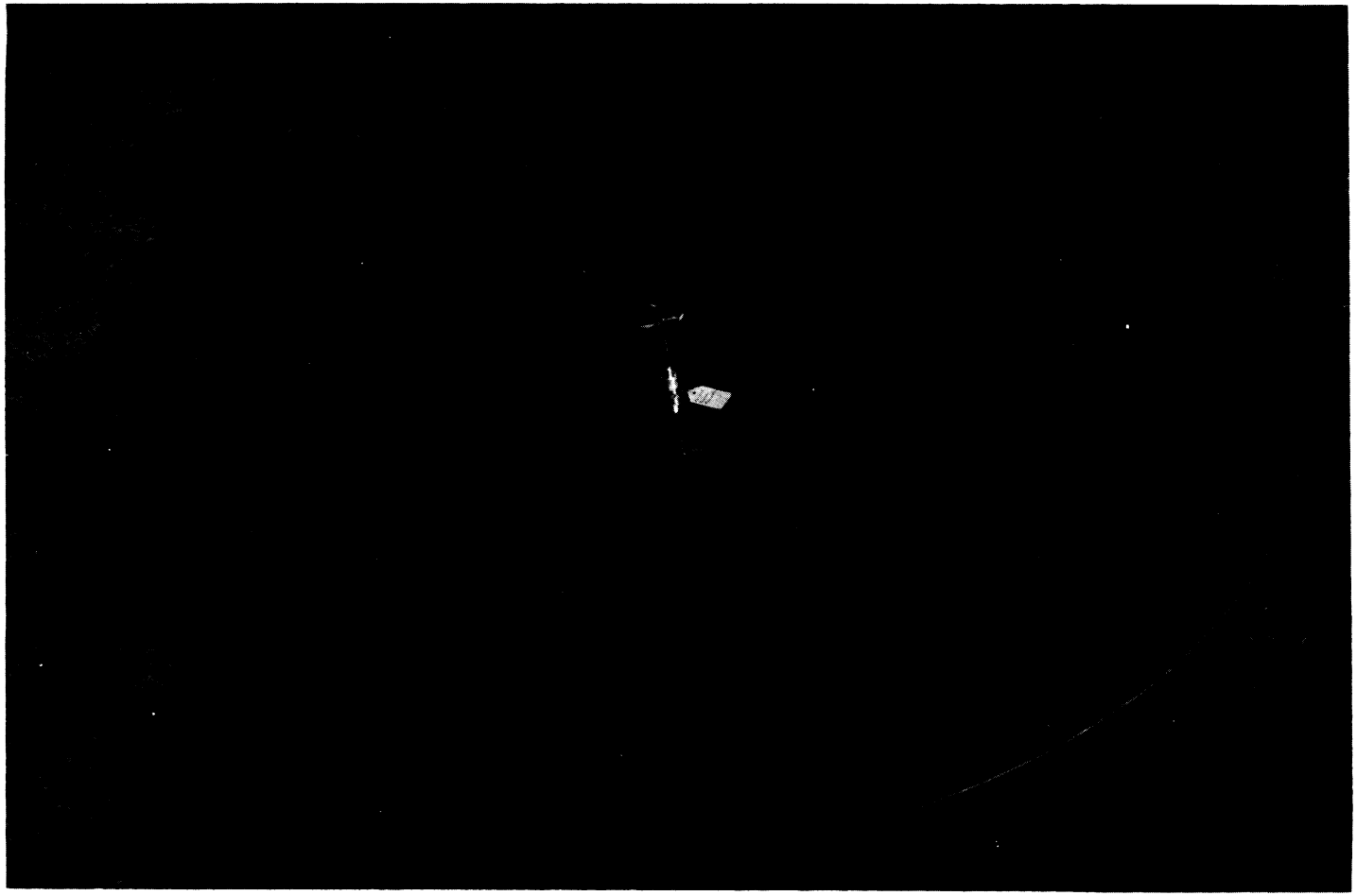

FIG. 2-3: PHOTOGRAPH OF THE ALFORD LOOP COUNTERPOISE ANTENNA MODEL.

model has been used as a receiving antenna. It is of some interest to mention here the following normalized physical parameters of the antenna used (see Fig. 2-1): $2A \sim 5.7\lambda$, $h \sim 0.44\lambda$, and $a \sim \lambda/10$.

2.4 Experimental Results and Comparison with Theory.

The measured elevation pattern of the Alford loop in the presence of a 5.2' diameter counterpoise is shown in Fig. 2-4. For comparison, the theoretical values of $S^A(\theta)$ as obtained from numerical computation of Eq.(2.2) are shown in the range $0 < \theta < \pi$ in Fig. 2-4. The general agreement between theory and experiment is considered to be excellent for this case. Elevation patterns of the same Alford antenna have been measured for 2A=4', 3' and 2' respectively and the agreement with theory has been found to be very good in all cases. The measured and theoretical patterns for the case with a 2' diameter counterpoise (kA=6.893) are shown in Fig. 2-5. It may thus be concluded that for $A \gtrsim \lambda$, Eq. (2.2) should predict quite accurately the radiation pattern produced by the Alford Loop counterpoise antenna. It is anticipated that the theory may give the pattern with reasonable accuracy even for $A < \lambda$. However, we have not tested the theory experimentally for such cases.

2.5 Omnidirectionality of the Pattern in Azimuth

As can be seen from Eq. (2 1) the far field is independent of the azimuthal angle ϕ. This is consistent with the physical symmetry of the theoretical model shown in Fig. 2-1. To test the omnidirectionality of the azimuthal pattern of the experimental model, elevation patterns have been measured in various meridian planes of the antenna (i.e. for different values of ϕ). The variation of the pattern as a function of ϕ is shown in Figs. 2-6a - c for three selected values of θ. As can be seen from Figs. 2-6a, b, the omnidirectionality of the pattern in azimuth may be considered to be very good in the horizontal plane and in the direction of the pattern maximum. The omnidirectionality for the case $\theta=10^o$(Fig. 2-6c) is found to be worse compared to the previous two directions.

2.6 Numerical Investigation

By using a high speed computer Eq.(2.2) has been computed for different values of A with constant kh=2.75. The computer program and numerical results are given in Appendices B and C. The computer used was the IBM 360/67. In the present section we discuss a few of the important radiation characteristics of the Alford loop counterpoise antenna on the basis of the numerical investigation. Pertinent information obtained from our experimental study will also be given for comparison.

2.6.1 Amplitude and Phase of the Radiation Field

As mentioned in Chapter I, the primary purpose of the investigation has been to shape the Alford loop counterpoise pattern near and below the horizon. For this purpose it is important to know both the variations of $|S^A(\theta)|$ and $\arg S^A(\theta)$ for $\theta \geq \pi/2$. Here we discuss the amplitude and phase variation of the field within the region $90^o \leq \theta \leq 120^o$ which is the most important region from the VOR point of view. Figure 2-7 shows the amplitude and phase of the radiation field as a function of θ. In general

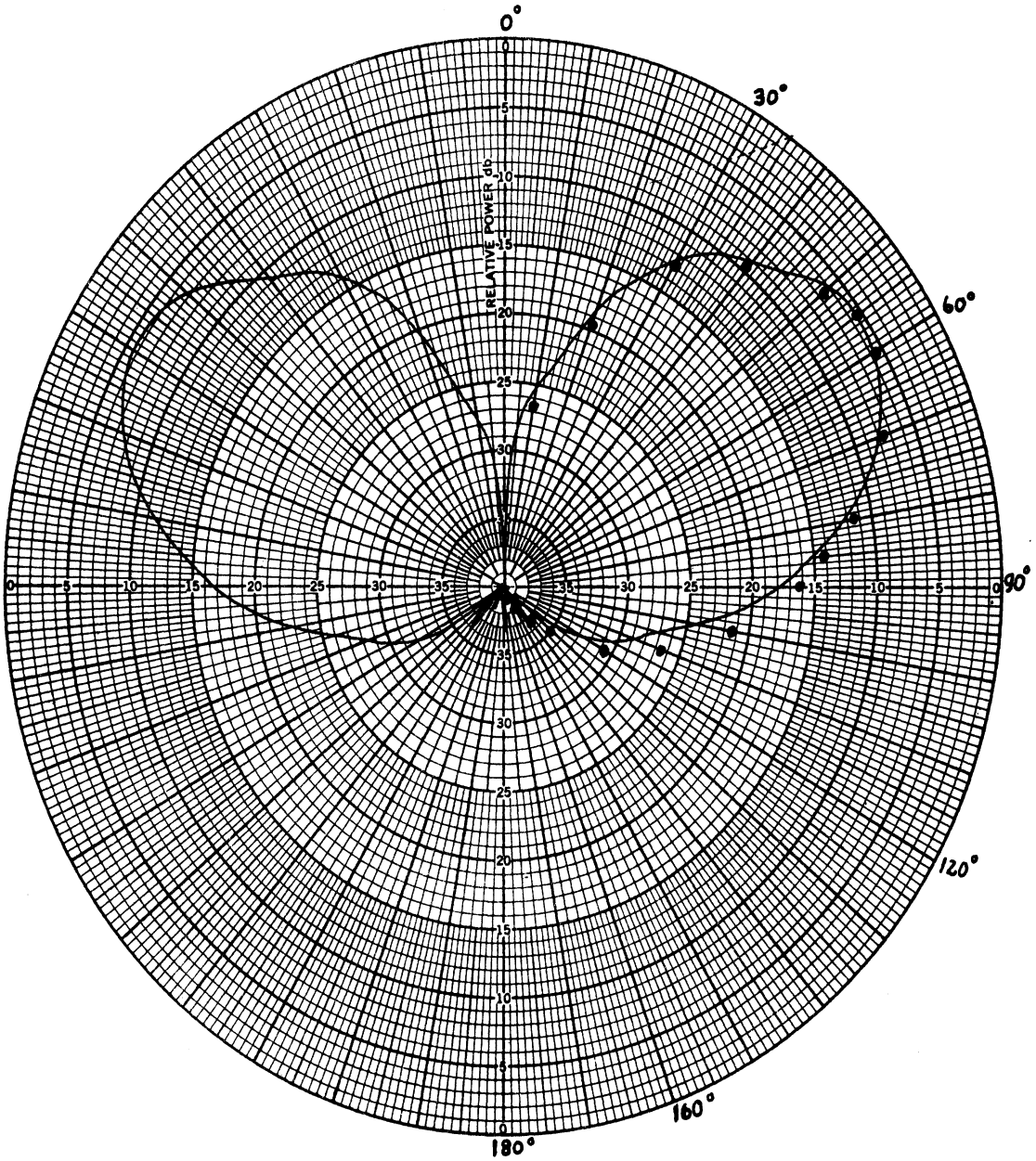

FIG. 2-4: ELEVATION RADIATION PATTERN OF ALFORD LOOP COUNTERPOISE ANTENNA, kh=2.75, kA=17.92, f=1080 MHz (—) Measured (• •) Theoretical.

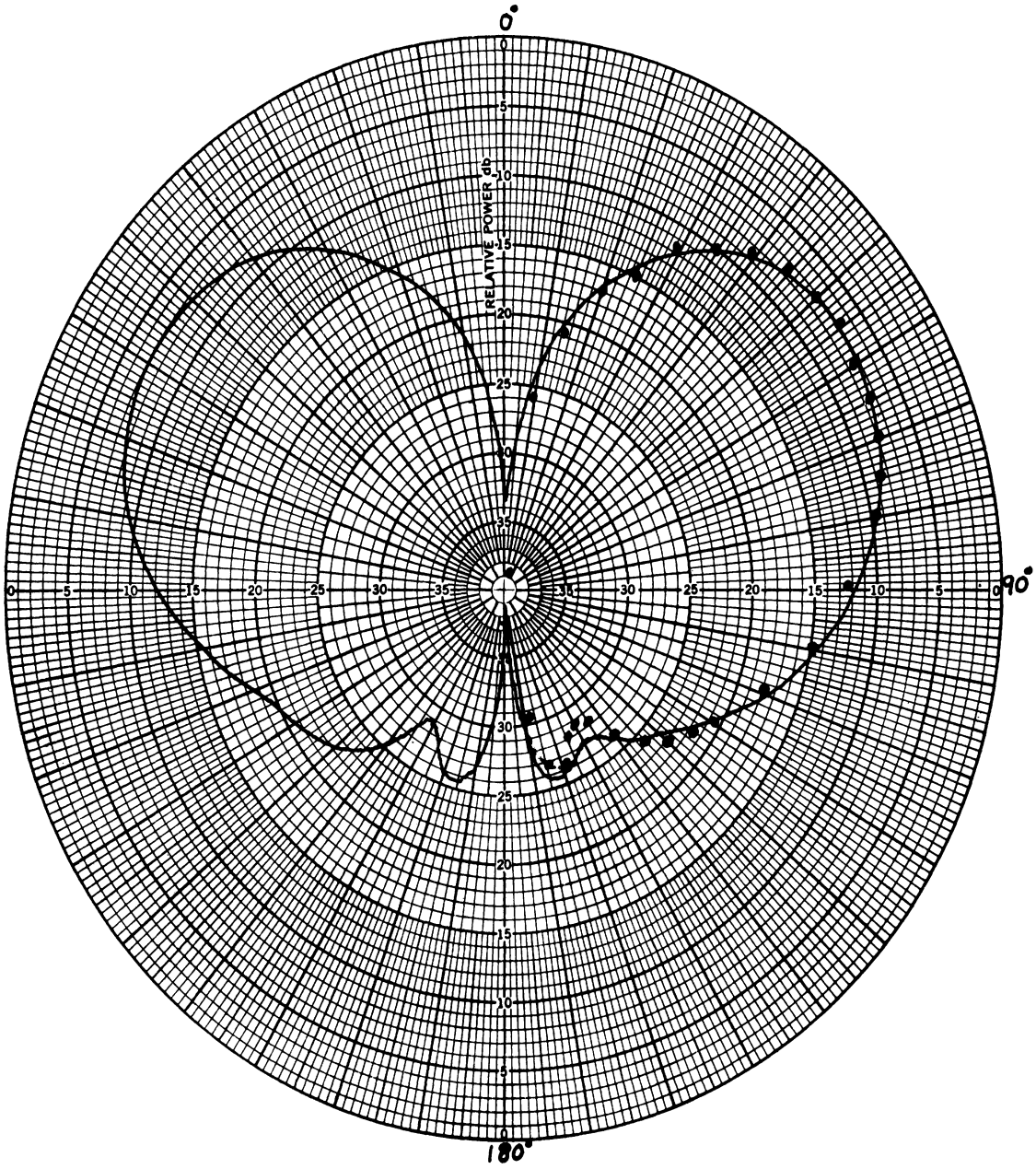

FIG. 2-5: ELEVATION RADIATION PATTERN OF ALFORD LOOP COUNTERPOISE ANTENNA. kh=2.75, kA=6.893, f=1080 MHz, (—)Measured, (• •) Theoretical.

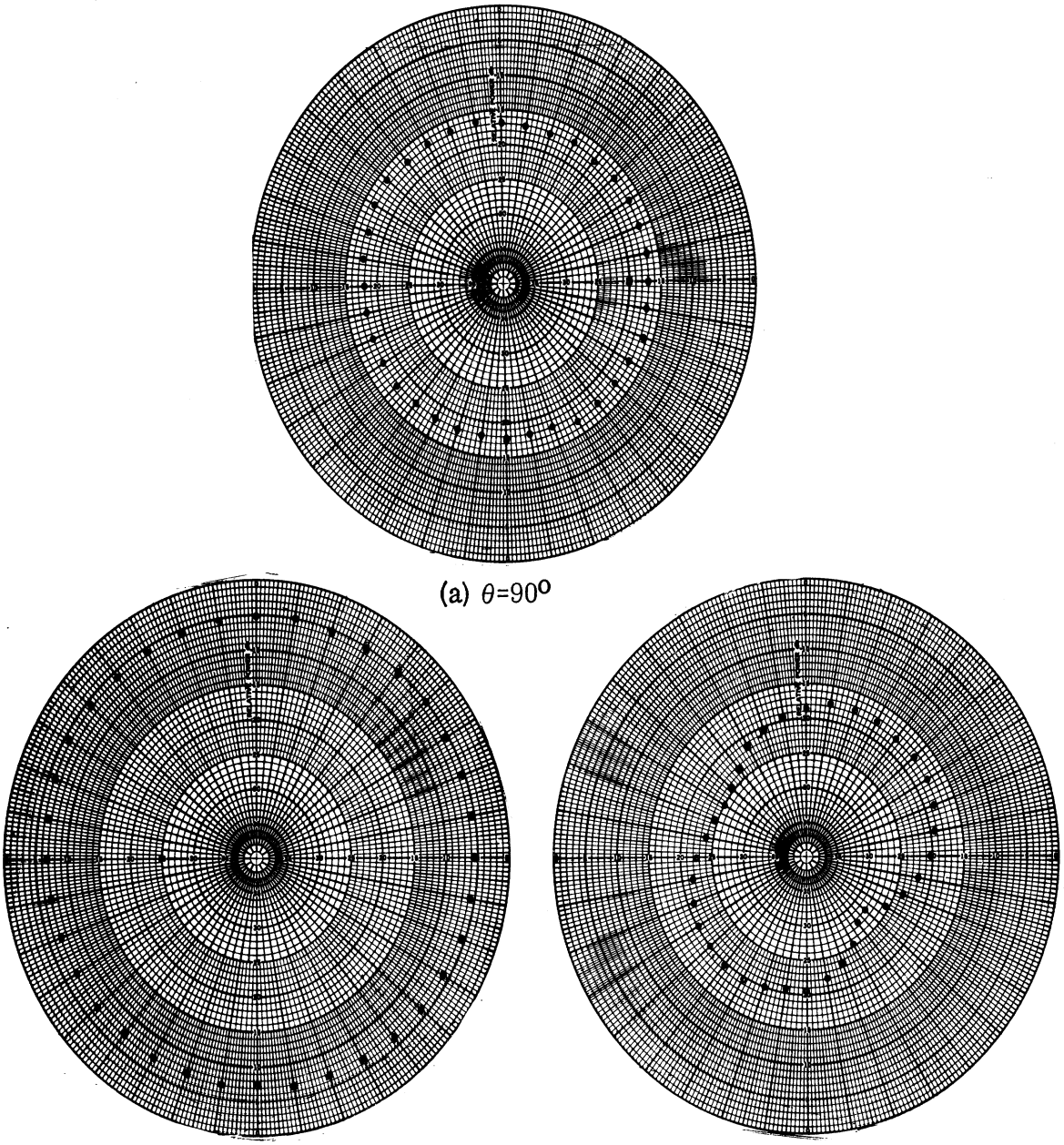

(a) θ=90°

(b) θ=55°

(c) θ=10°

FIG. 2-6: MEASURED AZIMUTHAL PATTERNS OF ALFORD LOOP COUNTERPOISE ANTENNA. kh=2.75, kA=17.92, f=1080 MHz

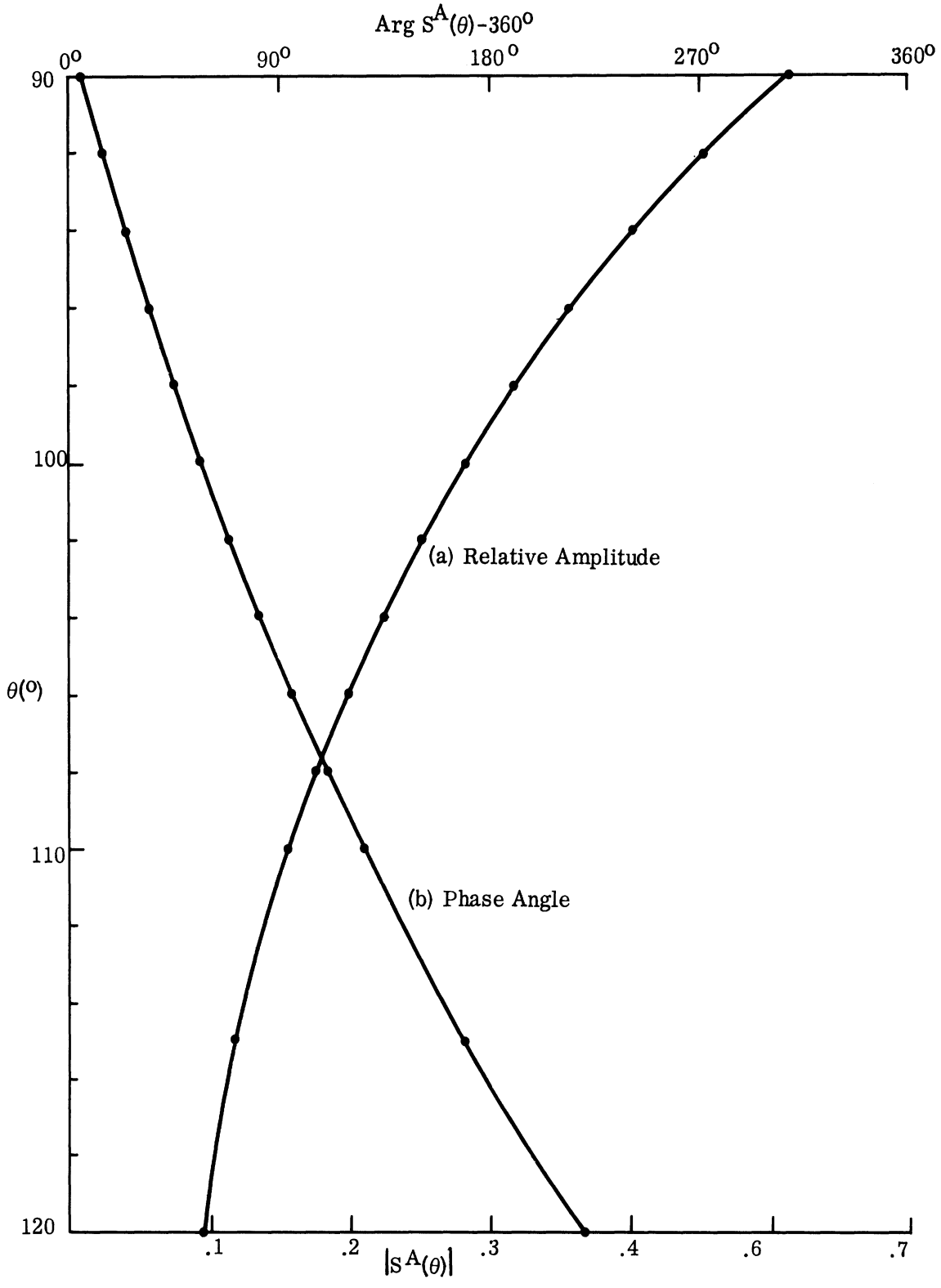

FIG. 2-7: THEORETICAL ELEVATION PATTERN CHARACTERISTICS OF ALFORD LOOP COUNTERPOISE ANTENNA BELOW HORIZON. kh=2.75, kA=17.92, f=1080 MHz.

it may be said that the phase varies quite rapidly around the horizontal direction $\theta=90^{o}$. It can be seen from Fig. 2-7 that for a change of 30^{o} in θ below the horizon the phase of the radiation field changes by about 212^{o}. The curves shown in Fig. 2-7 will be used later for the purpose of modifying the pattern below the horizon.

2.6.2 Pattern Characteristics as a function of the Counterpoise Size

In this section we discuss briefly the radiation pattern characteristics of the Alford loop counterpoise antenna as the counterpoise radius A is changed. The normalized radius kA of the counterpoise is varied from 6.893 to 51.69 at the frequency 1080 MHz, which corresponds to a variation of A from 1' to 7.5'. The results obtained from the numerical investigation are shown in graphical form in Fig. 2-8. Curve (a) shows the variation of the direction of principal maximum θ_{max} as A is varied. It may be concluded from curve (a) that as A is changed from about λ to 8λ, θ_{max} increases from 55^{o} to 60^{o}. Curve (b) shows the field gradient at the horizon as a function of the counterpoise size. The field gradient is defined to be the negative of the ratio field at $\theta=96^{o}$/ field at $\theta=90^{o}$, expressed in db. As expected, the field gradient at first increases substantially as A is increased, but for larger values of A, it increases very slowly. Curve (c) in Fig. 2-8 shows the variation of the field in the direction $\theta=90^{o}$ relative to that in the direction $\theta=\theta_{max}$ as A is increased. As the counterpoise size is increased the field in the direction $\theta=90^{o}$ decreases more and more relative to the field in the maximum direction. For a quick comparison, the theoretical and experimental values of the different quantities are shown in Table II-1. On the basis of the results discussed above we single out the following information regarding the pattern characteristics of an Alford loop above a 5.2' diameter counterpoise at the frequency of 1080 MHz:

$\theta_{max} = 55.3^{o}$,

field gradient = $\alpha_g = -20 \log_{10} \left| \frac{E(96^{o})}{E(90^{o})} \right| = 3.09$ db/6^{o}

field reduction = $\alpha_F = -20 \log_{10} \left| \frac{E(90^{o})}{E(\theta_{max})} \right| = 10.38$ db.

The above information will be found useful for later work.

TABLE II-1: ALFORD LOOP COUNTERPOISE ANTENNA PATTERN CHARACTERISTICS AT f=1080 MHz, kh=2.75 AND VARIABLE A.

2A (ft)	kA	θ_{max}(in ^{o})		α_g(in db)		α_F(in db)	
		Theory	Exp.	Theory	Exp.	Theory	Exp.
2	6.89	55	56	1.63	1.8	5.15	4.4
3	10.30	55	55.5	2.18	2.1	7.45	7.2
4	13.74	55	54.5	2.62	3.0	9.03	10.2
5.2	17.92	55	55.2	3.09	3.15	10.38	12.5
10	34.47	60	-	4.49	-	13.35	-
15	51.69	65	-	5.56	-	14.86	-

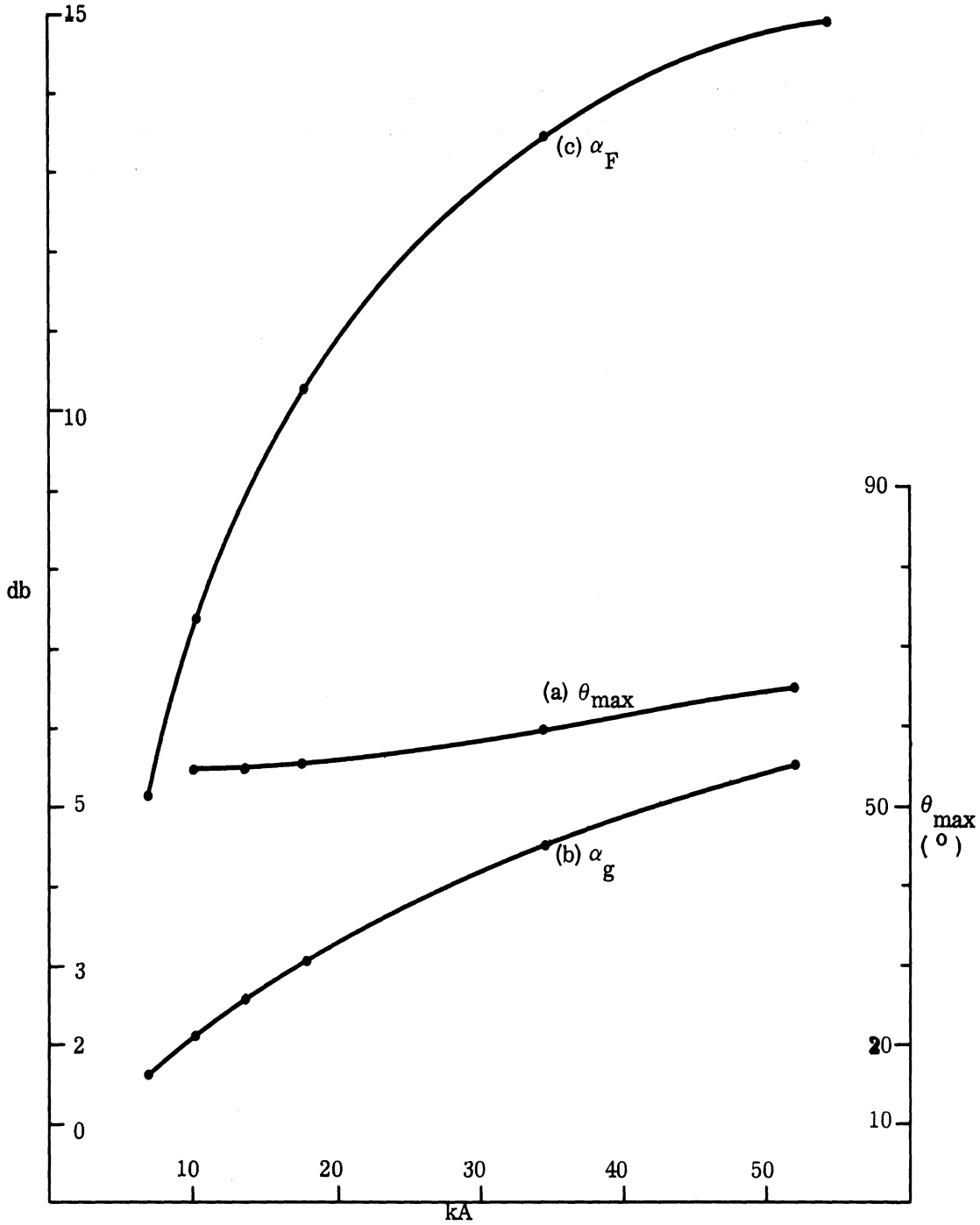

FIG. 2-8: THEORETICAL VARIATION OF ALFORD LOOP COUNTERPOISE RADIATION CHARACTERISTICS AS A FUNCTION OF COUNTERPOINT SIZE. f=1080 MHz, kh=2.75 (a) θ_{max} vs kA, (b) α_g vs kA (c) α_F vs kA .

2.7 Discussion

The radiation pattern characteristics of an Alford loop above a counterpoise have been discussed here both theoretically and experimentally. The results presented will be used later in evaluating and also improving the performance characteristics of the existing VOR antenna systems.

III

RADIATION FIELD OF A SINGLE PARASITIC LOOP COUNTERPOISE ANTENNA

3.1 Introduction

In the present chapter we investigate the radiation field produced by an Alford loop counterpoise antenna system as modified by the presence of a parasitic loop. The latter system is referred to as the parasitic loop counterpoise system and is shown schematically in Fig. 3-1. For theoretical analysis the Alford loop is represented by a small circular loop of radius a ($ka \ll 1$). The parasitic loop has a radius B and is placed at a height H above and parallel to the counterpoise. It is assumed to be made of conducting wire of radius b.

In the following sections we shall first develop a theoretical expression for the radiation field produced by the above antenna system. An experiment is then designed to obtain results so that the accuracy of the theory may be determined. Finally the various radiation properties of the antenna are discussed in general.

3.2 Far Field Expression

The parasitic loop receives its excitation from the Alford loop. The first step in the analysis is to obtain the current induced in the parasitic loop by the field produced by the excited loop. The radiation field produced by the parasitic current in the presence of the counterpoise is then determined. Finally this field is combined vectorially with the Alford loop counterpoise field given by Eq. (2.1) to obtain the far field produced by the parasitic loop counterpoise antenna.

3.2.1 Current Induced in the Parasitic Loop

From the symmetry of the system and the nature of the field produced by the excited loop, the current in the parasitic loop may be assumed to be of the form

$$\vec{I}_p = \hat{\phi} I_{p_o} e^{-i\omega t}, \tag{3.1}$$

where $\hat{\phi}$ is the unit vector in the ϕ-direction and I_{p_o} is a constant to be determined. In determining I_{p_o} it is assumed that the current at any point on the parasitic loop is equal to that induced by a longitudinally polarized (the electric field parallel to the axis) plane electromagnetic wave incident normally on a conducting cylinder of radius b and of infinite length (for example the cylinder is oriented parallel to the y-axis in Fig. 3-1). This is a basic assumption of geometrical optics and should be a reasonable approximation for the present problem as long as $kB \gg 1$. Using the

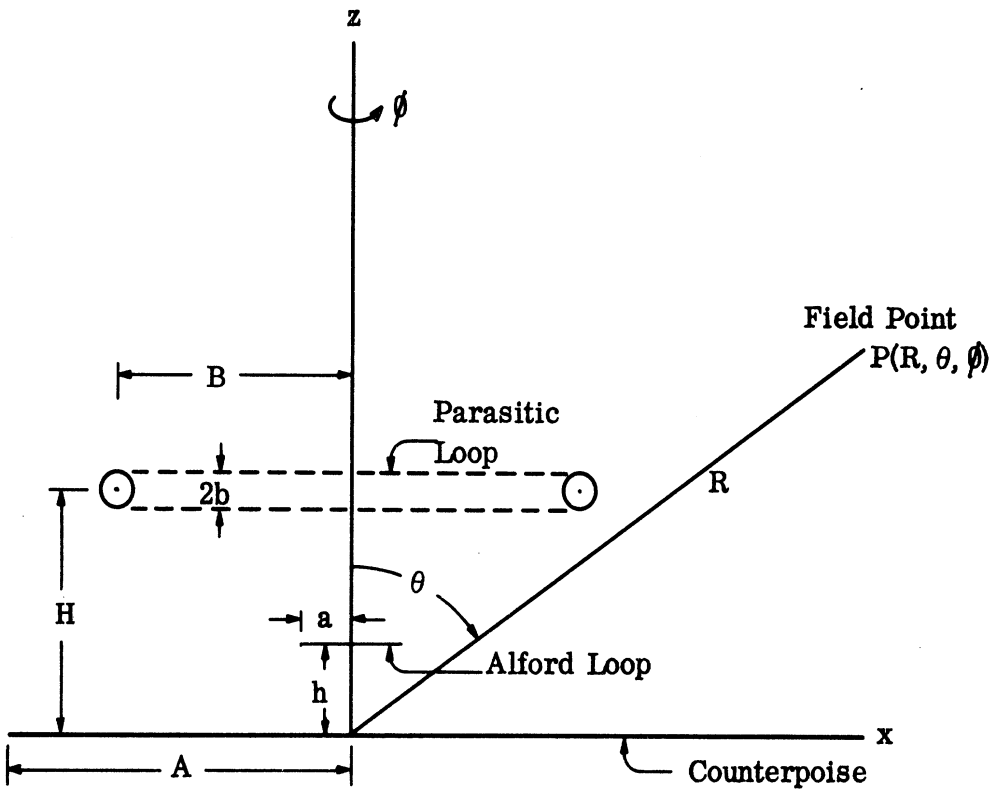

FIG. 3-1: GEOMETRIC REPRESENTATION OF PARASITIC LOOP COUNTERPOISE ANTENNA AND COORDINATE SYSTEM.

well-known results of the scattering of plane electromagnetic waves by a conducting cylinder of infinite length [3], it can be shown that

$$I_{p_o} = \frac{4}{\eta_o k} \sum_{n=-\infty}^{\infty}{}' \frac{i^n e^{in\phi'}}{H_n^{(1)}(kb)} E_\phi^{inc}(P) , \tag{3.2}$$

where

$E_\phi^{inc}(P)$ is the incident field at the position of the parasitic loop produced by the current $I_o e^{-i\omega t}$ in the small-excited loop,

$H_n^{(1)}$ is the Hankel function of the first kind and order n,

ϕ' is the azimuthal angle measured along the circumference of the cylinder,

and the other parameters are as explained before.

It is now assumed that $kb \ll 1$, so that it is sufficient to retain only the n=0 term in (3.2). After making the small argument approximation for the Hankel function we obtain the following from (3.2)

$$I_{p_o} \simeq \frac{2\pi}{i\eta_o kM} E_\phi^{inc}(P) , \tag{3.3}$$

where

$$M = 0.577 + \ell n \left(\frac{kb}{2}\right) - i\frac{\pi}{2} . \tag{3.4}$$

Thus the evaluation of the parasitic current I_{p_o} is reduced to the determination of the incident field at the position of the parasitic loop.

3.2.2 Incident Field at the Parasitic Element

The incident field $E_\phi^{inc}(P)$ at the point P on the parasitic loop is obtained from ray optics considerations. It is assumed that $E_\phi^{inc}(P)$ is due to the following rays originating from the phase center Q of the excited loop and reaching the point P (Fig. 3-2):

(i) direct and reflected rays 1 and 2 respectively originating from Q,
(ii) the rays 3 and 4 originating from Q and singly diffracted by the near and far edges of the counterpoise respectively,
(iii) a ray 5 from Q and singly diffracted by the diametrically opposite region P' of the parasitic loop before reaching P,
(iv) a ray 6 single diffracted by the parasitic loop at P and reflected back to P by the counterpoise.

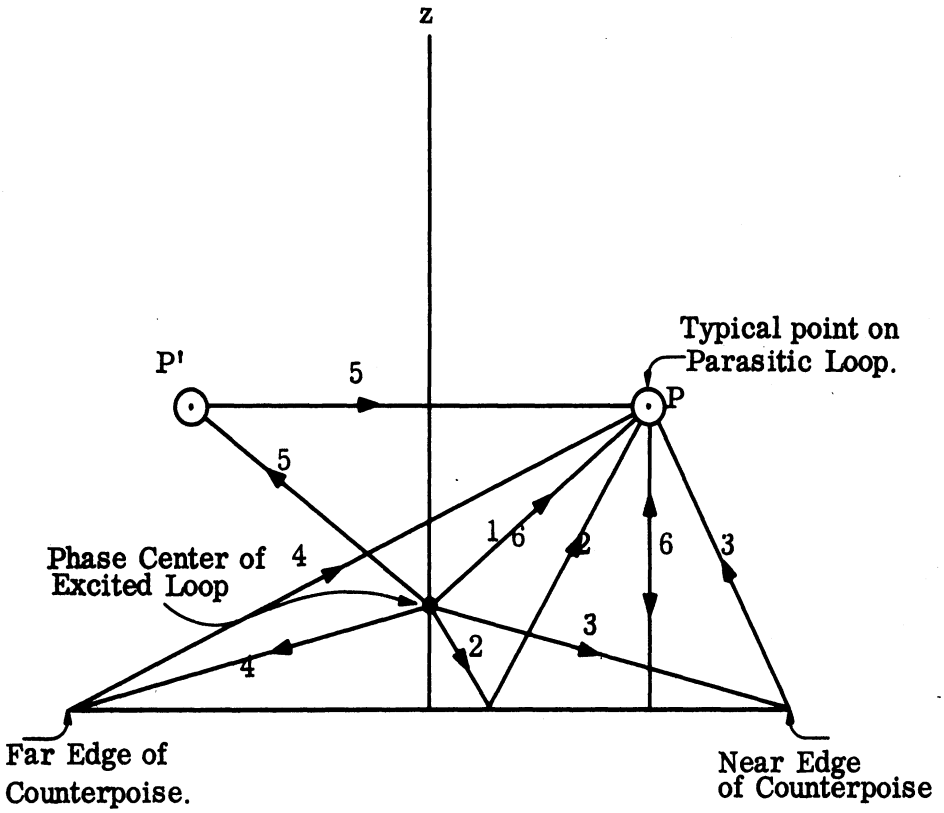

FIG. 3-2: DIAGRAM OF DIFFERENT RAYS CONTRIBUTING TO PARASITIC CURRENT.

There are other rays that may contribute to the field at P but they will be higher order diffracted and hence are neglected for the present purpose. It is clear from physical considerations that the contributions due to the direct and reflected rays will be predominant. It is also anticipated that for $kH \gg 1$ the contribution due to the diffracted rays will be of less importance. However, for small and moderate values of kH the diffracted ray contributions can no longer be neglected. Thus the incident field at the point P on the parasitic loop may be formally written as:

$$E_{\phi}^{inc}(P) = E_{\phi}^{12}(P) + E_{\phi}^{34}(P) + E_{\phi}^{56}(P) , \tag{3.5}$$

where the superscripts on the right hand side refer to the rays contributing to the field.

3.2.3 Evaluation of the Incident Field at the Parasitic Element

It is quite easy to obtain the field component $E_{\phi}^{12}(P)$ due to the direct and reflected rays. It can be shown to be given by

$$E_{\phi}^{12}(P) = \eta_o I_o \left(\frac{ka}{2}\right)^2 B \left[\frac{e^{ikr_1}}{r_1^2} - \frac{e^{ikr_2}}{r_2^2}\right] , \tag{3.6}$$

where

$$\left.\begin{aligned} r_1^2 &= B^2 + (H-h)^2 \\ r_2^2 &= B^2 + (H+h)^2 \end{aligned}\right\} . \tag{3.7}$$

The evaluation of the field $E_{\phi}^{34}(P)$ due to the near and far edge diffracted rays is not straightforward and hence we discuss the key steps involved in obtaining it. The near and far edge diffracted fields at P are determined separately and then combined to obtain $E_{\phi}^{34}(P)$. The coordinate system used in obtaining these fields is shown in Fig. 3-3. In obtaining these fields the results of Sommerfeld's theory of diffraction of plane waves by a half-plane[4] are used. The application of Sommerfeld's theory to the present type of problem has been discussed elsewhere[1] and will not be repeated here. It can be shown that the incident field at P due to the near-edge diffraction of the field originating from the phase center Q of the excited loop is given by

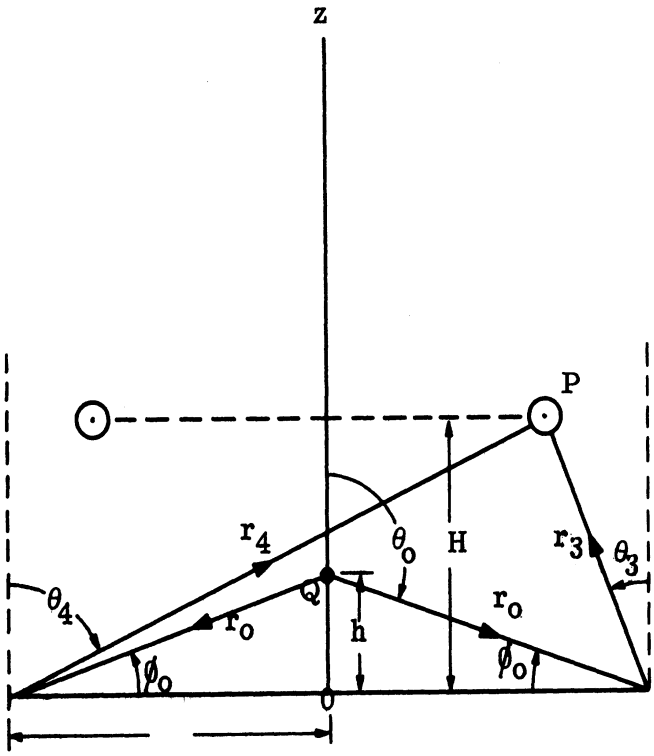

FIG. 3-3: COORDINATE SYSTEM FOR DETERMINING EDGE DIFFRACTED FIELDS.

$$E_{\phi}^{3}(P)=\left[\frac{A}{A-r_3\sin\theta_3}\right]^{1/2}\left(\frac{r_o}{r_3}\right)^{1/2}\frac{1-i}{i2\pi}\left(\frac{1}{p_3}-\frac{1}{p_3'}\right)e^{ikr_3}$$

$$\times\left[\eta_o I_o\left(\frac{ka}{2}\right)^2\sin\theta_o\,\frac{e^{ikr_o}}{r_o}\right],\qquad \text{for } kA\gg 1,\ kr_3\gg 1. \tag{3.8}$$

where

$$p_3=2\left(\frac{kr_o}{\pi}\right)^{1/2}\cos\left(\frac{\phi_o-\phi_3}{2}\right), \tag{3.9}$$

$$p_3'=2\left(\frac{kr_o}{\pi}\right)^{1/2}\cos\left(\frac{\phi_o+\phi_3}{2}\right), \tag{3.10}$$

and the other parameters are as explained in Fig. 3-3. In Eq. (3.8), the first factor $(A/A-r_3\sin\theta_3)^{1/2}$ is the near edge divergence factor which takes into account the circular geometry of the counterpoise. From the geometry shown in Fig. 3-3 it can be seen that

$$\left(\frac{A}{A-r_3\sin\theta_3}\right)^{1/2}=\left(\frac{A}{B}\right)^{1/2}\quad . \tag{3.11}$$

The last factor in (3.8) is the incident field at the near edge produced by the circular loop of radius a and carrying a current I_o. After introducing (3.11) into (3.8) and some algebraic manipulation, the following is obtained for the contribution of the incident field at P due to the near edge diffracted ray 3 :

$$E_{\phi}^{3}(P)=\eta_o I_o\left(\frac{ka}{2}\right)^2\frac{A}{r_o^2}\left(\frac{A}{B}\right)^{1/2}\left(\frac{1}{\pi kr_3}\right)^{1/2}e^{-i3\pi/4}$$

$$\times\ e^{ik(r_o+r_3)}\left[\sec\left(\frac{\phi_o-\phi_3}{2}\right)-\sec\left(\frac{\phi_o-\phi_3}{2}\right)\right]\quad . \tag{3.12}$$

Similarly it can be shown that the field produced at P due to the far-edge diffracted ray 4 is given by

$$E_{\phi}^{4}(P)=e^{-i\pi/2}\left(\frac{A}{r_4\sin\theta_4-A}\right)^{1/2}\left(\frac{r_o}{r_4}\right)^{1/2}\frac{1-i}{i2\pi}\left(\frac{1}{p_4}-\frac{1}{p_4'}\right)$$

$$\times\ e^{ikr_4}\left[-\eta_o I_o\left(\frac{ka}{2}\right)^2\sin\theta_o\,\frac{e^{ikr_o}}{r_o}\right]\quad ,\ \text{for } kA\gg 1, kr_4\gg 1, \tag{3.13}$$

where all the parameters are as defined in Fig. 3-3 and

$$P_4=2\left(\frac{kr_o}{\pi}\right)^{1/2}\cos\left(\frac{\phi_o-\phi_4}{2}\right), \tag{3.14}$$

$$p'_4=2\left(\frac{kr_o}{\pi}\right)^{1/2}\cos\left(\frac{\phi_o+\phi_4}{2}\right) \quad . \tag{3.15}$$

The interpretation of the different factors in (3.13) is similar to those in (3.8). The factor $e^{-i\pi/2}$ in front of (3.13) is due to the fact that the diffracted rays pass through the focal line (z-axis); the negative sign in the last factor is due to the reversal of the incident field polarization at the far edge of the counterpoise with respect to the near edge. After some rearrangement, (3.13) may be written as follows:

$$E_\phi^4(P)=-\eta_o I_o\left(\frac{ka}{2}\right)^2\frac{A}{r_o^2}\left(\frac{A}{B}\right)^{1/2}\left(\frac{I}{\pi kr_4}\right)^{1/2}\frac{e^{-i3\pi/4}}{2\sqrt{2}}e^{-i\pi/2}$$

$$\times e^{ik(r_o+r_4)}\left[\sec\left(\frac{\phi_o-\phi_4}{2}\right)-\sec\left(\frac{\phi_o+\phi_4}{2}\right)\right] \quad . \tag{3.16}$$

After combining (3.12) and (3.16) we obtain the following as the contribution to the incident field at P due to the near and far edge diffracted rays 3 and 4:

$$E_\phi^{34}(P)=\eta_o I_o\left(\frac{ka}{2}\right)^2\frac{A}{r_o^2}e^{ikr_o}\cdot\frac{e^{-i3\pi/4}}{2\sqrt{2}}\cdot\left(\frac{A}{B}\right)^{1/2}$$

$$\times\left[\left(\frac{1}{\pi kr_3}\right)^{1/2}e^{ikr_3}\left\{\sec\left(\frac{\phi_o-\phi_3}{2}\right)-\sec\left(\frac{\phi_o+\phi_3}{2}\right)\right\}\right.$$

$$\left.+i\left(\frac{1}{\pi kr_4}\right)^{1/2}e^{ikr_4}\left\{\sec\left(\frac{\phi_o-\phi_4}{2}\right)-\sec\left(\frac{\phi_o+\phi_4}{2}\right)\right\}\right]. \tag{3.17}$$

The contributions to the incident field at P due to the rays 5 and 6 are found in the following manner The geometry involved is as shown in Fig. 3-4, where P' is the cross section of the parasitic loop situated in a region diametrically opposite to P. To obtain the field at the point P due to the ray 5 we at first obtain the field at the point P due to the scattering of a plane electromagnetic wave of proper amplitude incident normally at an y-directed conducting and infinite cylinder of radius b located

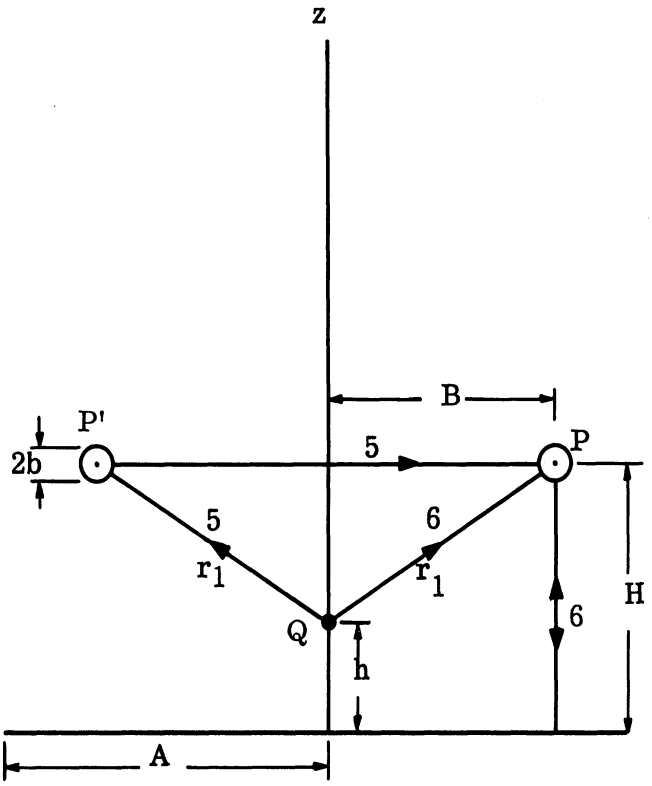

FIG. 3-4: COORDINATE SYSTEM USED TO DETERMINE FIELD DUE TO RAYS 5 AND 6 .

at P'. It is assumed that kb << 1 so that the low frequency approximation to the well-known results[3] of the scattering of electromagnetic waves by an infinite cylinder may be used for this purpose. The incident field at P' is that produced by the circular loop located at Q and its field is assumed to be locally a plane wave in the vicinity of P'. Thus it can be shown that the scattered field at P is

$$E_{\phi}^{s'}(P) \simeq \left[-\eta_o I_o \left(\frac{ka}{2}\right)^2 \frac{B}{r^2} e^{ikr_1}\right] \times \left[-\frac{\pi}{2iM}\left(\frac{1}{\pi kB}\right)^{1/2} e^{i(2kB-\pi/4)}\right], \qquad (3.18)$$

where M is as given by (3.4) and the other parameters are as explained before. The field at P due to the ray 5 is now assumed to be given by (3.18) multiplied by the proper divergence factor which takes into account the circular nature of the parasitic loop. The appropriate divergence factor in this case can be obtained from the divergence factor in front of (3.13) with A replaced by B and $r_4=2B$ and $\theta_4=\pi/2$. Thus the field at P due to the ray 5 is obtained as:

$$E_{\phi}^{5}(P) = -\eta_o I_o \left(\frac{ka}{2}\right)^2 \frac{\pi}{2M} \frac{B}{r_1^2} e^{ikr_1} \cdot \left(\frac{1}{\pi kB}\right)^{1/2} e^{i(2kB-\pi/4)} . \qquad (3.19)$$

The approximation involved in deriving (3.19) is valid for $kB \gg 1$.

Following a similar procedure the field at P due to the ray 6 can be obtained. It can be shown that it is given by:

$$E_{\phi}^{6}(P) = +\eta_o I_o \left(\frac{ka}{2}\right)^2 \frac{\pi}{i2M} \cdot \frac{B}{r_1^2} e^{ikr_1} \left(\frac{1}{\pi kH}\right)^{1/2} e^{i(2kH-\pi/4)} . \qquad (3.20)$$

Thus the combined field at P due to the rays 5 and 6 is obtained by the addition of (3.19) and (3.20) and is given by:

$$E_{\phi}^{56}(P) = -\eta_o I_o \left(\frac{ka}{2}\right)^2 \frac{\pi}{2iM} \frac{B}{r_1^2} e^{ikr_1} \times \left[\left(\frac{1}{\pi kB}\right)^{1/2} e^{i(2kB+\pi/4)} - \left(\frac{1}{\pi kH}\right)^{1/2} e^{i(2kH-\pi/4)}\right] . \qquad (3.21)$$

This completes the evaluation of the component incident fields in volved in Eq. (3.5).

3.2.4 Evaluation of the Parasitic Current

We are now in a position to evaluate the current I_{p_o} induced in the parasitic loop. After introducing Eq. (3.5) into (3.3), I_{p_o} is obtained in terms of the current

I_o and other physical parameters of the system. Following the same convention used in (3.5) we can write

$$I_{p_o} = I_{p_o}^{12} + I_{p_o}^{34} + I_{p_o}^{56} \quad . \tag{3.22}$$

Using (3.3), (3.4), (3.6), (3.7), (3.17) and (3.21) it can be shown that the component currents in (3.22) are given by the following set of equations.

$$I_{p_o}^{12} = I_o \left(\frac{ka}{2}\right)^2 \frac{2\pi B}{ikM} \left[\frac{e^{ikr_1}}{r_1^2} - \frac{e^{ikr_2}}{r_2^2}\right] , \tag{3.23}$$

$$\left.\begin{aligned} &r_1^2 = B^2 + (H-h)^2, \quad r_2^2 = B^2 + (H+h)^2 \\ &M = 0.577 + \ell n(kb/2) - i\pi/2 \end{aligned}\right\} \tag{3.24}$$

$$I_{p_o}^{34} = I_o \left(\frac{ka}{2}\right)^2 \frac{\pi}{ikM} \frac{A}{r_o^2} e^{ikr_o} \cdot \frac{e^{-i3\pi/4}}{\sqrt{2}} \left(\frac{A}{B}\right)^{1/2}$$

$$\times \left[\left(\frac{1}{\pi kr_3}\right)^{1/2} e^{ikr_3} \left\{\sec\left(\frac{\phi_o - \phi_3}{2}\right) - \sec\left(\frac{\phi_o + \phi_3}{2}\right)\right\}\right.$$

$$\left. + i\left(\frac{1}{\pi kr_4}\right)^{1/2} e^{ikr_4} \left\{\sec\left(\frac{\phi_o - \phi_4}{2}\right) - \sec\left(\frac{\phi_o + \phi_4}{2}\right)\right\}\right], \tag{3.25}$$

$$\left.\begin{aligned} &r_3^2 = (A-B)^2 + H^2; \quad r_4^2 = (A+B)^2 + H^2; \quad r_o^2 = A^2 + h^2 \\ &\tan\phi_3 = H/(A-B); \quad \tan\phi_4 = H/(A+B); \quad \tan\phi_o = h/A \end{aligned}\right\} , \tag{3.26}$$

$$I_{p_o}^{56} = I_o \left(\frac{ka}{2}\right)^2 \frac{\pi^2 (kB)}{M^2} \frac{e^{ikr_1}}{(kr_1)^2} \times \left[\left(\frac{1}{\pi kB}\right)^{1/2} e^{i(2kB + \pi/4)} - \left(\frac{1}{\pi kH}\right)^{1/2} e^{i(2kH - \pi/4)}\right] . \tag{3.27}$$

This completes the evaluation of the current induced in the parasitic loop element. As mentioned before the approximations involved in the derivation makes the above set of equations valid for the cases when $kB \gg 1$ and $kA \gg 1$, i. e. when both the parasitic loop and the counterpoise diameters are large compared to the wavelength. For ϕ_o sufficiently small and the present polarization of the field produced by the excited loop, it can be seen that the contribution due to the $I_{p_o}^{34}$ term is much less than the other terms. More will be discussed about this later.

3.2.5 Far Field of a Large Circular Loop Above a Counterpoise

In this section we give the theoretical expression for the radiation field produced by a large circular loop of radius B(i. e. kB $\gg$ 1) and carrying a current of the form

$$\vec{I}_p = \hat{\phi} I_{p_o} e^{-i\omega t}$$

and placed at a height H above a counterpoise of radius A. The method of analysis is similar to the one used by Weston et al [2] to obtain the radiation field produced by a small circular loop above a counterpoise. The derivation of the expression is discussed in Appendix A. With reference to Fig. 3-5, it can be shown that the far field at the point $P(\pi, \theta, \phi)$ is given by the following expression, valid in the region $0 < \theta < \pi$:

$$E_\phi \sim \eta_o I_{p_o} \left(\frac{kB}{2}\right) \frac{e^{i(kR-\pi/4)}}{R} F(\theta) , \tag{3.28}$$

where

$$F(\theta) = \frac{J_1(kB\sin\theta)}{\sqrt{2}} F^p(\theta) e^{-ikA\sin\theta} + \frac{\cos\theta \sin\left(\frac{\phi_p}{2}\right)}{\sqrt{\pi\, kr_p \sin\theta}} e^{ikr_p} L^p(\theta) , \tag{3.29}$$

$$L^p(\theta) = \frac{e^{i(\pi/2-kA\sin\theta)}}{\sqrt{1-\sin\theta}} \left[\frac{\cos^{1/2}\phi_p J_1(kB\cos\phi_p) - \sin^{1/2}\theta\, J_1(kB\sin\theta)}{\cos\phi_p - \sin\theta} \right]$$

$$- \frac{e^{ikA\sin\theta}}{\sqrt{1+\sin\theta}} \left[\frac{J_1(kB\cos\phi_p)\cos^{1/2}\phi_p}{\cos\phi_p + \sin\theta} \right] , \tag{3.30}$$

$$F^p(\theta) = e^{ikr_p\sin(\theta-\phi_p)} \int_{-\infty}^{p_5} e^{i\pi t^2/2}\, dt - e^{ikr_p\sin(\theta+\phi_p)} \int_{-\infty}^{p_6} e^{i\pi t^2/2}\, dt , \tag{3.31}$$

$$p_5 = 2\left(\frac{kr_p}{\pi}\right)^{1/2} \cos\left(\frac{\phi_p - \theta - \pi/2}{2}\right) , \tag{3.32}$$

$$p_6 = 2\left(\frac{kr_p}{\pi}\right)^{1/2} \cos\left(\frac{\phi_p + \theta + \pi/2}{2}\right) , \tag{3.33}$$

$$\left.\begin{aligned} r_p^2 &= A^2 + H^2 \\ \tan\phi_p &= H/A \end{aligned}\right\} , \tag{3.34}$$

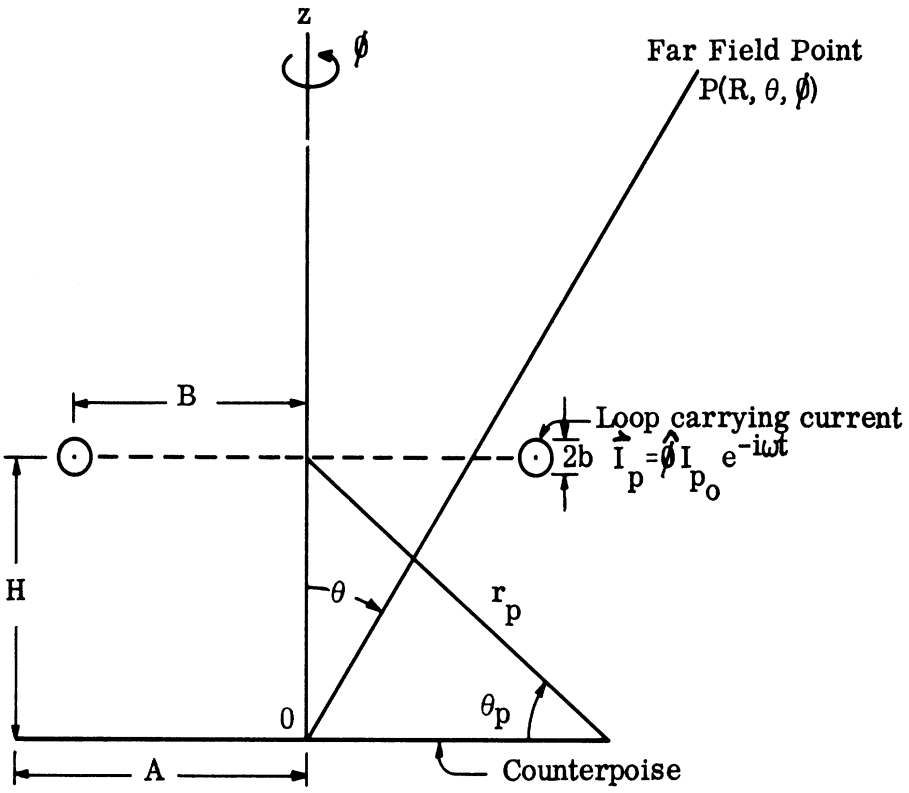

FIG. 3-5: COORDINATE SYSTEM USED TO DETERMINE FAR FIELD OF LARGE LOOP ABOVE COUNTERPOISE.

and J_1 is the usual notation for the Bessel function of the first kind and first order.

3.2.6 The Radiation Field of a Parasitic Loop Counterpoise Antenna

The radiation field produced by the parasitic loop counterpoise antenna shown in Fig. 3-1 can now be obtained by superposing the fields given by (2.1) and (3.28) with the parasitic loop current I_{p_o} in (3.28) being given by (3.22) - (3.27). Thus it can be shown that in the range $0 < \theta < \pi$ the far field may be expressed in the form

$$E_{\phi} = \eta_o I_o \left(\frac{ka}{2}\right)^2 \frac{e^{i(kR-\pi/4)}}{R} S(\theta) \quad , \tag{3.35}$$

where

$$S(\theta) = S^A(\theta) + S^p_{12}(\theta) + S^p_{34}(\theta) + S^p_{56}(\theta) \quad . \tag{3.36}$$

In (3.35), $S(\theta)$ is identified as the complex far field pattern produced by the parasitic loop counterpoise antenna. In (3.36) the terms $S^A(\theta)$ is the free space complex far field pattern produced by the small loop only above the counterpoise and is given by Eq. (2.2). The last three terms in (3.36) constitute the complex far field pattern produced by the parasitic loop only in the presence of the counterpoise. The subscripts in the terms on the right hand side of (3.36) refer to the approximation used in evaluating the corresponding parasitic current. The conventional radiation pattern of the loop counterpoise antenna is given by $|S(\theta)|$. Explicit expressions for the terms in (3.36) are given below for future reference.

$$S^A(\theta) = \left\{ \frac{F^o(\theta)\sin\theta}{\sqrt{2}} e^{-ikA\sin\theta} + \frac{|\cos\theta| \sin(\frac{\phi_o}{2})}{\sqrt{\pi kr_o \sin\theta}} e^{ikr_o} L^o(\theta) \right\} \quad , \tag{3.37}$$

$F^o(\theta)$, $L^o(\theta)$ are as defined by (2.3) - (2.8).

$$S^p_{12}(\theta) = \frac{\pi(kB)^2}{iM} \left[\frac{e^{ikr_1}}{(kr_1)^2} - \frac{e^{ikr_2}}{(kr_2)^2} \right] F(\theta) \quad , \tag{3.38}$$

$$S^p_{34}(\theta) = \frac{\pi(kA)(kB)}{iM} \frac{e^{-i\pi/4}}{2\sqrt{2}} \frac{e^{ikr_o}}{kr_o} \left(\frac{A}{B}\right)^{1/2} \times \left[\left(\frac{1}{\pi kr_4}\right)^{1/2} e^{ikr_4} \left\{ \sec\left(\frac{\phi_o - \phi_4}{2}\right) - \sec\left(\frac{\phi_o + \phi_4}{2}\right) \right\} \right.$$

$$\left. - i\left(\frac{1}{\pi kr_3}\right)^{1/2} e^{ikr_3} \left\{ \sec\left(\frac{\phi_o - \phi_3}{2}\right) - \sec\left(\frac{\phi_o + \phi_3}{2}\right) \right\} \right] F(\theta), \tag{3.39}$$

$$S^{p}_{56}(\theta) = \frac{\pi^2 (kB)^2}{2M^2} \frac{e^{ikr_1}}{(kr_1)^2} \left[\left(\frac{1}{\pi kB}\right)^{1/2} e^{i(2kB + \pi/4)} \right.$$

$$\left. - \left(\frac{1}{\pi kH}\right)^{1/2} e^{i(2kH - \pi/4)} \right] F(\theta) \ , \qquad (3.40)$$

where $F(\theta)$ is as given by (3.29) - (3.34) and all the other parameters are as defined before.

It is appropriate at this stage to list the following approximations involved in the derivation of (3.37) - (3.40):

$$kA \gg 1, \ kB \gg 1, \ kH \gg 1, \ kb \ll 1 \text{ and } kA > kB \ . \qquad (3.41)$$

The influence of each of the parameters, A, B, H and b on the pattern as well as the relative importance of each of the terms in (3.36) will be discussed later. This completes the derivation of the theoretical expression for the radiation field produced by the parasitic loop counterpoise antenna.

3.3 Description of the Experimental Arrangement

For experimental investigations a parasitic loop was positioned coaxially with the axis of an active Alford loop antenna. Both the parasitic element and Alford loop were mounted above a counterpoise having $2A \sim 5.7\lambda$ at an operating frequency of 1080 MHz and is shown in Fig. 3-6. All pattern measurements were carried out in the θ-variable plane of Fig. 3-6. The basic Alford loop counterpoise antenna is similar to the one described in Section 2.3 and was not varied during the experiment. The parasitic loops were held in position by a polystyrene foam structure as shown in Fig. 3-7. As can be seen from both figures, the parasitic loops are made of conducting strips rather than conducting wires as assumed in the theory. This has been done for mechanical simplicity. In comparing the experimental results with theory it is assumed[5] that a conducting strip of width w is electrically equivalent to a conducting cylinder of radius b , which is a reasonable assumption provided $w = 4b$ and $w, b \ll \lambda$. The parasitic elements were fabricated from brass strips $9.15 \times 10^{-3}\lambda$ thick at 1080 MHz and oriented as shown in Fig. 3-6. Two basic parasitic elements having w = 1" and w = 2" were used during the experiment. These two widths correspond to $9.15 \times 10^{-2}\lambda$ and $1.83 \times 10^{-1}\lambda$ respectively at the frequency 1080 MHz. Employing each of these basic parasitic loop configurations in the Alford loop counterpoise system, the effects of the variation of H and B (Fig. 3-6) on the patterns were studied. All the patterns were measured in an anechoic chamber. It should be noted that the height H of the parasitic loop is measured from the top surface of the counterpoise to the center (w/2) of the parasitic element.

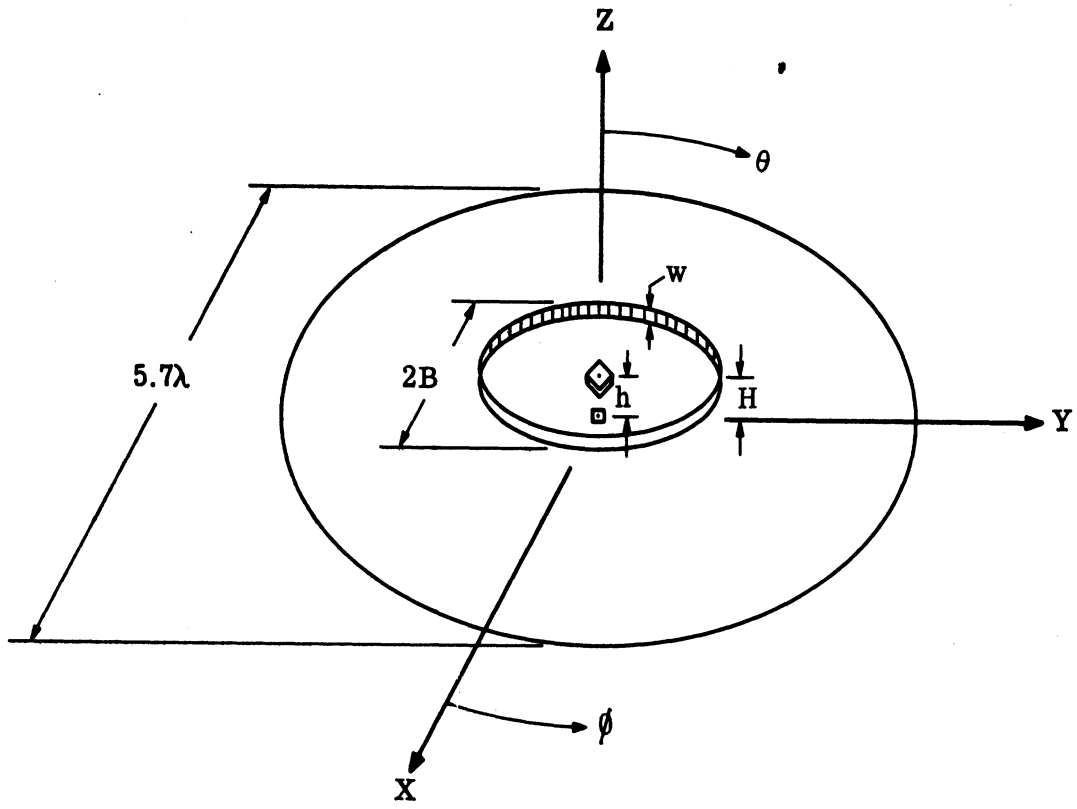

FIG. 3-6: SCHEMATIC DIAGRAM OF THE EXPERIMENTAL PARASITIC LOOP COUNTERPOISE ANTENNA.

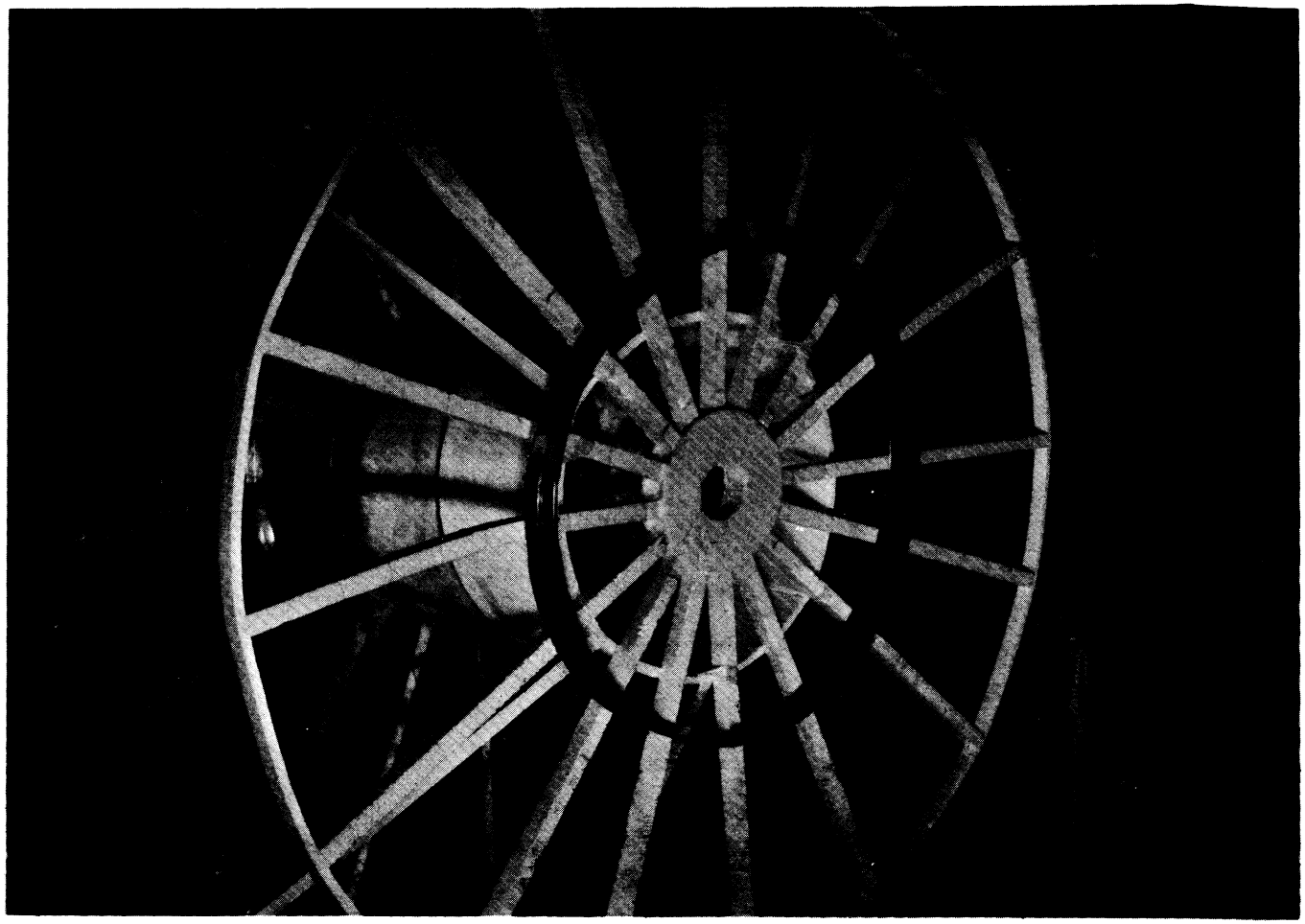

FIG. 3-7: PHOTOGRAPH OF THE PARASITIC LOOP COUNTERPOISE ANTENNA.

3.4 Comparison Between Theory and Experiment

A typical measured elevation pattern of the loop counterpoise antenna system with one parasitic loop is shown in Fig. 3-8. This particular value of H was chosen here because it was anticipated that the disagreement between theory and experiment would be more for smaller values of H. Theoretical points as obtained from numerical computation of

$$|S^{A}(\theta)+S^{p}_{12}(\theta)|$$

of Eq. (3.36) are shown as dots in Fig. 3-8. It can be seen that with this first order approximate theory, the agreement between theory and experiment is fairly good over most of the range of θ despite the fact that the pattern has been computed by neglecting all diffraction effects in the determination of the parasitic current. Diffraction effects on the parasitic current are taken into account by numerically computing $|S^{A}(\theta)+S^{p}_{12}(\theta)+S^{p}_{56}(\theta)|$ of Eq. (3.36). These computed points are shown as crosses in Fig. 3-8, which shows a slight improvement in the agreement between the theory and experiment due to the inclusion of the term $S^{p}_{56}(\theta)$. The improvement is found to be more than 3 db for values of θ near 0^{o} and for $\theta > \pi/2$. Numerical computations indicated that the term $S^{p}_{34}(\theta)$ in (3.36) is negligible compared to the other terms. For this reason, in the theoretical calculations discussed below, this term was not considered and was also neglected for all subsequent calculations.

Figure 3-9 shows the measured and theoretical elevation patterns produced by an antenna system with a parasitic element having a larger value of b. The agreement between theory and experiment here may be considered to be satisfactory in the range $0 < \theta \lesssim 80^{o}$. For $\theta > 80^{o}$ the disagreement between the two is found to be worse than that considered in Fig. 3-8. This is attributed to the fact that the values of b, B and H used in obtaining the theoretical pattern in Fig. 3-9 lie in the extreme end of the range of validity of the approximation mentioned in (3.41). For larger values of B and H the agreement will be better.

The present theory may be further improved by taking into account higher order diffraction terms in obtaining the induced current in the parasitic loop. However it is anticipated that for larger values of H and B the present theory should agree better with experiment. This is borne out in Fig. 3-10 where the agreement between the two may be considered to be excellent.

On the basis of our comparative study of numerical and experimental patterns it may be said that the theory given in Section 3.2 can be used with satisfactory

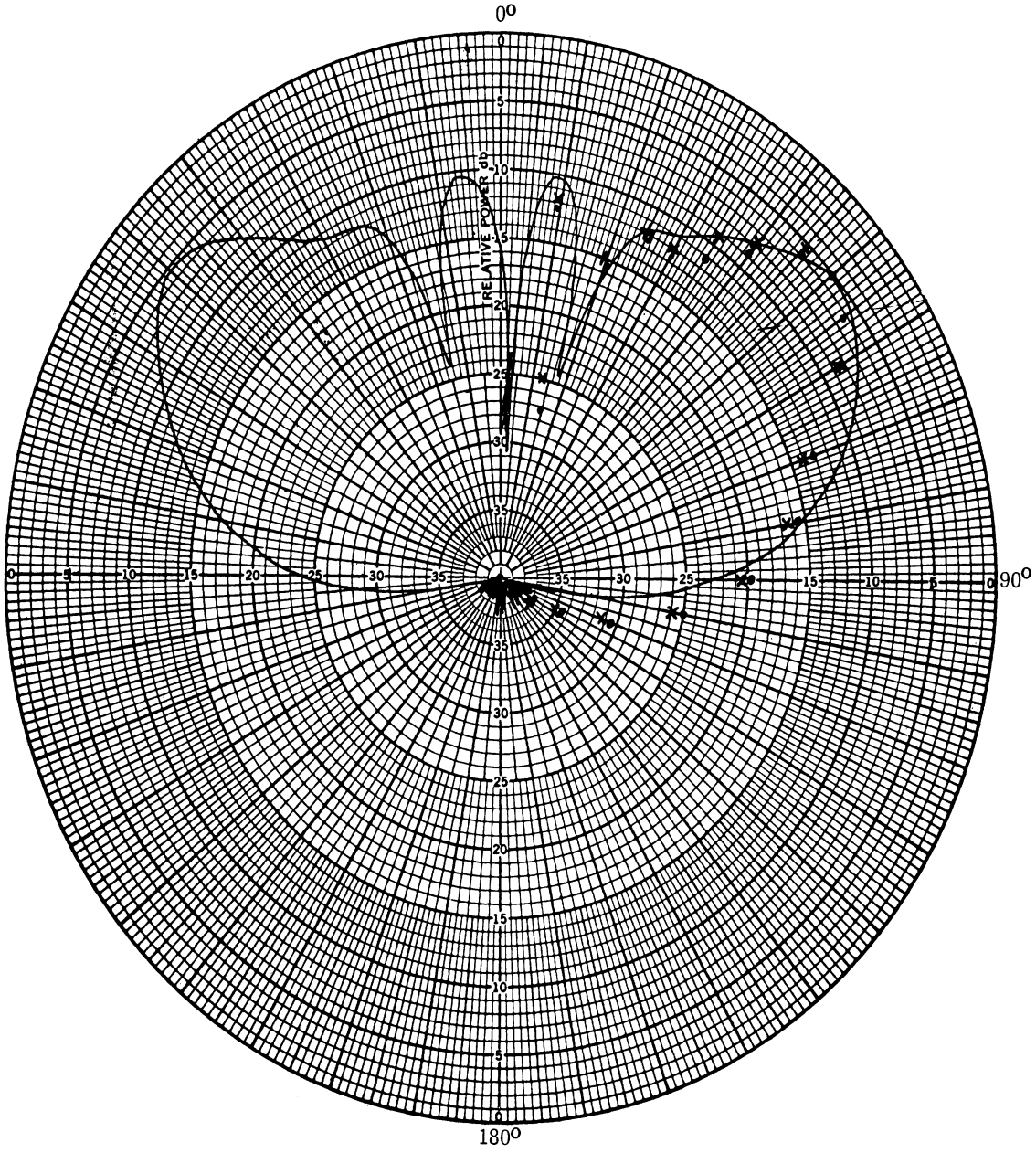

FIG. 3-8: FREE SPACE FAR FIELD ELEVATION PATTERN PRODUCED BY SINGLE PARASITIC LOOP COUNTERPOISE ANTENNA.
ka=2.75, kH=3.75, kA=17.92, kb=0.15, kB=4π, f=1080 MHz
(—) Experimental, (••) $\left|S^{A}(\theta)+S^{P}_{12}(\theta)\right|$ Theoretical, (××) $\left|S^{A}(\theta)+S^{P}_{12}(\theta)+S^{P}_{56}(\theta)\right|$ Theoretical.

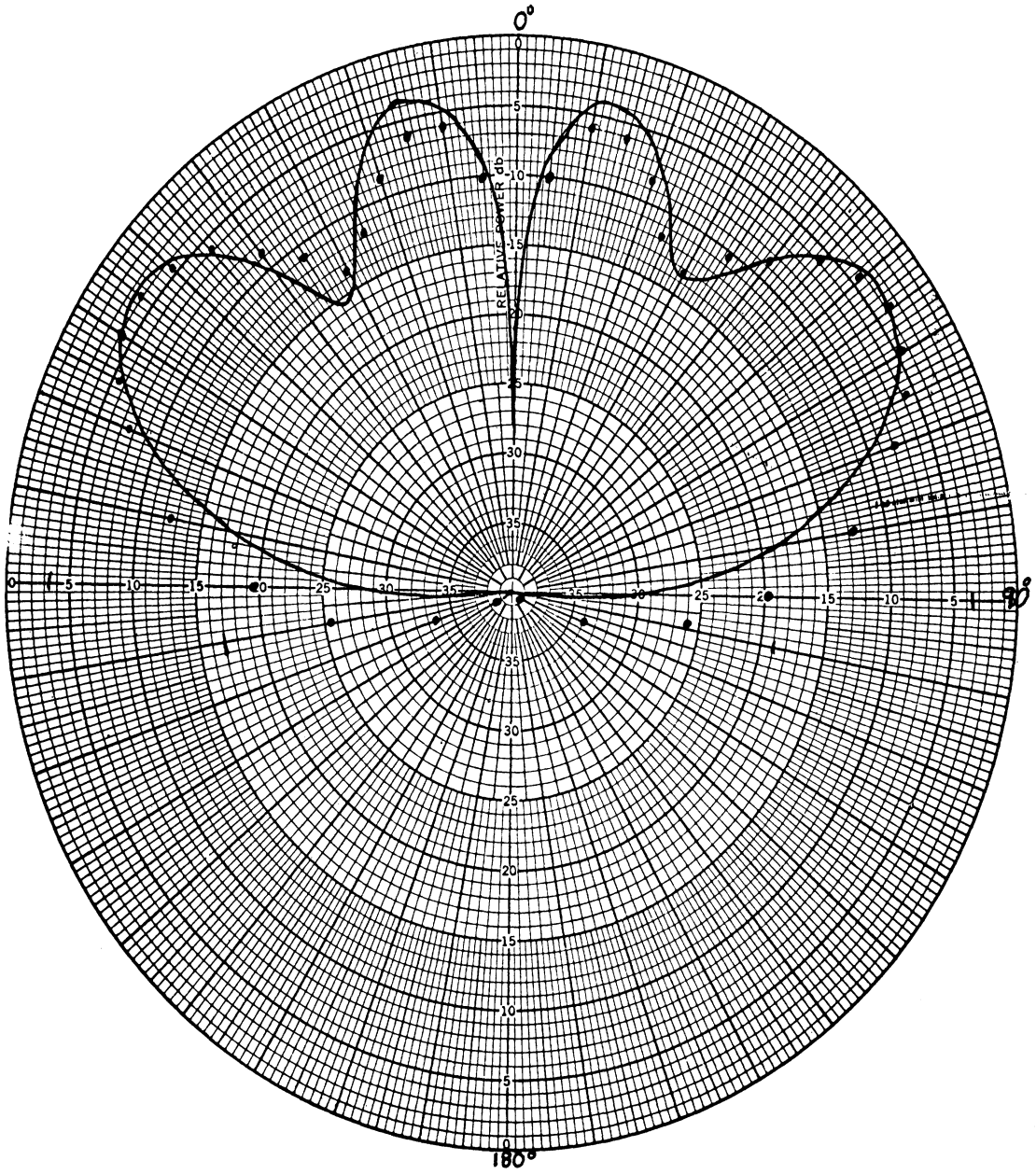

FIG. 3-9: FREE SPACE FAR FIELD ELEVATION PATTERN PRODUCED BY SINGLE PARASITIC LOOP COUNTERPOISE ANTENNA. kh=2.75, kH=3.75, kA=17.92, kb=0.287, kB=2.5π, f=1080 MHz (—) Experimental, (•,•) Theoretical.

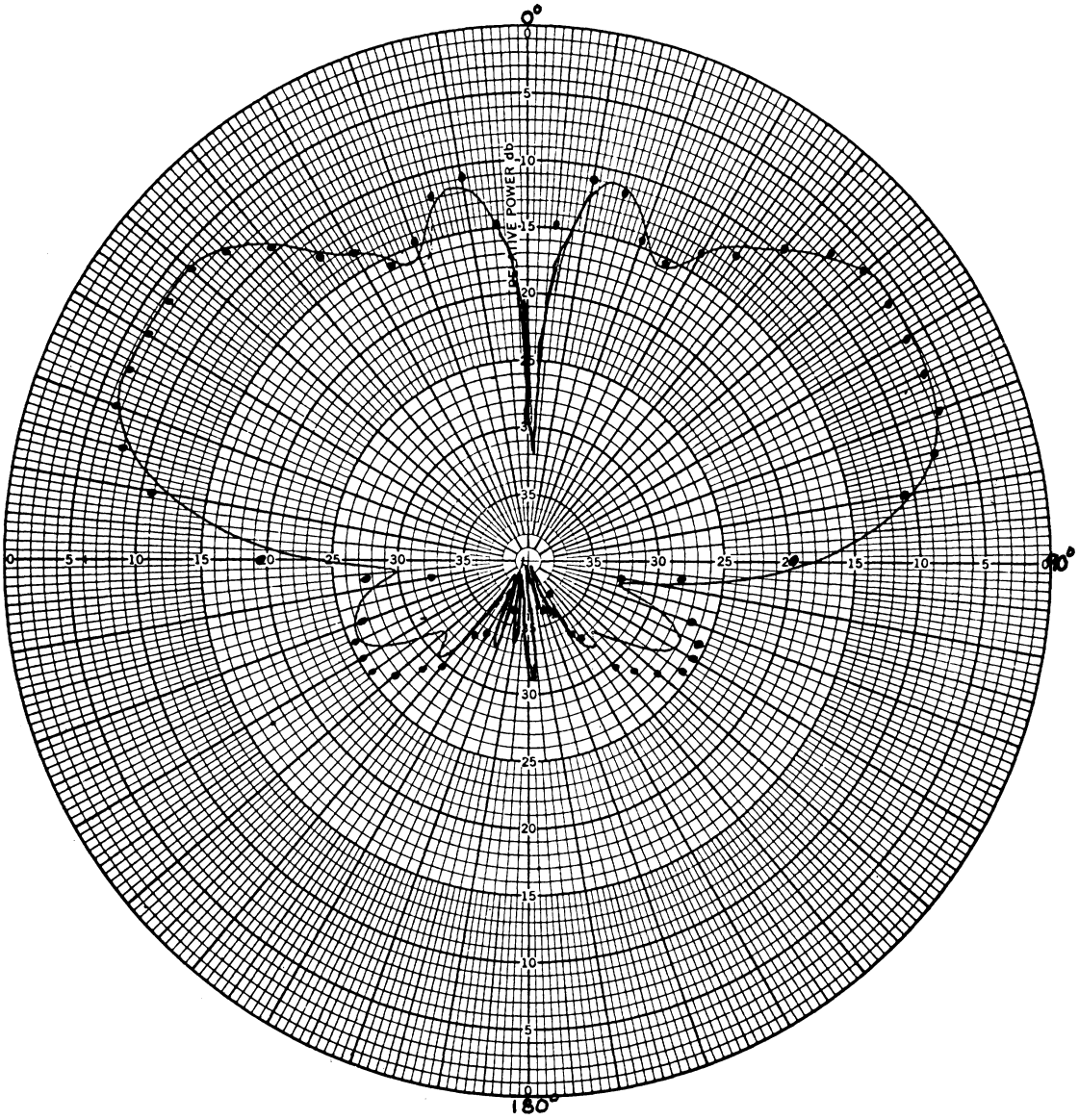

FIG. 3-10: FREE SPACE FAR FIELD ELEVATION PATTERN PRODUCED BY SINGLE PARASITIC LOOP COUNTERPOISE ANTENNA. kh=2.75, kH=11.78, kA=17.92, kb=0.15, kB=2.5π, f=1080 MHz (—) Experimental, (••) Theoretical.

accuracy for $kb \lesssim 0.25$ and $kB \gtrsim 2.5\pi$ and $kH \geq 3.75$. The accuracy will be better for larger values of B and H and smaller values of b.

3.5 General Effects of the Parasitic Loop on the Radiation Pattern

The elevation pattern of the basic Alford loop counterpoise antenna was discussed in Chapter II. The considerable response of the antenna for $\theta \geq \pi/2$ as shown in Fig. 2-4 is due to the effects produced by the counterpoise edge diffraction. After comparing the patterns given in Figs. 3-8 through 3-10 with that given in Fig. 2-4, it can be said that, in general, the parasitic loop reduces the effects of counterpoise edge diffraction considerably. This is evident from the fact that the parasitic loop counterpoise antenna patterns discussed in Section 3.4 show much reduced response in directions $\theta \geq \pi/2$ than that shown in Fig. 2-4. This effect is particularly true for small values of H and all values of B. In addition to this the introduction of a parasitic loop increases the average response of the antenna near the axial directions. This observation has also been reported by us elsewhere[6]. The parasitic loop can thus be utilized to shape the loop counterpoise antenna patterns in the regions near $\theta=0^{o}$ and also $\theta \geq 90^{o}$. We shall discuss this in more detail in a later section.

3.6 The Effects of Variation of the Parasitic Loop Parameters

In this section we discuss qualitatively the general effects of the variation of the parasitic loop parameters b, H and B on the parasitic loop counterpoise radiation patterns. Quantitative discussions of these effects will be given in later sections. The following observations are made from a general study of the numerical and experimental results.

The parameter b (or w) has been found to be quite critical. For $kb \ll 0.15$, (i. e. $w \ll 0.09\lambda$) the parasitic loop does not receive enough excitation to affect the pattern appreciably (Eq. 3.3). As kb is increased beyond 0.15, the amount of reduction in field response in directions $\theta \geq 90^{o}$ at first increases, but for $kb > 0.3$ the overall pattern becomes too much distorted as compared with Fig. 2-4.

It was mentioned in Section 3.5 that for small values of H the parasitic loop produces strong effects on the overall pattern. This is due to the fact that as H is increased the magnitude of the parasitic current $|I_{p_o}|$ decreases. A study of (3.23) - (3.27) reveals the fact that $|I_{p_o}|$ becomes maximum near $H \simeq h$, i. e. the parasitic loop lying near the plane of the Alford loop. With kb = 0.15 it has been found both theoretically and experimentally that for $H > 2\lambda$ the effect of the parasitic loop on the radiation pattern near the direction $\theta \geq 90^{o}$ is negligible.

The effects of the parameter B has been found to be quite strong whenever 2B is of the same order of some multiple of a wavelength. The position and amplitude of the minor lobes in the parasitic loop counterpoise antenna pattern near the axial region is found to depend in a complicated manner on both B and H.

3.7 Discussion

In the present chapter we have developed a theory for the radiation field produced by a parasitic loop counterpoise antenna. Within the range of approximation the theory has been found to agree satisfactorily with experimental results. It may thus be concluded that the theory can be used for theoretical investigation of the various radiating properties of the present antenna configuration as the different parameters are varied.

IV

RADIATION CHARACTERISTICS OF A SINGLE PARASITIC LOOP COUNTERPOISE ANTENNA

4.1 Introduction

In the present chapter we investigate in more detail various aspects of the radiation characteristics of a single parasitic loop counterpoise antenna. The parasitic loop counterpoise radiation patterns are compared with the pattern produced by the basic Alford loop above the counterpoise. The effects of the different parasitic loop parameters on the patterns are also discussed. The investigation is divided into two main parts. The first part presents and discusses the results of an experimental investigation of the radiation properties of the antenna as the parasitic loop parameters are varied. The second part gives the results obtained from numerical computation of the theoretical expressions given by Eqs. (3.37) - (3.40). These contain information about the amplitude and phase variation of the far field as functions of the different parameters of the parasitic loop.

4.2 Experimental Results

The experimental arrangement has been described in Section 3.3. The basic system was the Alford loop placed at a height 0.44λ above the 5.7λ diameter counterpoise as described in Sections 2.3 and 3.3. Two sets of parasitic loops having $w=0.0915\lambda$ and $w=0.183\lambda$ and variable B and H (Fig. 3-6) were used during the experiment. With the first type of parasitic elements ($w=0.0915\lambda$) the elevation patterns of the system were measured at 1080 MHz by varying the height H from 0.23λ to 1.88λ in steps of 0.18λ increments and the diameter 2B from 1.0λ to 5.0λ in 0.5λ increments. Similar measurements were carried out for the antenna with the second type of parasitic elements ($w=0.183\lambda$) with the corresponding variations of H from 0.46λ to 0.82λ and of 2B from 1.0λ to 5.0λ. All the measurements were carried out at 1080 MHz.

4.2.1 General Behavior of the Patterns

The radiation patterns obtained for single parasitic loop counterpoise antenna as a function of the parasitic loop parameters are presented in Figs. 4-1 and 4-2. Although the details are lost these figures may be found useful in ascertaining the general behavior of the patterns with the variation of H and B. Figures 4-1 and 4-2 should be compared with the pattern produced by the basic Alford loop counterpoise antenna as given in Fig. 2-4. It should be noted that the Alford loop is located at a

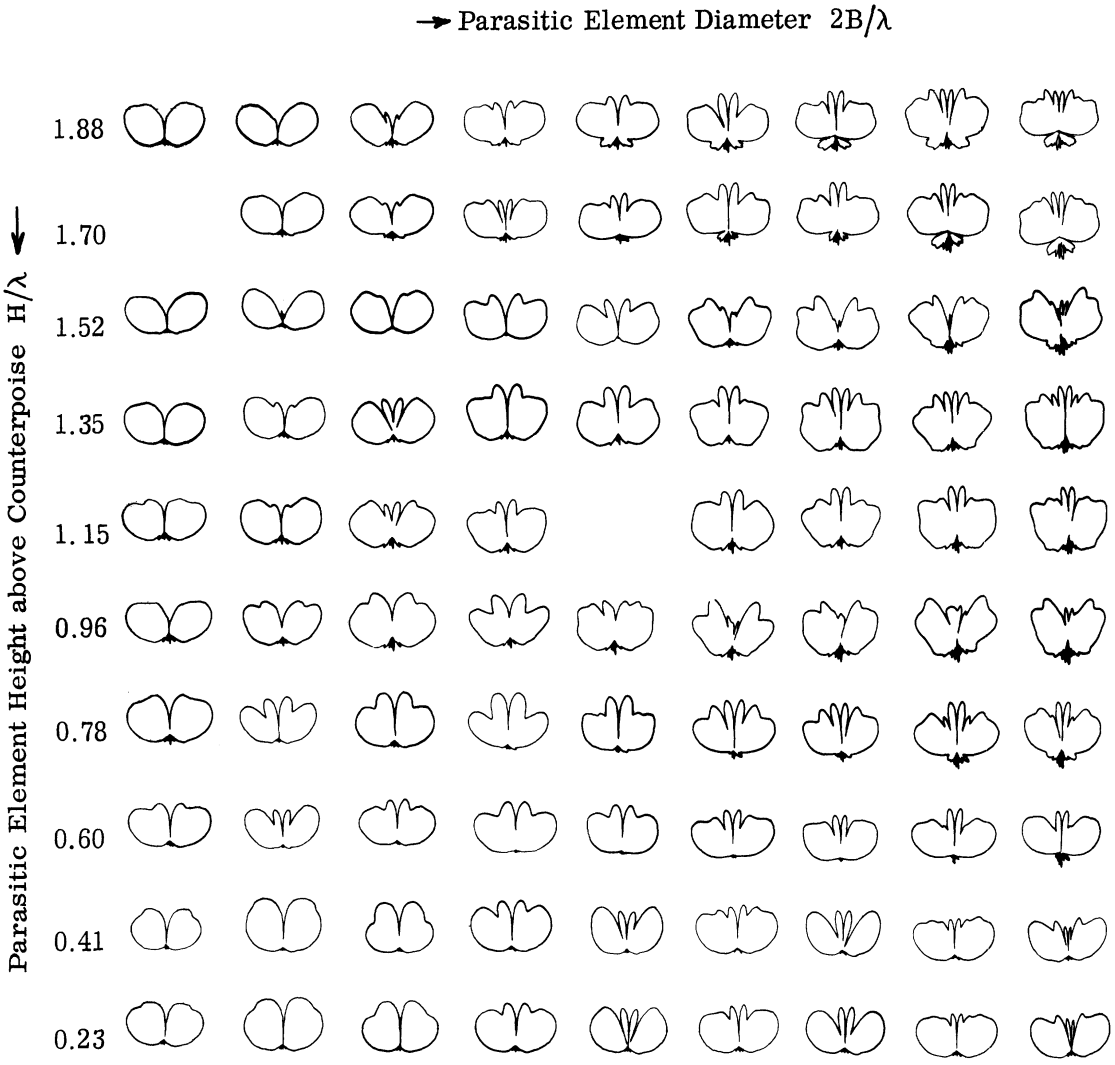

FIG. 4-1: MEASURED FAR FIELD ELEVATION PATTERNS OF SINGLE PARASITIC LOOP COUNTERPOISE ANTENNA. h=0.44λ, w=0.092λ, A=5.7λ, f=1080 MHz, 2B and H variable.

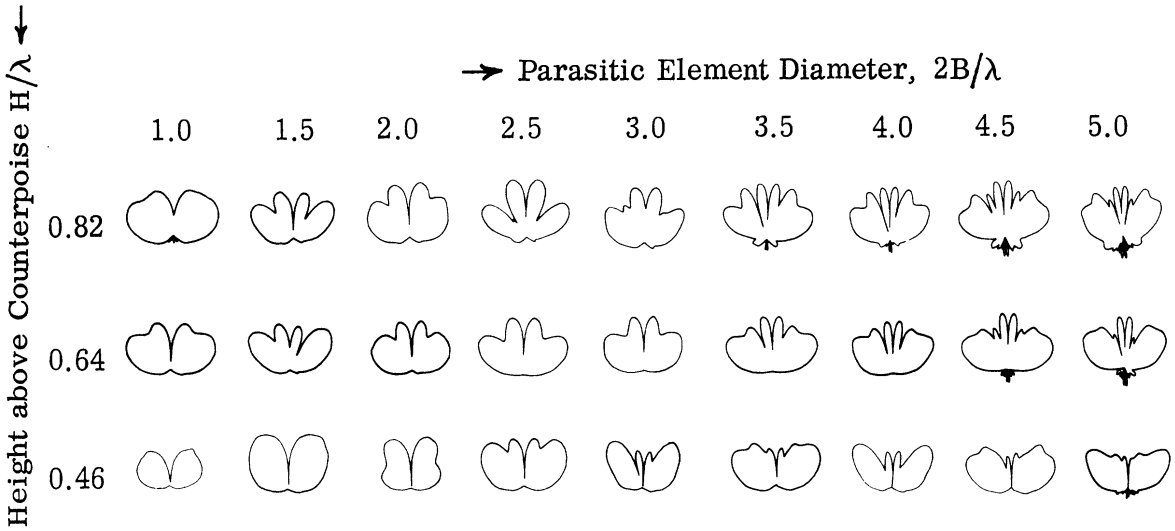

FIG. 4-2: MEASURED FAR FIELD ELEVATION PATTERNS OF SINGLE PARASITIC LOOP COUNTERPOISE ANTENNA. h=0.44λ, w=0.183λ, A=5.7λ, f=1080 MHz, 2B and H variable.

height h=0.44λ above the counterpoise. After comparing Figs. 4-1 and 4-2 with Fig. 2-4 it is found that in general the behavior of the pattern near the principal maximum is not altered appreciably due to the introduction of the parasitic loop. The principal maximum of the basic Alford loop counterpoise antenna is in the direction $\theta=55^{o}$ (Fig. 2-4). The direction of principal maximum in the pattern of the parasitic system varied between 50^{o} to 60^{o} over most of the range of variations of H and B shown in Figs. 4-1 and 4-2. The main effects of the parasitic loop are observed in the two regions of space. New lobes appear in the pattern in the region near $\theta=0^{o}$. The position of maximum of this lobe has been found to lie within 10^{o} to 20^{o} off the axial direction. In general the amplitude of this lobe has been found to be of the order of the main maximum but it may become larger than the main maximum for larger values of B. For large values of B there appeared more than two secondary maxima near the region $\theta=0^{o}$.

In the second region of space defined as $\theta \geq 90^{o}$ the general effects of the parasitic loop has been found to reduce the average level of response of the antenna, i. e. the counterpoise edge diffraction effects are reduced by the parasitic loop.

The above effects depend, in a complicated manner, on the parameters w, B and H, so that it is not possible to give any rule for the effects produced by the variation of these parameters. In the following sections we give a few quantitative observations obtained from more careful study of the experimental patterns.

4.2.2 A Few Observations

(1) For $H < 0.44\lambda$, i. e. when the parasitic loop lies below the Alford loop the direction of the principal maximum moves towards the direction $\theta = 0^{o}$, for values of 2B in the range $1 - 2\lambda$. This has been found more pronounced for the case $w=0.183\lambda$ where the principal maximum occurred near the direction $\theta=35^{o}$.

(2) For $H \leq 0.44\lambda$ and all the values of B the parasitic loop is found to be ineffective in modifying the pattern shape in the directions $\theta \geq 90^{o}$.

(3) For $H \sim 0.6\lambda$ the parasitic loop is found to be most effective in reducing the field in directions $\theta \geq 90^{o}$. This effect has been observed for all values of B. The amount of reduction is found to increase with increasing w. For example the maximum field reduction in the direction $\theta=90^{o}$ is found to be about 24 db for $H=0.64\lambda$, $2B=2.5\lambda$ and $w=0.183\lambda$ and 20 db for $H \simeq 0.6\lambda$, $2B=2.5\lambda$ and $w=0.092\lambda$. For the basic system this factor was 10.3 db.

(4) The effect of the generation of the secondary maxima near $\theta=0^{o}$ and the reduction of field in directions $\theta \geq 90^{o}$ increase with increasing w. This can be seen from the typical patterns shown in Fig. 4-3

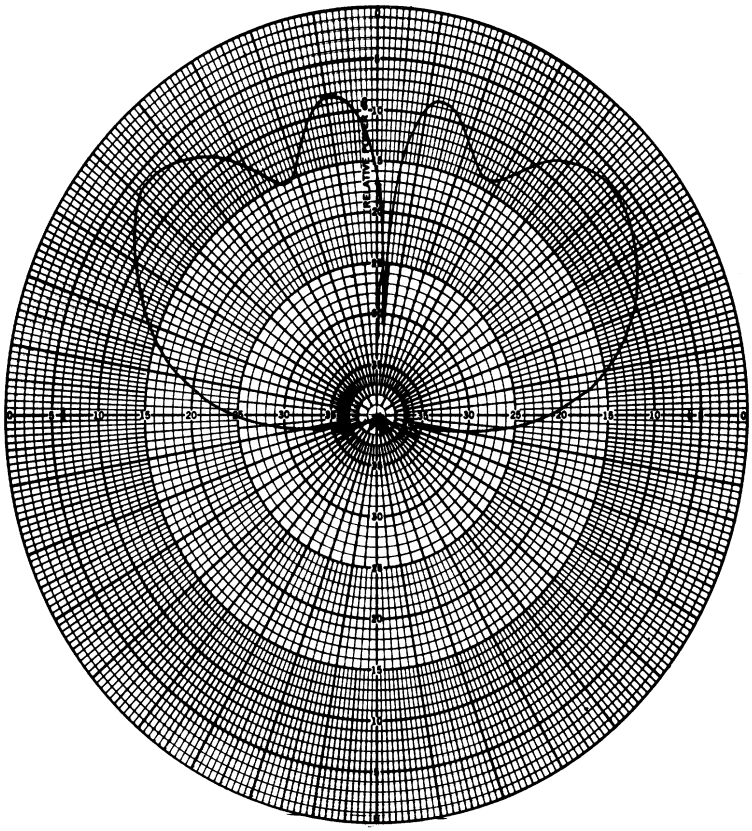

(a) w=1", H= 6.5"

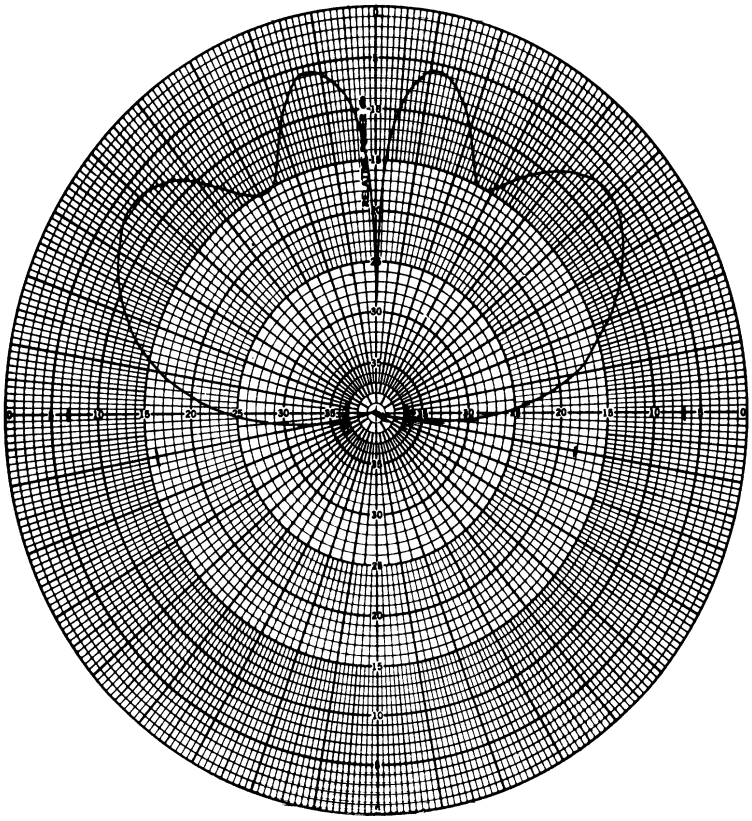

(b) w=2", H=7"

FIG. 4-3: MEASURED FAR FIELD ELEVATION PATTERNS SHOWING EFFECTS OF PARAMETER w. h=4.8", A=5'2", f=1080 MHz.

(5) The gradient of the field at the horizon is not much improved for small values of H. The improvement is found to take place for longer values of H and B. This is because for these values of H and B there appears a minimum in the pattern a few degrees below the direction $\theta=90^{o}$. With a single parasitic loop system the best theoretical field gradient obtained was 8.4 db/6^{o} with the system shown in Fig. 3-10.

4.3 Numerical Results

In this section we discuss the theoretical behavior of the patterns produced by the parasitic loop counterpoise antenna system in the region below the horizon defined as $90^{o} \leq \theta \leq 120^{o}$. The reason for choosing this region of space is that it is in this region the existing VOR antenna patterns need to be improved. The experimental investigation discussed above indicated that for largers values of H and B the parasitic loop can improve the horizontal field gradient considerably. The pattern behavior is discussed for the parasitic loop counterpoise system having kb=0.15, and $kH > 10.00$ and $kB \geq 3\pi$. As discussed in Section 3.4 within this range of parameters the theory predicts the pattern with satisfactory accuracy. The results discussed below have been obtained by numerically computing Eq. (3.36) without the term $S^{p}_{34}(\theta)$. In the sections below the following notations are used to represent the various pattern functions.

$S^{A}(\theta)$ = complex far field pattern produced by the basic Alford loop above the counterpoise,

$S(\theta)=S^{A}(\theta)+S^{p}_{12}(\theta)+S^{p}_{56}(\theta)$ = complex far field pattern produced by the parasitic loop counterpoise antenna,

$S^{p}(\theta)=S^{p}_{12}(\theta)+S^{p}_{56}(\theta)$ = complex far field pattern produced by the parasitic loop only above the counterpoise,

α_{g} = field gradient at the horizon = $-20 \log_{10} \left| \frac{E_{\phi}(96^{o})}{E_{\phi}(90^{o})} \right|$,

α_{F} = field reduction at the horizon = $-20 \log_{10} \left| \frac{E_{\phi}(90^{o})}{E_{\phi}(\theta_{max})} \right|$.

4.3.1 Field Gradient Characteristics

As mentioned in Section 2.6.2 the field gradient at the horizon obtained from the basic Alford loop counterpoise antenna is 3.09 db. Experimental results discussed in Section 4.2 and numerical investigations indicate that for small values of H (i.e. $H < 1.5\lambda$) although the parasitic loop considerably reduces the response of the parasitic loop antenna in the directions $\theta \geq 90^{o}$, it only improves slightly (1 or 2 db) the

field gradient compared to that obtained in the basic system. Usually α_g takes on large values whenever B is some multiple of λ. This can be seen from Fig. 4-4 which shows the theoretical variation of α_g as a function of kH with kB as the parameter. It is found that significant improvement in the field gradient can be obtained only for some specific values of B and H. Within the ranges of variables shown in Fig. 4-4 a parasitic loop with $kB=3\pi$ and kH=11.7 is found to be the optimum and it yields a maximum value of α_g=8.43 db. This is confirmed by the experimental pattern shown in Fig. 3-10, which is also found to be the optimum pattern from this point of view. The curves given in Fig. 4-4 can thus be used to obtain the best field gradient characteristics from a single parasitic loop counterpoise system.

4.3.2 Pattern Behavior Near the Horizon

The behavior of the parasitic loop counterpoise antenna radiation pattern in the region near and below the horizon ($90^o \leq \theta \leq 120^o$) is shown in Figs. 4-5a - 4-5c for various values of B and H. The range of values of B and H are chosen to be the same as considered in Section 4.3.1 so that direct comparison of results may be possible. It is found that for each value of kB considered a minimum in the pattern appears in $|S(\theta)|$ for some value of kH. As kH is increased the position of this minimum moves towards the horizontal direction; at the same time the amplitude of the minimum assumes a largest value for some intermediate value of kH. On comparing Figs. 4-4 and 4-5a-c, it can be seen that an optimum parasitic system producing the best field gradient may not necessarily yield the deepest minimum in the far field pattern below the horizon. Using the curves given in Figs. 4-4 and 4-5a-c, a best compromise can be made under a given practical situation.

4.3.3 Parasitic Field Near the Horizon

In a practical situation it may be desirable to control the position and amplitude of the minimum in $|S(\theta)|$ below the horizon. For the system considered here this can be done, in principle, by adjusting the phase of the parasitic field $S^P(\theta)$ to be 180^o out of phase from that of $S^A(\theta)$. The variation of the amplitude and phase of $S^A(\theta)$ has been discussed in Section 2.6.1. In this section the behavior of the complex field $S^P(\theta)$ near the horizon is discussed. Figure 4-6 shows the complex parasitic field $S^P(\theta)$= Re $S^P(\theta)$+ i Im $S^P(\theta)$ as a function of H for some selected values of θ below the horizon. Note that the curves in Fig. 4-6 are given for constant B and that the values of kH are marked on the individual curves. It is important to note that the phase of the parasitic field, as shown here, lies in the fourth quadrant. These curves combined with those given in Fig. 2-7 may be found convenient in the design of single parasitic counterpoise antennas having a required field characteristic near the horizon.

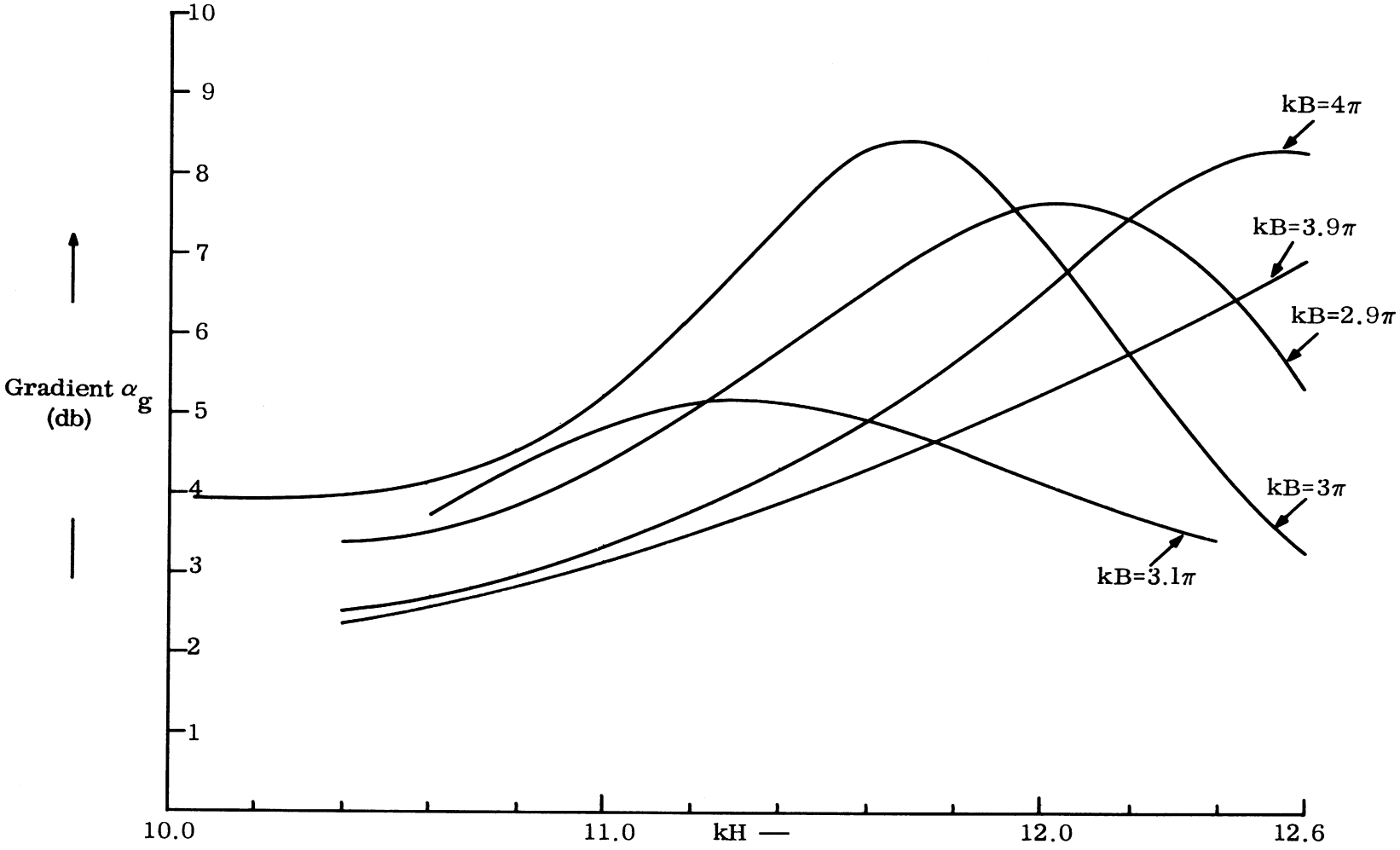

FIG. 4-4: THEORETICAL FIELD GRADIENT NEAR HORIZON OF SINGLE PARASITIC LOOP COUNTERPOISE ANTENNA ELEVATION PATTERN. kh=2.75, kA=17.92, kb=0.15, kB and kH variable.

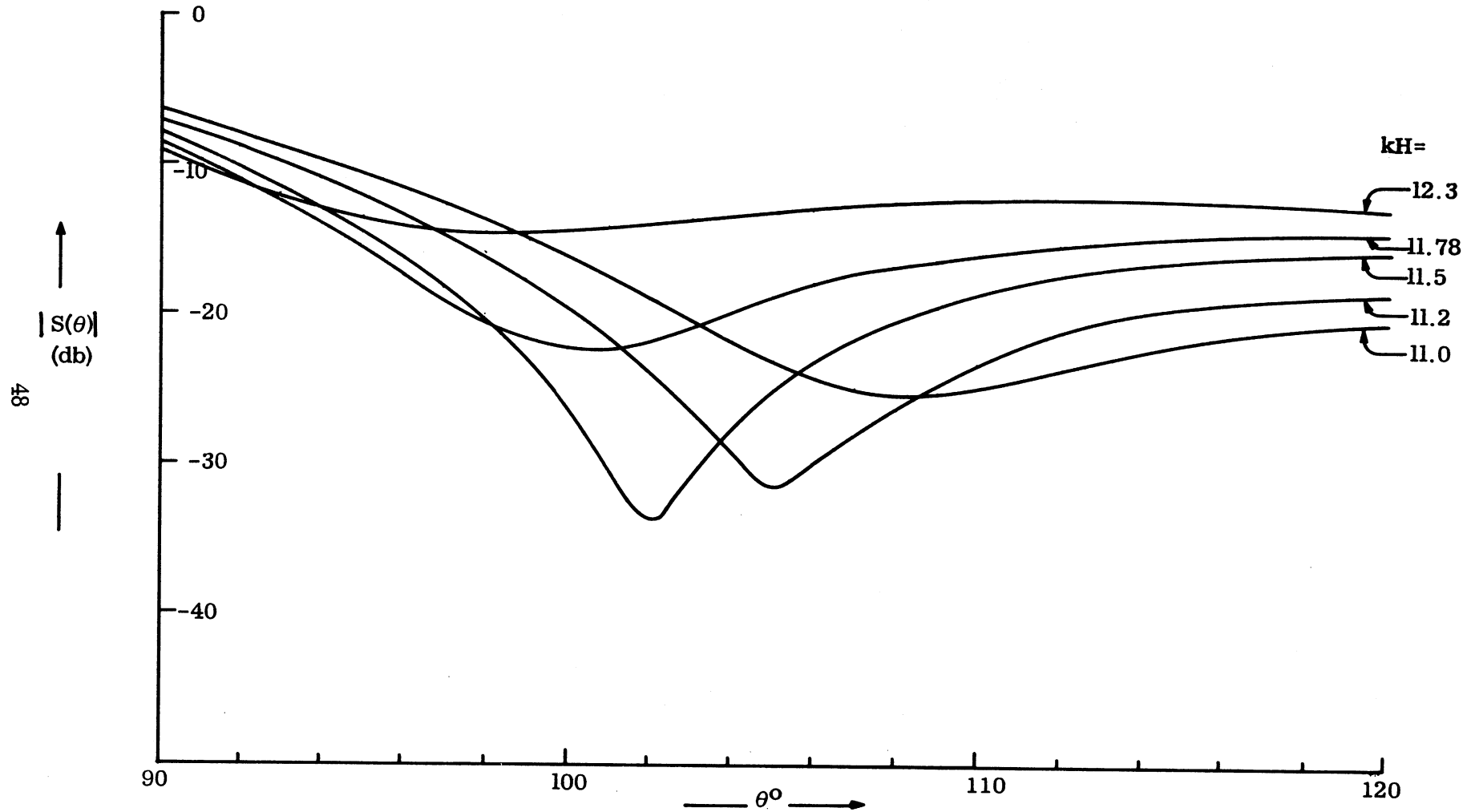

FIG. 4-5a: THEORETICAL VARIATION OF PARASITIC LOOP COUNTERPOISE ANTENNA ELEVATION PATTERN $|S(\theta)|$ BELOW HORIZON. kh=2.75, kA=17.92, kb=0.15, kB=3π, kH variable.

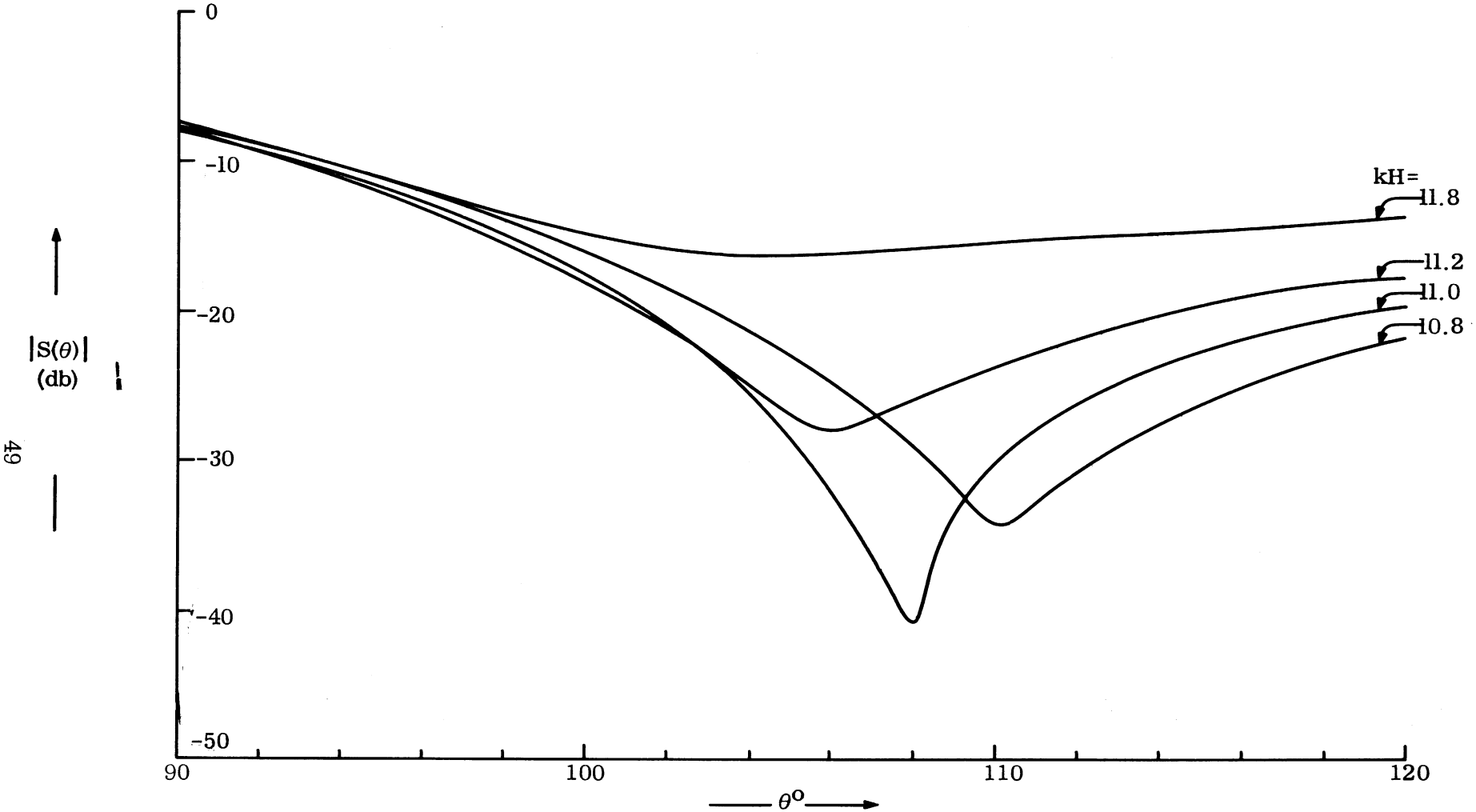

FIG. 4-5b: THEORETICAL VARIATION OF PARASITIC LOOP COUNTERPOISE ANTENN ELEVATION PATTERN $|S(\theta)|$ BELOW HORIZON. kh=2.75, kA=17.92, kb=0.15, kB=3.1π, kH variable.

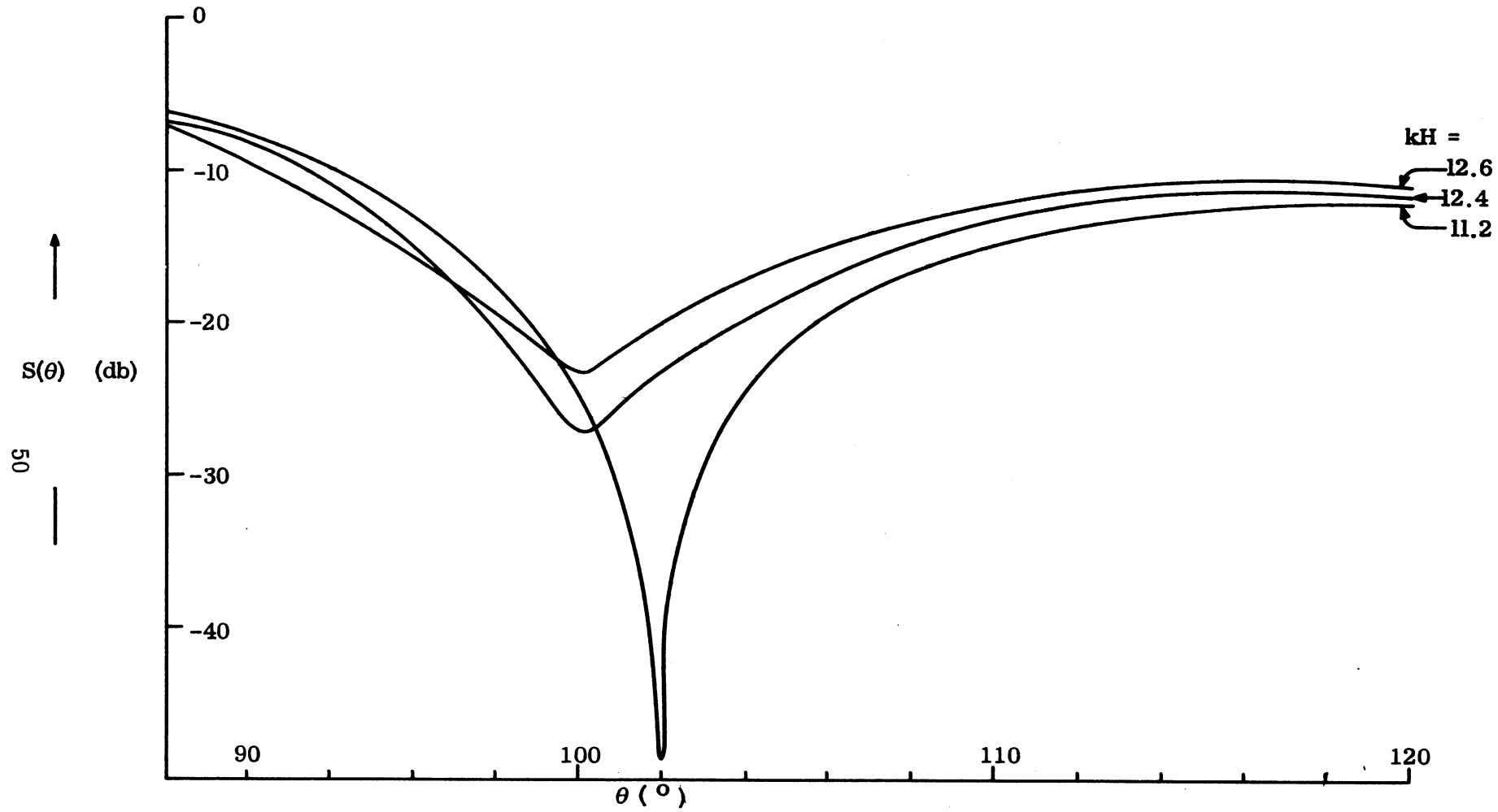

FIG. 4-5c: THEORETICAL VARIATION OF PARASITIC LOOP COUNTERPOISE ANTENNA ELEVATION PATTERN $S(\theta)$ BELOW HORIZON. kh=2.75, kA=17.92, kb=0.15, kB=4π, kH variable.

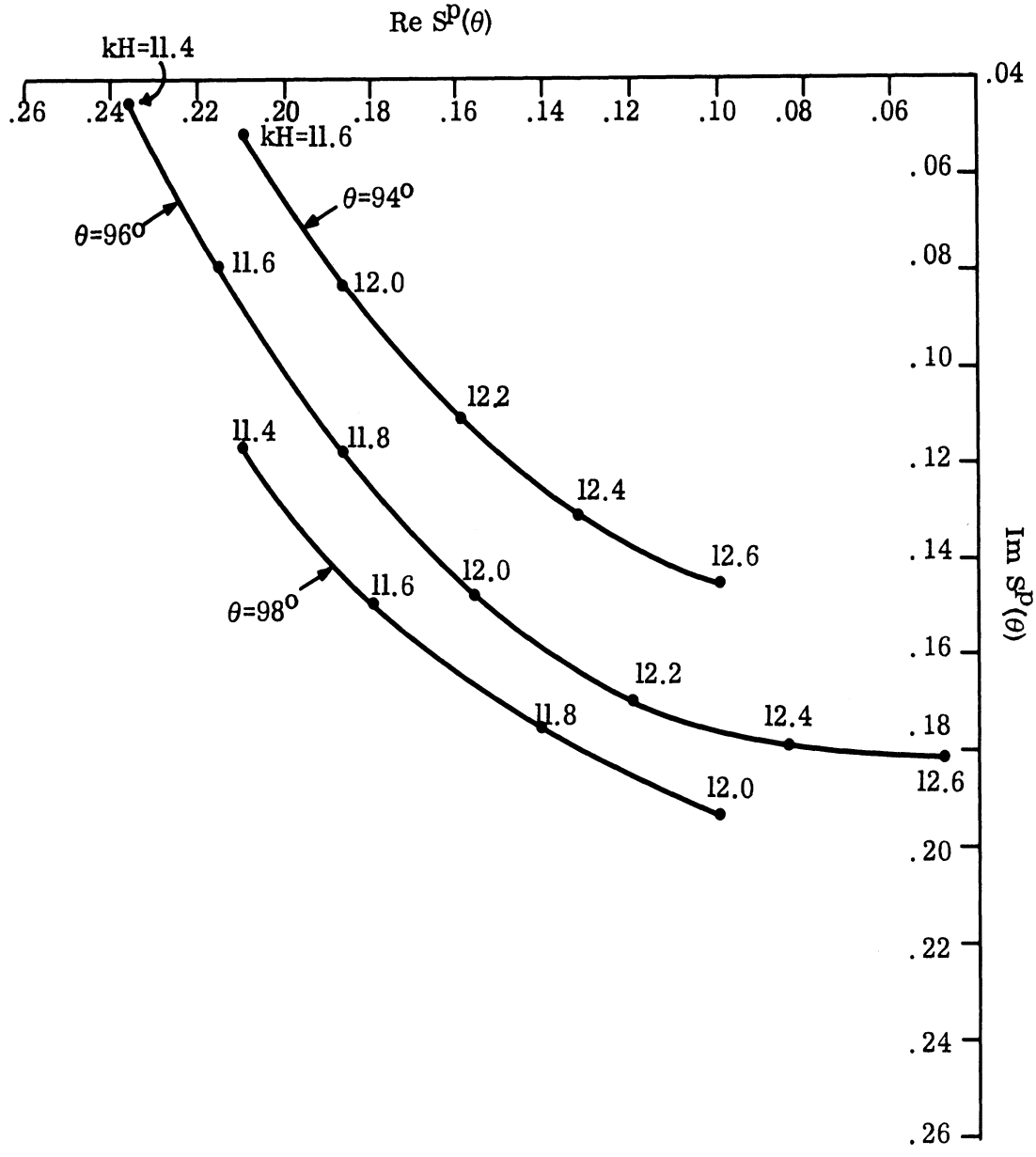

FIG. 4-6: THEORETICAL VARIATION OF PARASITIC FAR FIELD $S^p(\theta)$ BELOW HORIZON. kh=2.75, kA=17.92, kB=3π, kb=0.15.

4.3.4 Far Field of the Parasitic System Near the Horizon

As discussed in the previous sections, a parasitic loop counterpoise antenna with $H \sim 0.6\lambda$ and $B \geq 1.5\lambda$ reduces the overall response of the antenna in directions $\theta \geq 90^{o}$. However, the field gradient characteristics of such an antenna is not much superior to that of the basic Alford loop counterpoise antenna. As will be discussed later, it may be necessary to use such a single parasitic loop system as the basic antenna and to use another parasitic loop above it so that the pattern produced by the complete system will yield a very large value of α_g. For this purpose it would be convenient to have information about $S(\theta)$ near the horizon. Figures 4-7a - d show the variation of $-S(\theta)$ as functions of kB and kH for selected values of θ below the horizon. Each curve is for a constant kH and the variable kB values are marked on each. Note that the curves show the negative of $S(\theta)$, the reason for doing this will be discussed later. It is interesting to note the regions A and B of Fig. 4-7c for $\theta=96^{o}$. It can be seen that in these two regions $S(\theta)$ is insensitive to small variations in B and H. Thus an antenna system designed to operate in this region will not change its field characteristics near the horizon for small changes in B and H. This observation may be found convenient in some practical situations. The curve $S_2^p(96^{o})$ shown in Fig. 4-7c is superposed here for future reference and will be discussed in a later section.

4.3.5 Some Useful Results

In this section a few useful quantities pertaining to the radiation pattern produced by a single parasitic loop counterpoise antenna are given in tabular form in Table IV-1. These tables are meant to provide quick estimates of the variation of the various quantities as the parasitic loop parameters are changed. The variation of the following quantities will be tabulated:

θ_o = the direction of the principal maximum,

α_F = the field reduction factor,

α_g = the field gradient/6^{o} at the horizon in db,

ρ = the field ratio = $20 \log_{10} \left| \frac{E(100^{o})}{E(90^{o})} \right|$,

θ_{01} = the directions of the maximum of the minor lobes near the region $\theta=0^{o}$,

α_{01} = the minor lobe amplitude relative to the maxima at $\theta=\theta_o$, in db,

$E(\theta_o)$ = amplitude of the field in the direction $\theta=\theta_o$, in db .

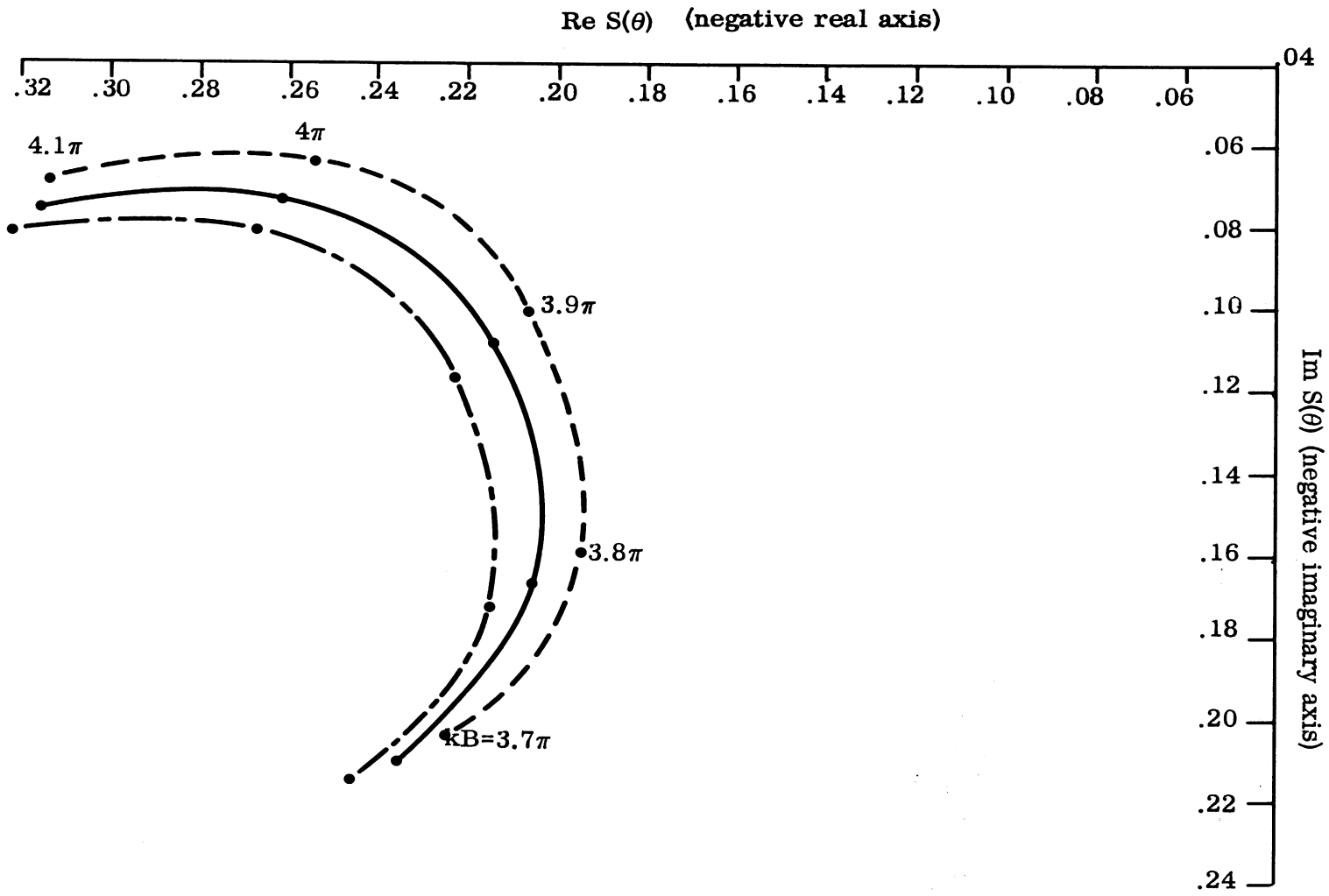

FIG. 4-7a: THEORETICAL FAR FIELD S(θ) OF PARASITIC LOOP COUNTERPOISE ANTENNA IN DIRECTION θ=92°. kh=2.75, kA=17.92, kb=0.15 (--)kH=3.8, (—)kH=3.7)(———)kH=3.6.

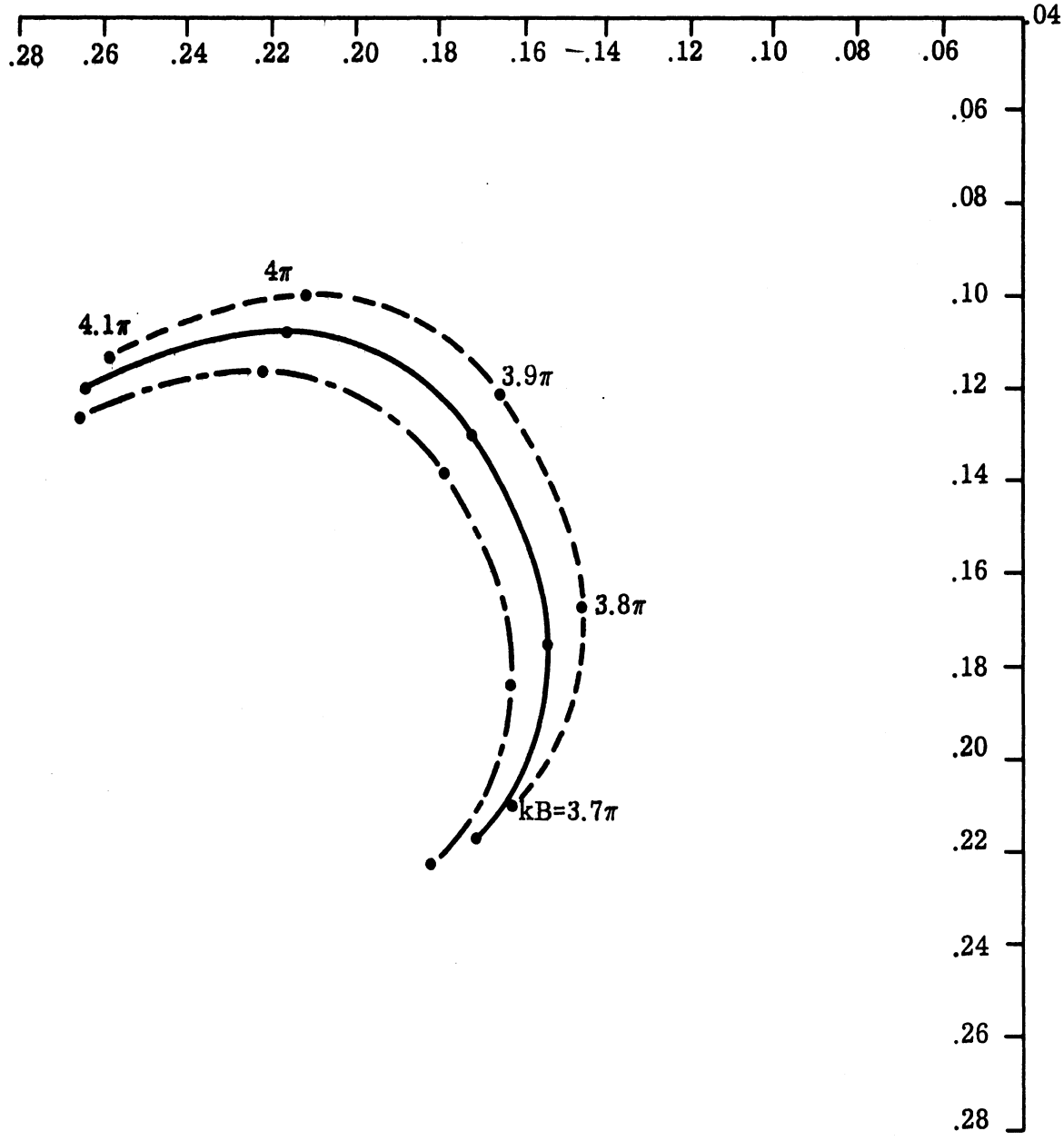

FIG. 4-7b: THEORETICAL FAR FIELD S(θ) OF PARASITIC LOOP COUNTERPOISE ANTENN IN DIRECTION θ=94°. kh=2.75, kA=17.92, kb=0.15 (- -)kH=3.8 (—)kH=3.7 (— - —)kH=3.6.

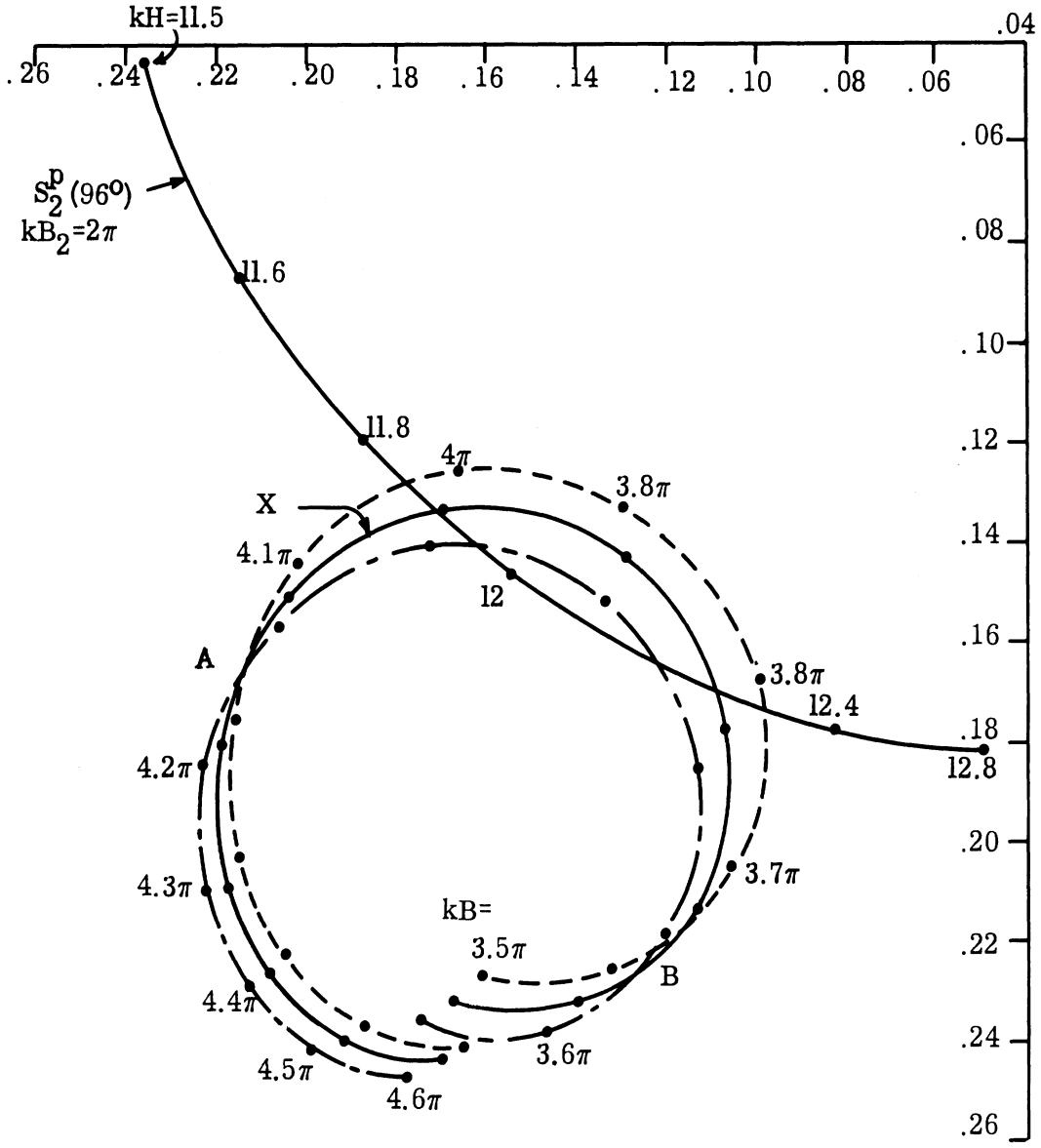

FIG. 4-7c: THEORETICAL FAR FIELD $S(\theta)$ OF PARASITIC LOOP COUNTERPOISE ANTENNA IN DIRECTION $\theta=90^o$. kh=2.75, kA=17.92, kb=0.15, (---)kH=3.8, (—)kH=3.7, (— - —)kH=3.6.

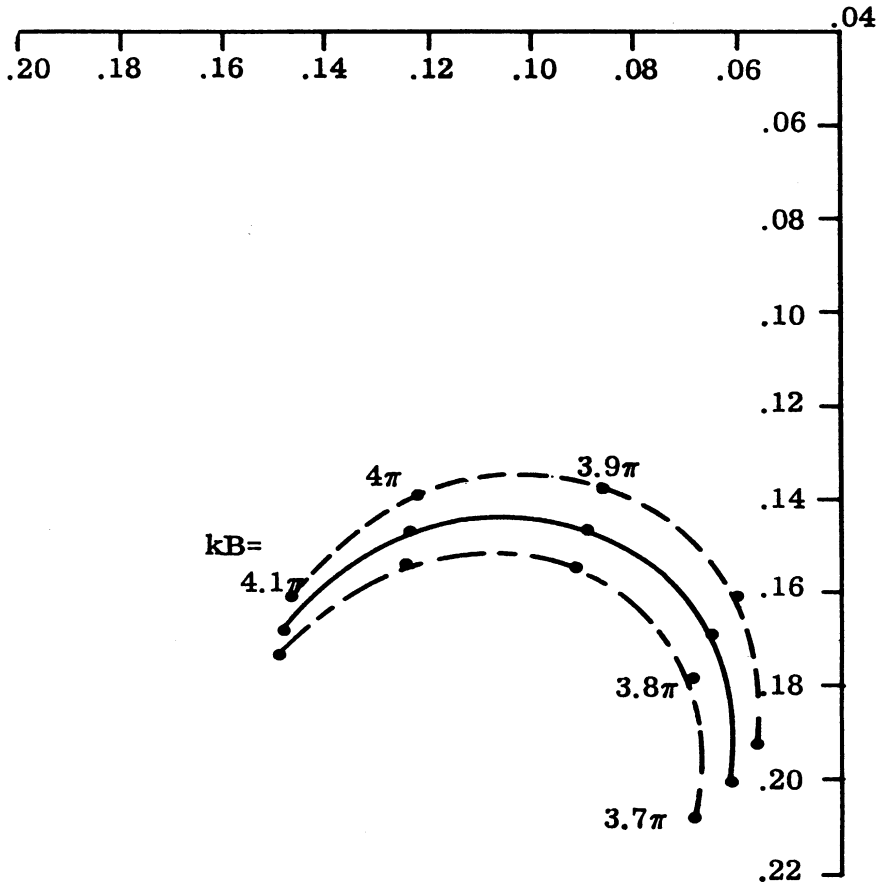

FIG. 4-7d: THEORETICAL FAR FIELD $S(\theta)$ OF PARASITIC LOOP COUNTERPOISE ANTENNA IN DIRECTION $\theta=98^{o}$. kh=2.75, kA=17.92, kb=0.15, (--)kH=3.8), (—)kH=3. 7, (— — —)kH=3.6

4.4 Discussion

The results given here indicate that a single parasitic loop placed suitably above an Alford loop counterpoise antenna is capable of improving the field characteristics of such an antenna in the region below the horizon. The field pattern near the principal maximum direction is not altered much. Near the region $\theta=0^{o}$ the antenna response increases considerably and new lobes appear in the pattern. Numerical results given here should be found useful for the purpose of shaping the radiation pattern of an Alford loop counterpoise antenna with the help of one or more parasitic loops.

TABLE IV-1: RADIATION PATTERN CHARACTERISTICS OF A SINGLE PARASITIC LOOP COUNTERPOISE ANTENNA

(a):kh=2.73, kH=4.00, kb=0.15, kA=17.92, kB is variable

kB (π)	θ_o (^{o})	$E(\theta_o)$	α_F	α_g	θ_{01} (^{o})	α_{01}	ρ
2.50	55	5.87	15.31	3.97	15	-3.38	-6.37
2.75	50	4.80	19.46	3.65	10	-0.93	-6.29
3.00	45	3.33	14.74	3.53	10	+1.58	-5.87
3.25	60	5.15	12.55	3.89	10	-1.98	-6.51
3.50	55	5.83	13.64	3.85	10	-4.84	-6.51
3.75	55	5.74	16.60	3.58	10	-3.73	-6.21
4.00	50	5.08	16.14	3.01	10	-2.55	-5.31
4.25	60	4.18	11.52	3.71	10	-3.07	-6.24
4.50	60	5.42	12.49	3.74	5	-5.33	-6.33
4.75	55	6.19	15.27	3.56	5	-5.90	-6.21
5.00	50	5.70	15.62	2.95	5	-2.88	-5.10

(b): kh=2.75, kH=4.00, kb=0.287, kA=17.92, kB is variable

2.50	55	5.95	15.13	4.05	15	-2.17	-6.85
2.75	50	4.84	17.72	3.62	10	+0.34	-6.28
3.00	45	3.58	19.20	3.37	10	+3.27	-5.89
3.25	60	4.82	12.70	3.99	10	+0.57	-6.69
3.50	55	5.76	13.18	3.83	10	-3.09	-6.48
3.75	50	5.68	15.17	3.53	10	-1.80	-6.14
4.00	50	5.41	18.78	2.55	10	-0.71	-4.65
4.25	50	3.80	11.57	3.69	10	-0.77	-6.19
4.50	60	5.23	11.98	3.68	5	-4.03	-6.24
4.75	55	6.20	14.26	3.53	5	-2.45	-6.18
5.00	50	6.15	17.20	2.56	5	-1.30	-4.89

TABLE IV-1 (continued

(c): kh=2.75, kb=0.15, kB=3π, kA=17.92, Kh is variable

kH	θ_o (^{o})	$E(\theta_o)$	α_F	α_g	θ_{01} (^{o})	α_{01}	ρ
10.63	50	3.67	8.81	3.94	10	-3.70	-6.89
10.90	50	3.83	9.96	4.83	10	-2.93	-8.69
11.20	50	3.98	11.20	6.26	10	-2.86	-12.30
11.50	50	4.11	12.30	7.92	10	-3.52	-17.95
11.78	50	4.18	13.00	8.40	10	-4.75	-13.52
12.00	50	4.21	13.29	7.29	15	-6.15	-8.91
12.30	50	4.20	13.27	5.07	15	-7.99	-5.30
12.50	50	4.16	14.05	3.80	20	-9.18	-3.77

The corresponding quantities for the basic Alford loop counterpoise antenna are:

kh=2.75, kA=17.92, $\theta_o=55^o.3$, $E(\theta_o)=+4.59$, $\alpha_F=10.38$, $\alpha_g=3.09$, $\rho=-5.15$.

V

INVESTIGATION OF A DOUBLE PARASITIC LOOP COUNTERPOISE ANTENNA

5.1 Introduction

From the results discussed in the previous chapters it is found that a single parasitic loop counterpoise antenna is capable of producing good field gradient characteristics near the horizon while maintaining the characteristics in the regions near the principal maximum similar to those of an Alford loop counterpoise antenna. The largest value of α_g obtained for such an optimum system was found to be 8.4 db. It is conceivable that by using another parasitic system it may be possible to obtain larger values of α_g. In the present chapter we investigate the feasibility of using two parasitic loops in conjunction with the basic Alford loop counterpoise antenna in order to achieve better field gradient characteristics.

5.2 Double Parasitic Loop Counterpoise System

A double-parasitic loop counterpoise antenna system is shown in Fig. 5-1. It consists of two parasitic loops placed parallel to each other and to the plane of the counterpoise. Sometime this will be referred to as a colinear system in contrast to the coplanar system where the parasitic loops are placed in the same plane. It is assumed that the two parasitic loops have the same b (or w in the experimental model). Additional control may be obtained by using different values of b. The principle of the design is to choose the parameters H_1, B_1 and H_2, B_2 such that the combined field produced by the parasitic loops in a certain direction below the horizon be such that when it is superposed with the Alford loop field in that a direction a deep minimum is produced in the pattern. The choice of the H_1, B_1 and H_2, B_2 may be facilitated by using the results of the previous chapter.

5.3 Theoretical Expression for the Radiation Field

If the distance between the two parasitic loops are small, then the mutual coupling effects between them must be taken into account and the theoretical analysis of the radiation field becomes complicated. However, after studying the phase of the parasitic field (arg $S^p(\theta)$) below the horizon (as discussed before), it is found that the phase of the parasitic field in this region opposes that of the basic Alford loop field for values of H near 0.6λ and 2λ. It is thus anticipated that for the present purpose the two parasitic loops should be separated by a distance at least of the order of λ or more. In such cases the mutual effects may be neglected. In a coplanar parasitic loop system mutual coupling effects may be neglected if $B_2 - B_1 \gtrsim \lambda$.

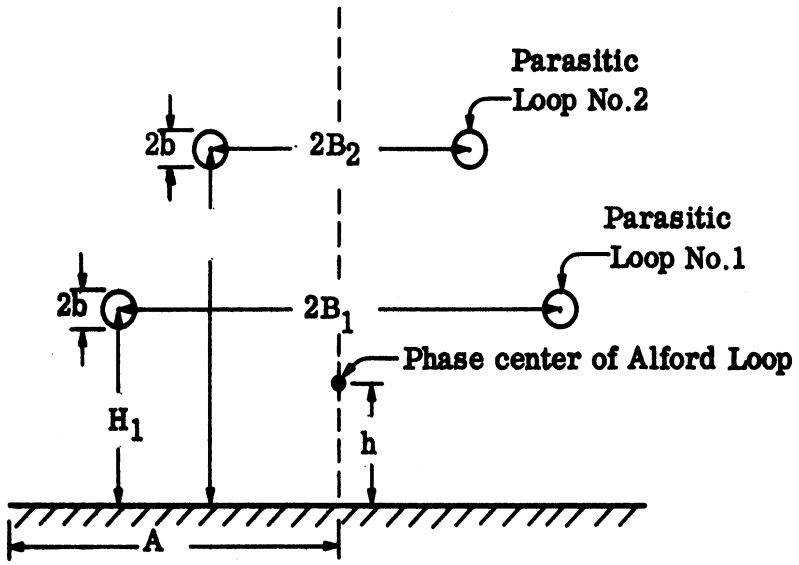

FIG. 5-1: DIAGRAM OF DOUBLE PARASITIC LOOP COUNTERPOISE ANTENNA.

In the absence of mutual coupling between the parasitic loops the theoretical expression for the radiation field produced by a double-parasitic loop system can be obtained by a simple modification of the theory given in Section 3.2 for the single parasitic loop system.

Thus the far field produced by the system consisting of the Alford loop, the parasitic loop No. 1 and the counterpoise can be written as

$$E_{\phi_1} = \eta_o I_o \left(\frac{ka}{2}\right)^2 \frac{e^{i(kR-\pi/4)}}{R} S_1(\theta) , \tag{5.1}$$

where

$$S_1(\theta) = S^A(\theta) + S^p_{12}(\theta) + S^p_{34}(\theta) + S^p_{56}(\theta) \tag{5.2}$$

and all the other notations are as explained in Section 3.2.6. All the parameters involved in the detailed expressions of (5.2) (see Eqs. 3.37 - 3.40) should pertain to the parasitic loop No. 1.

Similarly, the far field produced by the parasitic loop No. 2 only above the counterpoise can be written as

$$E_{\phi_2} = \eta_o I_o \left(\frac{ka}{2}\right)^2 \frac{e^{i(kR-\pi/4)}}{R} S^p_2(\theta) , \tag{5.3}$$

where

$$S^p_2(\theta) = S^{p'}_{12}(\theta) + S^{p'}_{34}(\theta) + S^{p'}_{56}(\theta) . \tag{5.4}$$

In (5.4) the terms on the right hand side are given by (3.38) - (3.40) with the understanding that the different parameters involved pertain to the parasitic loop No. 2. Thus the far field produced by the double-parasitic loop counterpoise system in the range $0 < \theta < \pi$ is given by the following expression:

$$E_\phi = \eta_o I_o \left(\frac{ka}{2}\right)^2 \frac{e^{i(kR-\pi/4)}}{R} \left[S_1(\theta) + S^p_2(\theta)\right] . \tag{5.5}$$

The approximations involved in (5.5) are same as discussed in Section 3.2.6. Thus, $S_1(\theta) + S_2(\theta)$ gives the complex far field of the double parasitic loop counterpoise antenna.

5.4 An Example

In the present section we outline the method of designing a double-parasitic loop counterpoise antenna so that there may be a deep null in the radiation pattern in a direction $\theta = 96^o$. Let us choose the normalized height of the first parasitic

loop to be $kH_1=3.70$. This particular value of H is chosen because a single parasitic loop system with this value of H yields maximum field reduction factor α_{F_1}. The negative of the complex far field $S_1(\theta)$ in the direction $\theta=96^o$ as a function of kB_1 is then given by the curve marked with a cross in Fig. 4-7c. In the same figure we have also given $S_2^p(\theta)$ for $\theta=96^o$ as a function of kH_2 for the second parasitic loop with $kB_2=3\pi$. The points of intersection of the curves $S(96^o)$ and $S_2^p(96^o)$ in Fig. 4-7c will give the undetermined parameters kB_1 and kH_2. It is thus anticipated from Fig. 4-7c that for $kB_1=4\pi$, $kH_1=3.70$ and $kB_2=3\pi$, $kH_2=11.9$ a sharp minimum will be produced in the pattern in the direction $\theta=96^o$. The complete far field pattern produced by the system may be obtained from Eq. (5.5). The measured elevation pattern produced by such an antenna is shown in Fig. 5-2. The theoretical points obtained by numerical computation of Eq. (5.5) are also shown in Fig. 5-2 in the range $0<\theta<\pi$. The agreement between the two may be considered to be satisfactory.

5.5 Optimum Double-Parasitic Loop Counterpoise Antenna

In the example given above and with reference to Fig. 4-7c, it can be seen that for the particular parameters chosen $S_1(\theta)$ and $S_2^p(\theta)$ do not completely cancel each other in the direction $\theta=96^o$. It may thus be possible to obtain a larger value of α_g from the antenna by slight adjustments of the parameters H_1, B_1 and H_2, B_2. This was done experimentally as follows. The parameters B_1 and H_1 were fixed at $kB_1=4\pi$, $kH_1=3.70$. Then H_2 and B_2 were adjusted slightly and for each setting of H_2, B_2 a complete pattern of the system was measured. During this adjustment it was found that the setting of the parameter H_2 was more critical. In this way an optimum system was obtained which yielded the maximum value α_g. The optimum pattern obtained is shown in Fig. 5-3. The field gradient obtained is $21\,db/5^o.5$ and the field reduction factor $\alpha_F=23\,db$.

In order to observe the effects of the parameter w on the pattern a parasitic system was fabricated with strips of $w_1=w_2=0.183\lambda$ (i.e. $kb_1=kh_2=0.3$) and the system pattern was optimized experimentally by adjusting the parameters. The measured elevation pattern of this second optimum double-parasitic loop counterpoise antenna is shown in Fig. 5-4. This pattern has $\alpha_g=12\,db$ and $\alpha_F=16\,db$. On comparing Figs. 5-3 and 5-4 it is found that the field gradient is better in the former but the response of the antenna beyond the minimum below the horizon is much less in the second antenna. This may be found useful in some practical situations.

The basic principle by which high field gradient is obtained is the cancellation of the Alford loop counterpoise field in a certain direction by the parasitic fields in that direction. It is therefore anticipated that the performance of any optimum system thus designed will be highly frequency sensitive. The radiation pattern produced by the first optimum antenna system was measured over the frequency range

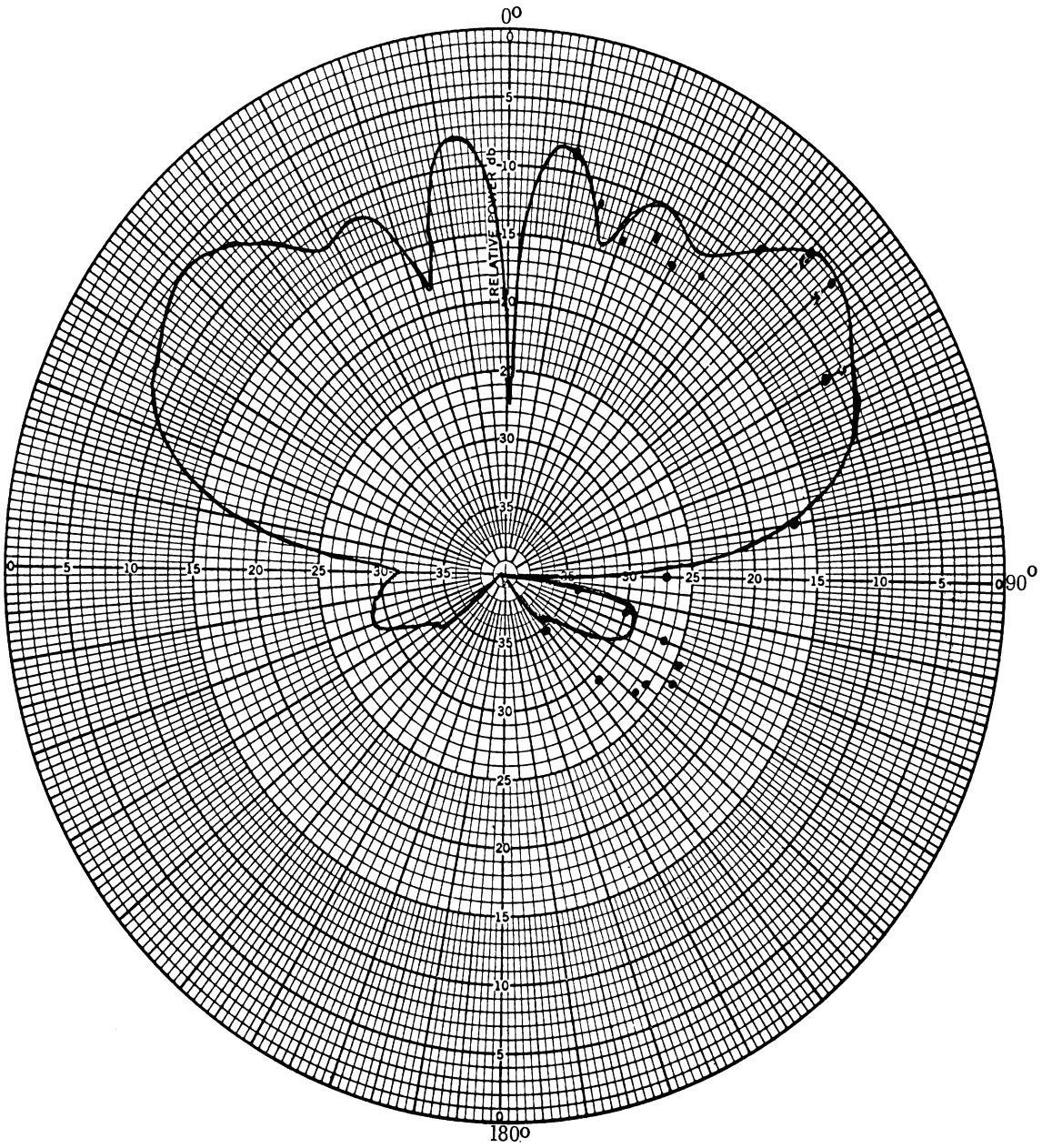

FIG. 5-2: FAR FIELD ELEVATION PATTERN PRODUCED BY DOUBLE PARASITIC LOOP COUNTERPOISE ANTENNA. $kh=2.75$, $kH_1=3.70$, $kB_1=4\pi$, $kH_2=11.78$, $kB_2=0.15$, f=1080 MHz. (—) Experimental (• •) Theoretical

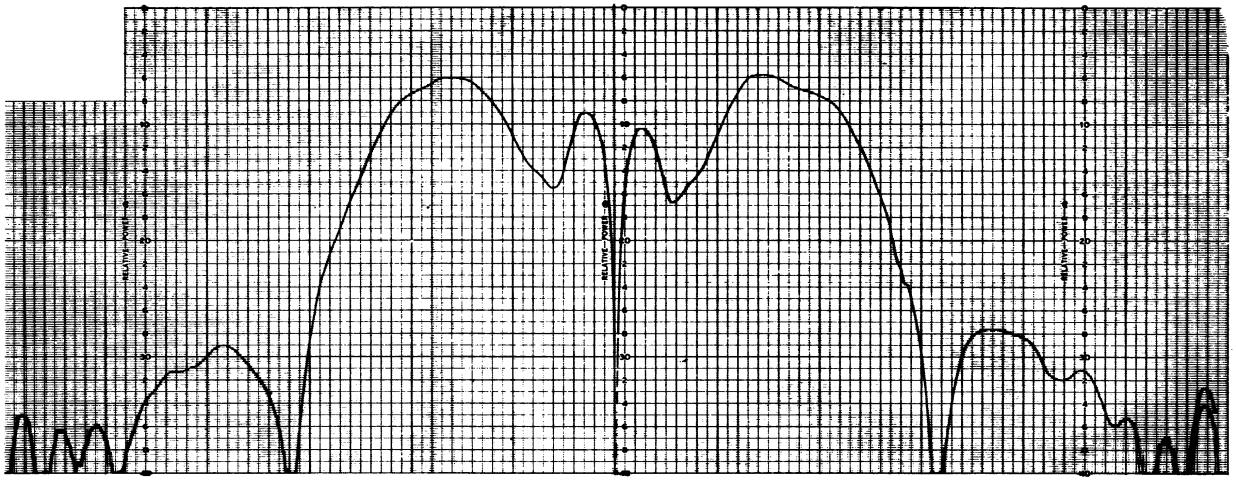

FIG. 5-3: MEASURED FAR FIELD ELEVATION PATTERN OF OPTIMUM DOUBLE PARASITIC LOOP COUNTERPOISE ANTENNA. kh=2.75, kA=17.92, kb_1=0.15, $kB_1=4\pi$, kH_1=3.7, kb_2=0.15, kB_2=10.27, kH_2=10.63, f=1080 MHz.

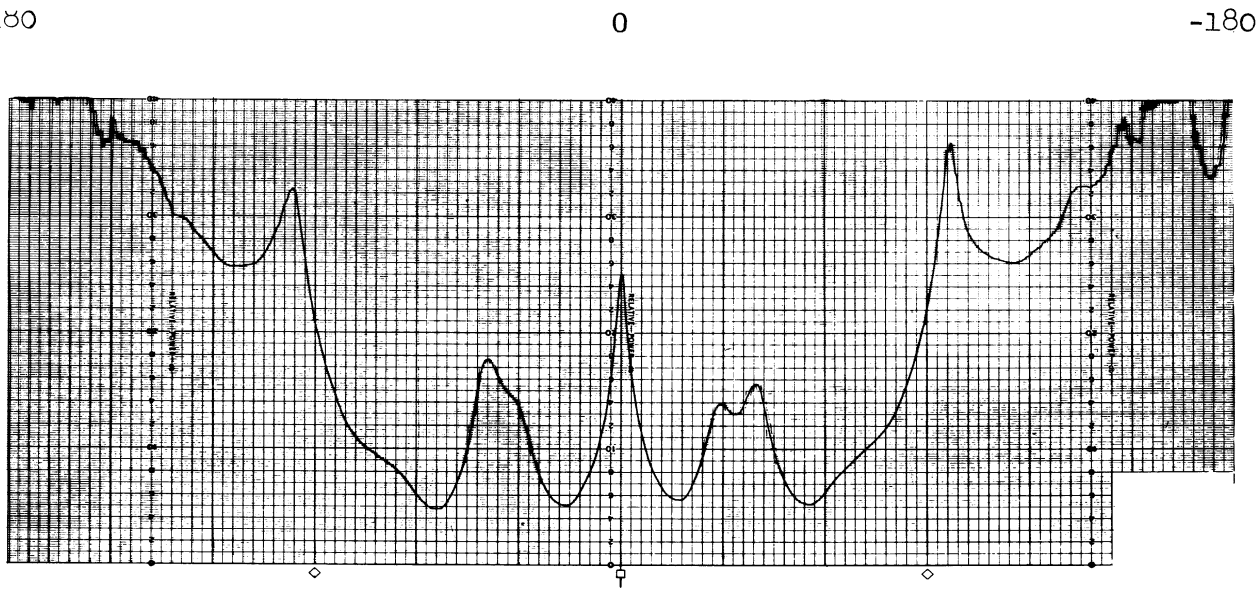

FIG. 5-4: MEASURED FAR FIELD ELEVATION PATTERN OF AN OPTIMUM DOUBLE PARASITIC LOOP COUNTERPOISE ANTENNA. $w_1=w_2=0.183\lambda$, $2B_1=2B_2=2.5\lambda$, $H_1=0.64\lambda$, $H_2=2.29\lambda$, f=1080 MHz.

of 1080 - 1180 MHz. The overall shape of the pattern near the principal maximum did not change appreciably as the frequency was varied. However, the field characteristics below the horizon changed considerably as can be seen from Figs. 5-5a - g . The variation of the different quantities with frequency is shown in Table V-1. These values are obtained from the measured patterns.

5.6 Pattern Variation with H_2

During the optimization of the antenna to obtain large field gradients it was found that the parameter H_2 influences the pattern behavior considerably. In order to study this effect more carefully the patterns produced by a two-loop system, having $2B_1=2B_2=2.5\lambda$, $H_1=0.65\lambda$, $w_1=w_2=0.183\lambda$ and H_2 variable, were measured. The results of this investigation are shown in Fig. 5-6 .

5.7 Impedance Characteristics

The impedance characteristics of the double loop antenna have been measured in the frequency range 1080 - 1180 MHz in 20 MHz increments. The objective of this investigation was to determine the influence of the parasitic loops on the impedance of the basic Alford loop above the counterpoise.

In the experimental arrangement there was a 4.8" long section of 50 ohm coaxial transmission line between the impedance measuring point and the terminals of the Alford loop. Because of the high input VSWR associated with the Alford loop, efforts were made to match the Alford loop (employing a double stub tuner) to have a VSWR of less than 1.2:1. The measured impedances referred to by the input connector, of the Alford loop above the counterpoise are shown in Fig. 5-7. The corresponding VSWR obtained are shown in Table V-2. As can be seen from the table, the values of VSWR at 1160 and 1180 MHz are somewhat higher and are probably caused by the double stub tuner needing to be positioned differently along the line.

The two colinear parasitic rings were constructed from 2" wide strips each having a diameter of 27" (i.e. $2B \simeq 2.5\lambda$ at 1080 MHz). They were positioned so that the lower loop was 7" ($\simeq 0.6\lambda$ at 1080 MHz) and the upper loop was 22" ($\simeq 2\lambda$ at 1080 MHz) above the counterpoise. The VSWR characteristics obtained at the input terminals of the two parasitic loop antenna are shown in Table V-2. As can be seen from the table, the parasitic loops have very little effect on the VSWR characteristics.

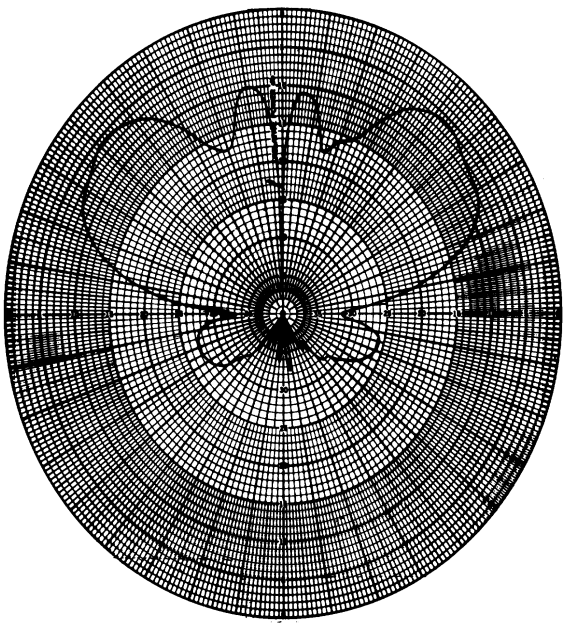

(a) f = 1060 MHz

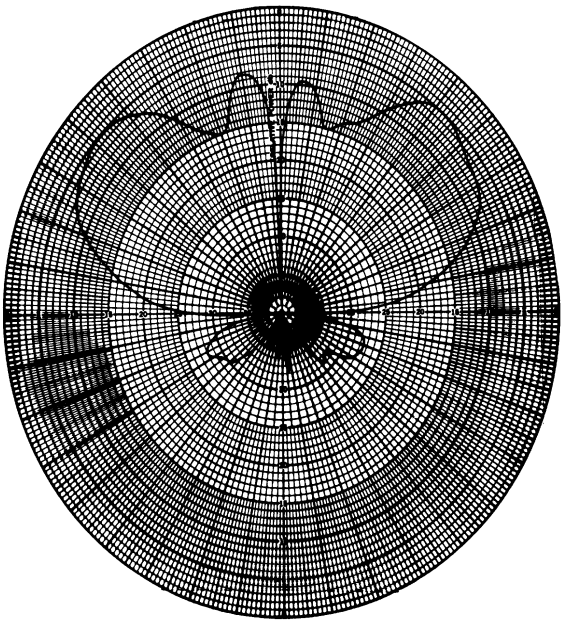

(b) f = 1080 MHz

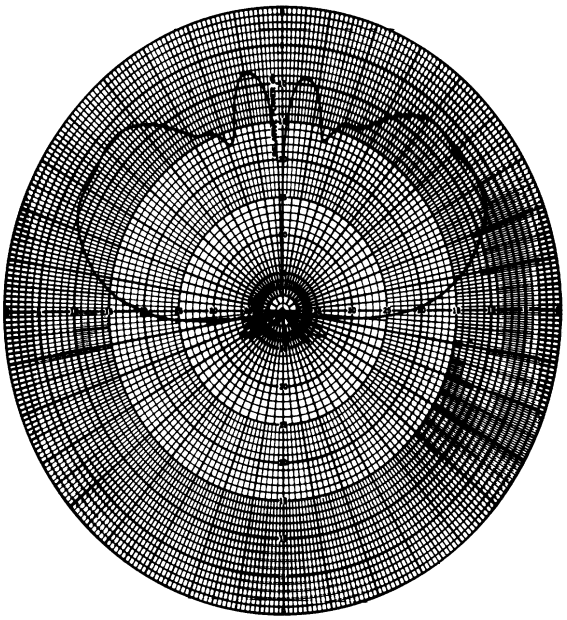

(c) f = 1110 MHz

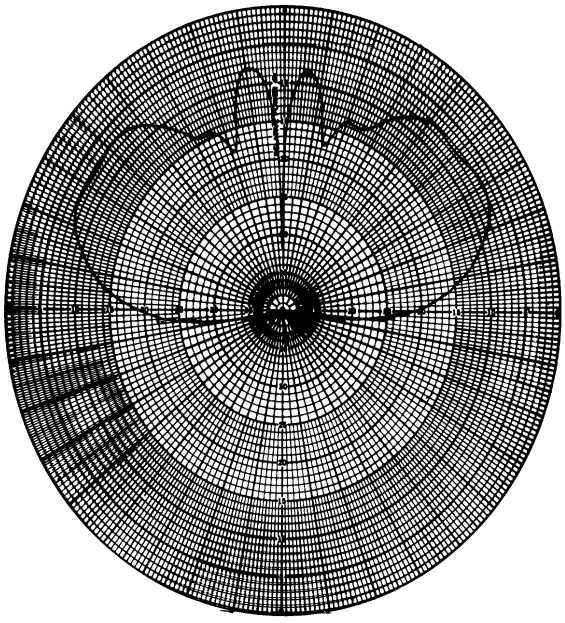

(d) f = 1120 MHz

FIG. 5-5 a-d: MEASURED FAR FIELD ELEVATION PATTERNS OF OPTIMUM DOUBLE PARASITIC LOOP COUNTERPOISE ANTENNA. kh=2.75, kA=17.92, kb_1=0.15, $kB_1=4\pi$, kH_1=3.7, kb_2=0.15, kB_2=10.27, kH_2=10.63 .

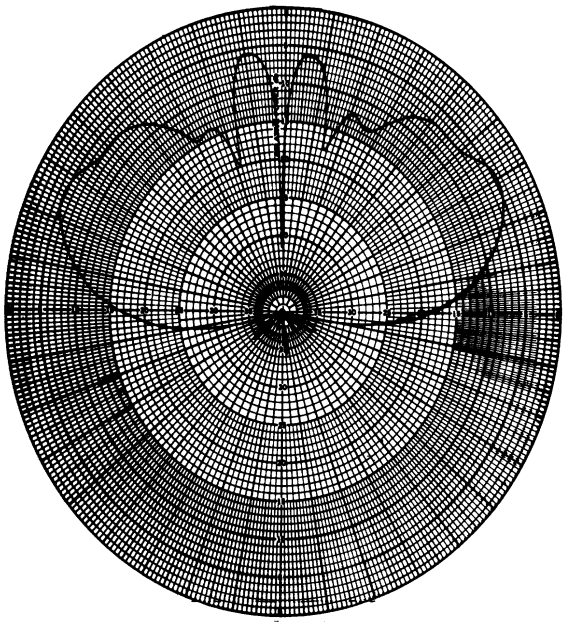

(e) f = 1140 MHz

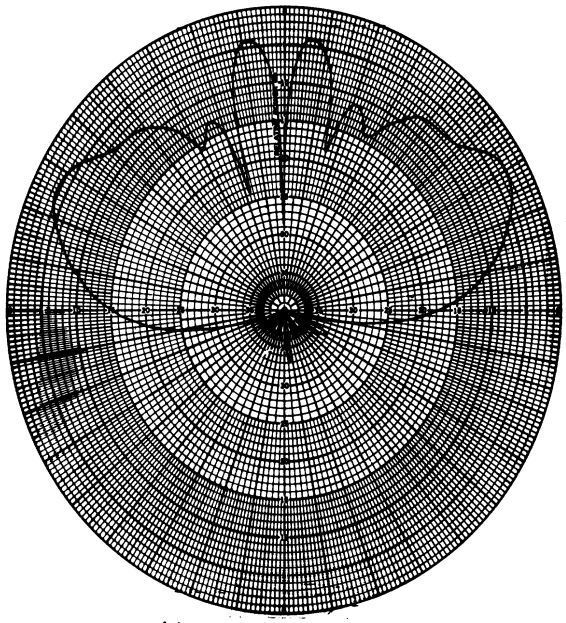

(f) f = 1160 MHz

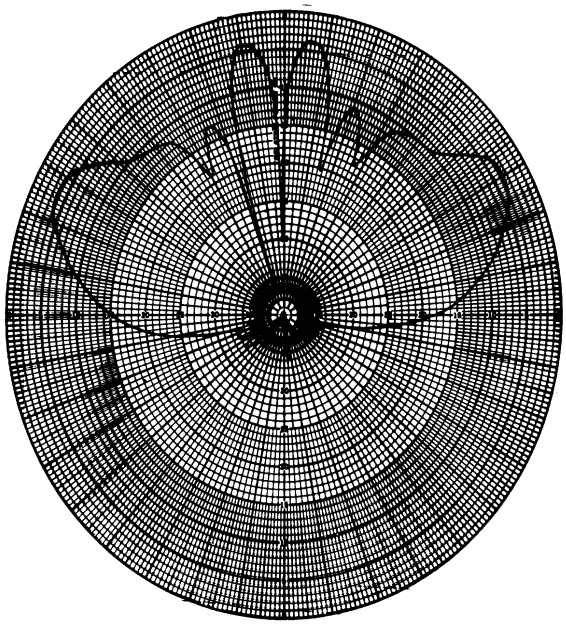

(g) f = 1180 MHz

FIG. 5-5e-g: MEASURED FAR FIELD ELEVATION PATTERN OF OPTIMUM DOUBLE PARASITIC LOOP COUNTERPOISE ANTENNA.
kh=2.75, kA=17.92, kb_1=0.15, $kB_1=4\pi$, kH_1=3.7, kb_2=0.15, kB_2=10.27, kH_2=10.63.

TABLE V-1: PATTERN CHARACTERISTICS FOR THE OPTIMUM DOUBLE PARASITIC LOOP COUNTERPOISE ANTENNA

f (MHz)	θ_{min} (^{o})	E_{min} (db)	θ_{max} (^{o})	E_{max} (db)	α_g (db)	α_F (db)
1050	2	-0.2	15	+0.7	-	20.7
1060	2	-0.3	21	+8.2	-	26.4
1070	2.5	-7.0	24	+9.5	-	29.0
1080	5.5	-21.0	25	+0.5	$21/5^o.5$	23.0
1090	8	-24.6	27	-4.9	14.6	18.9
1100	11	-26.4	28.5	-8.8	12.3	12.3
1110	14	-27.8	29	-11.1	7.9	13.8
1120	16	-26.6	37	-13.4	6.5	12.7
1130	19	-30.0	40	-15.2	6.4	12.8
1140	20	-32.0	41	-16.7	5.8	12.6

θ_{min} = position of the first minimum in degrees below $\theta=90^o$,

E_{min} = amplitude of the field at $\theta=\theta_{min}$ relative to the field at $\theta=90^o$,

θ_{max} = position of the first maximum in degrees below $\theta=90^o$,

E_{max} = amplitude of the field at $\theta=\theta_{max}$ relative to the field at $\theta=90^o$,

α_g = field gradient = $-20 \log_{10} \left| \frac{E(96^o)}{E(90^o)} \right|$

α_F = field reduction = $-20 \log_{10} \left| \frac{E(90^o)}{E(\text{main max})} \right|$.

Note that in the column for α_g, the values are not given for the first three frequencies because at these frequencies the gradient per 6^o cannot be defined. The field gradient for f = 1080 MHz is defined to be for $5^o.5$ instead of 6^o.

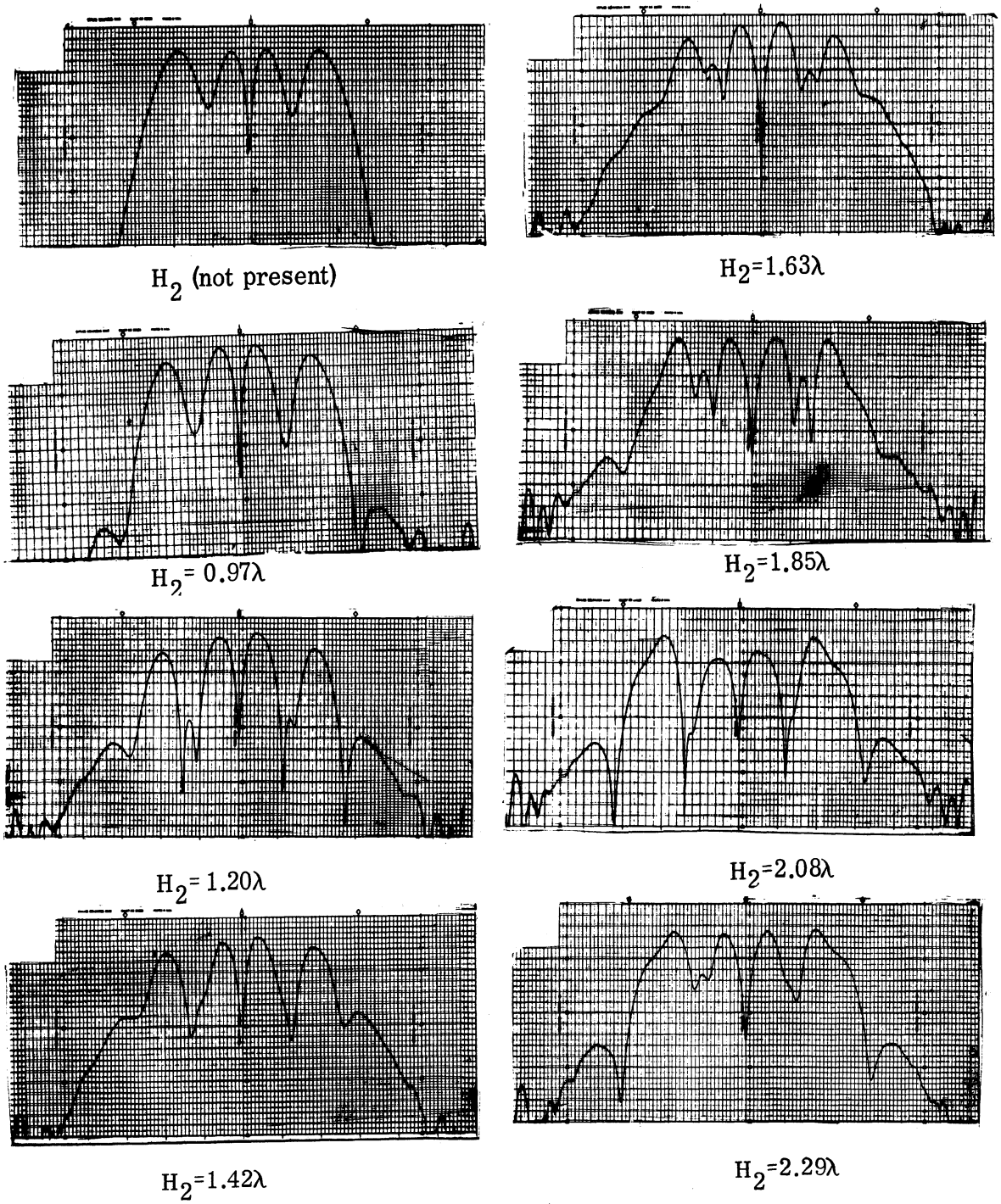

FIG. 5-6: MEASURED ELEVATION PATTERNS OF DOUBLE PARASITIC LOOP COUNTERPOISE ANTENNA. $2B_1=2B_2=2.5\lambda$, $H_1=0.64\lambda$, f=1080 MHz, H_2 Variable.

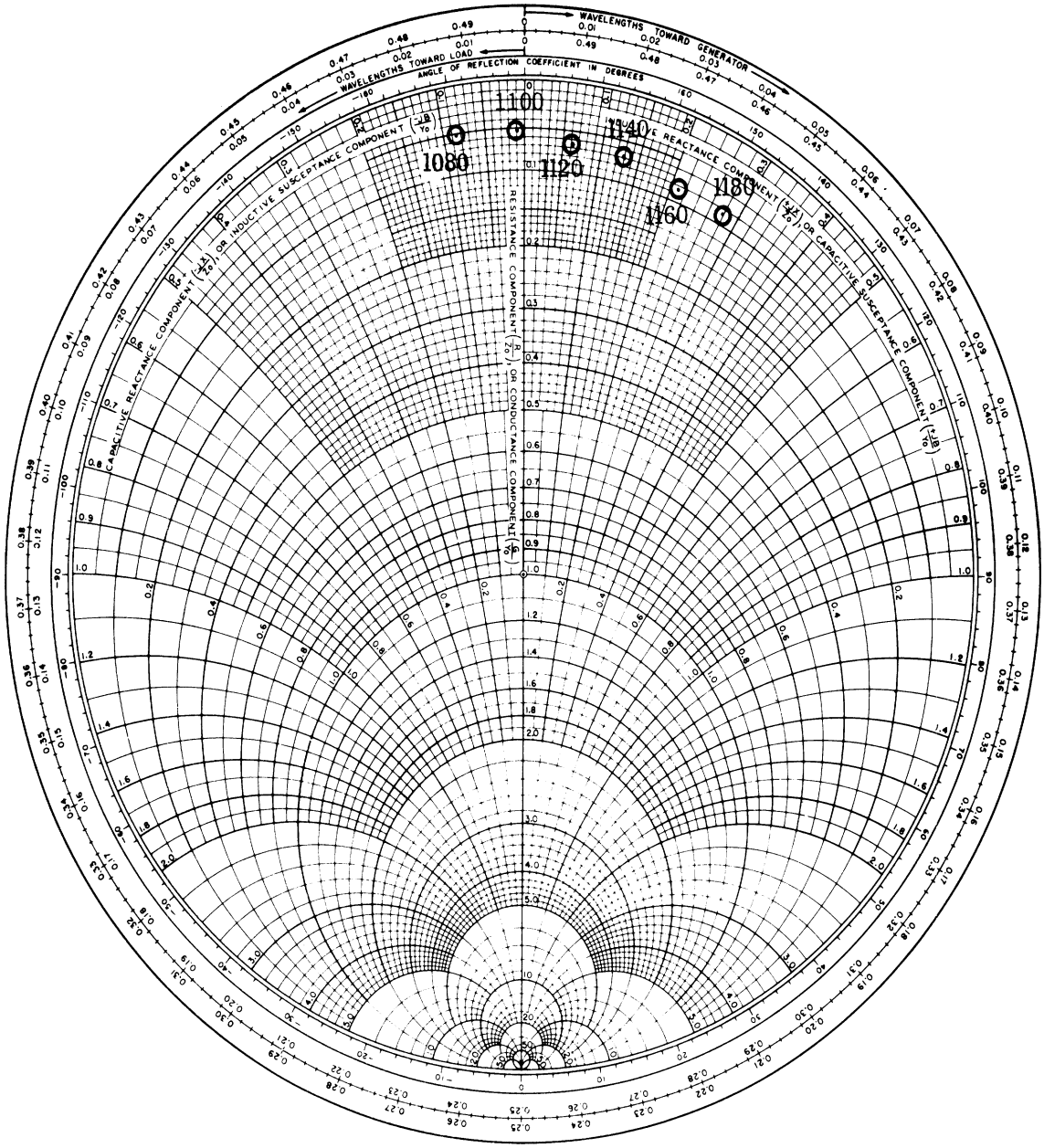

FIG. 5-7: IMPEDANCE CHARACTERISTICS OF ALFORD LOOP COUNTERPOISE ANTENNA (Freq. = MHz) .

TABLE V-2: VSWR CHARACTERISTICS OF DOUBLE PARASITIC LOOP COUNTERPOISE ANTENNA

Frequency (MHz)	VSWR without two 2" rings	VSWR with two 2" rings
1080	1.14	1.18
1100	1.12	1.16
1120	1.14	1.14
1140	1.16	1.16
1160	1.40	1.50
1180	1.80	2.00

5.8 Double Coplanar Parasitic Loop System

It may be convenient in many situations to use two parasitic loops in the same plane instead of different planes as considered above. Such a system is referred to as the double coplanar parasitic loop system. The measured patterns produced by such an antenna are shown in Fig. 5-8. The average values obtained for α_g and α_F are indicated on the patterns. The general features of the patterns here are that the response of the antenna in directions $\theta \geq 90^o$ are considerably reduced and the response near the region $\theta=0^o$ is increased substantially.

The general behavior of the patterns of such an antenna as the different parameters are varied, is shown in Fig. 5-9 .

5.9 Comparison with Single Parasitic Loop System

The general pattern characteristics of single and double parasitic loop counterpoise antenna systems are found to be similar. The double-loop system offers additional parameters to shape the pattern near the horizon. From the results discussed above it can be seen that with the addition of the second parasitic loop it is possible to achieve a much deeper minimum in the pattern below the horizon. It is because of this, the double parasitic loop system produced a field gradient much better than that obtained from a single parasitic loop antenna.

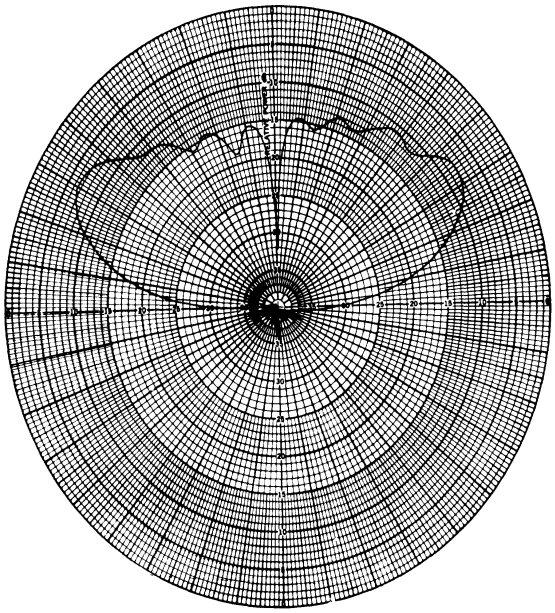

(a) $2B_2=3.5\lambda$, $H_1=H_2=0.06\lambda$

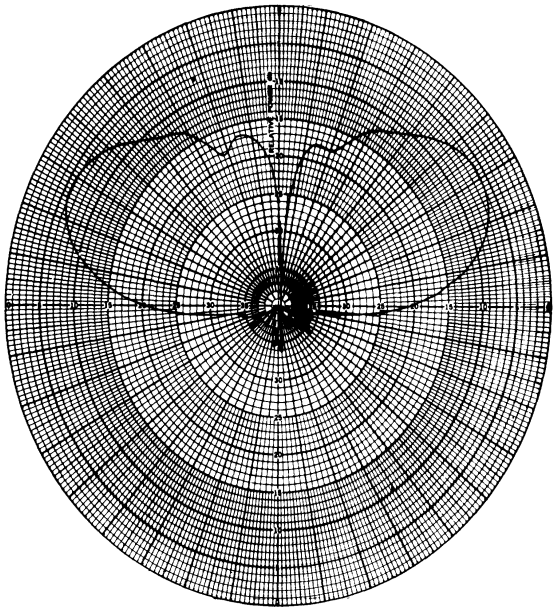

(b) $2B_2=1.5\lambda$, $H_1=H_2=1.7\lambda$

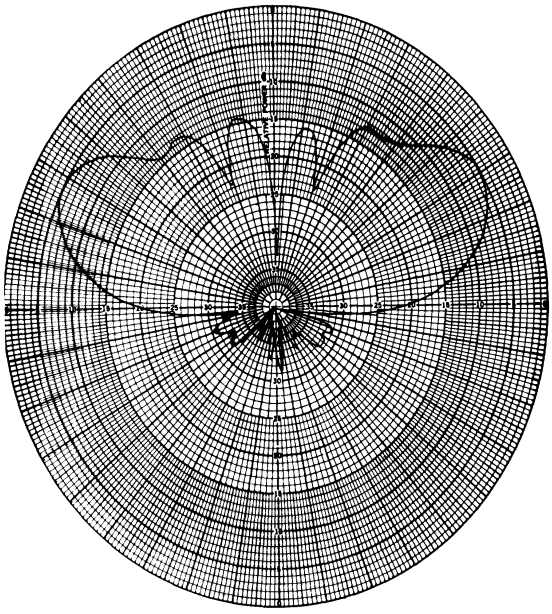

(c) $2B_2=2.5\lambda$, $H_1=H_2=1.7\lambda$

FIG. 5-8: MEASURED ELEVATION PATTERNS OF DOUBLE COPLANAR PARASITIC LOOP COUNTERPOISE ANTENNA. kh=2.75, kA=17.92, $w=0.09\lambda$, $2B_1=2\lambda$, f=1080 MHz.

(a) $\alpha_{g(avg)}=23.3$ db, $\alpha_{F(avg)}=5$ db. (b) $\alpha_{g(avg)}=7.8$ db, $\alpha_{F(avg)}=16.1$ db

(c) $\alpha_{g(avg)}=8.5$ db, $\alpha_{F(avg)}=16$ db.

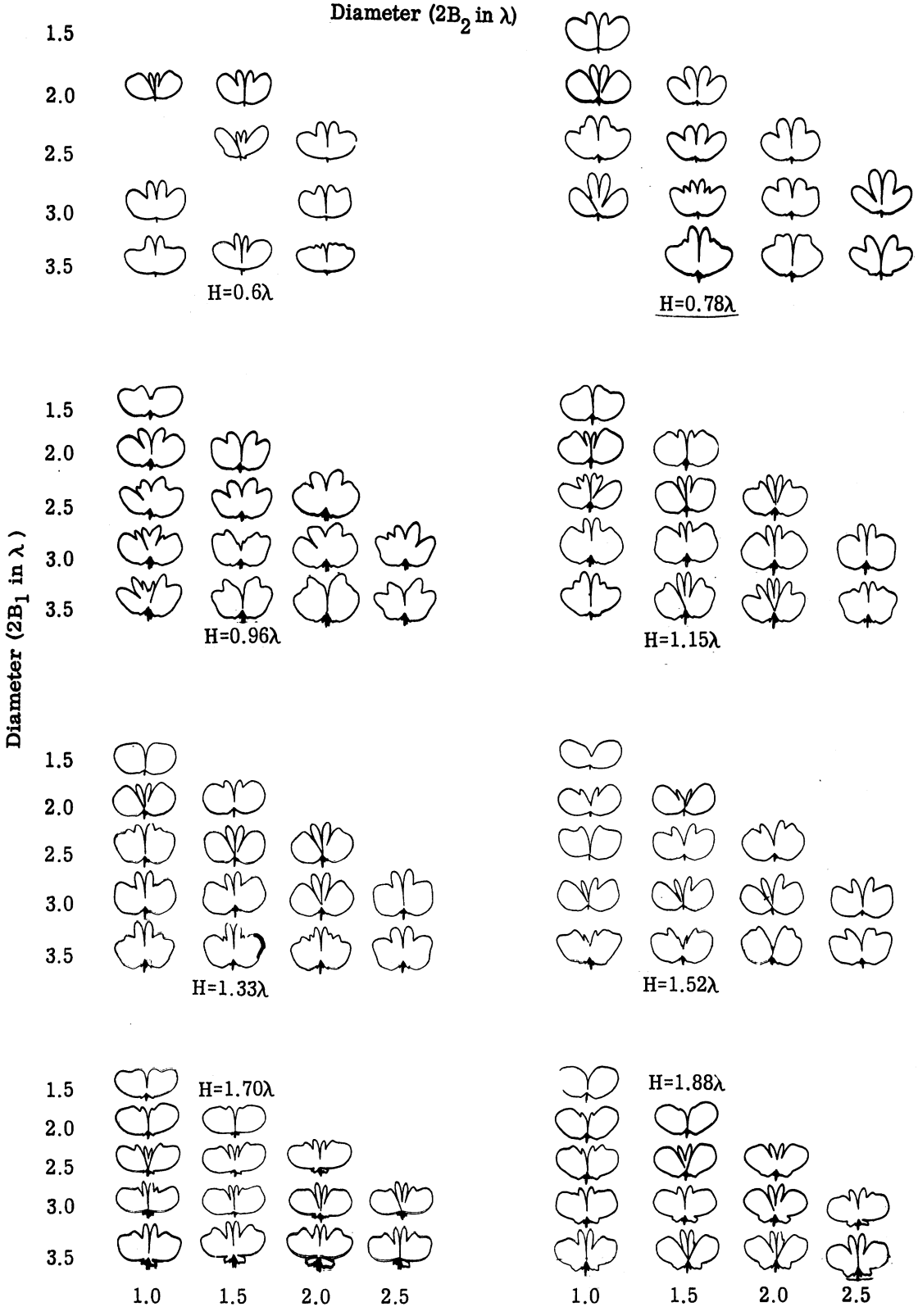

FIG. 5-9: MEASURED ELEVATION PATTERNS OF DOUBLE COPLANAR PARASITIC LOOP COUNTERPOISE ANTENNA. h=0.44λ, 2A=5.7λ, H_1=H_2=H and f= 1080 MHz.

5.10 Discussion

The radiation properties of a double parasitic loop counterpoise antenna have been discussed above in detail. For the case of large separation between the two parasitic elements the patterns can be analyzed theoretically. The choice of the specific parameters for a particular antenna will depend on the requirements on the pattern behavior. The influence of the different parameters on the patterns produced can be obtained from the results given above.

VI

MULTIPLE PARASITIC LOOP COUNTERPOISE ANTENNA

6.1 Introduction

In this chapter the results of a limited experimental investigation of the radiation patterns produced by a multiple parasitic loop counterpoise antenna are discussed. This study was undertaken in order to determine whether it is possible to obtain increased response from the antenna along and above the horizon by using more than two parasitic loops.

6.2 Description of a Multiple Parasitic Loop Antenna

A multiple parasitic loop antenna is shown schematically in Fig. 6-1. It consists of the basic Alford loop located at a height h above the counterpoise of radius A. Four coplanar parasitic loops of variable diameters were placed at a height H above and parallel to the counterpoise. During the experiment the diameters of the parasitic loops were fixed at 1, 2, 3 and 4 λ respectively and the height H was varied from 0.23 λ to 1.88 λ in steps of 0.18 λ. All the patterns were measured at 1080 MHz.

6.3 Radiation Patterns

The measured elevation patterns of the four parasitic loops antennas of Fig. 6-1 are shown in Fig. 6-2 as a function of the height H. The general behavior of the pattern appears to be similar to the single and double parasitic loop antennas discussed earlier in the report. However, it can be seen from Fig. 6-2 that the use of four parasitic loops gives rise to more lobes in the pattern near the region $\theta=0^{o}$. Three of the patterns given in Fig. 6-2 are shown separately in Figs. 6-3a-c so that the details may be studied more carefully.

6.4 Discussion

It can be seen from Fig. 6-2 and 6-3 that the response in the direction of the horizon does not increase due to the increased number of parasitic elements. For some values of H the increased number of elements produced more uniform coverage in the half plane above the counterpoise. Although a multiple loop system offers more adjustable parameters for pattern shaping, further study is needed to determine its usefulness as compared to the single and double loop systems.

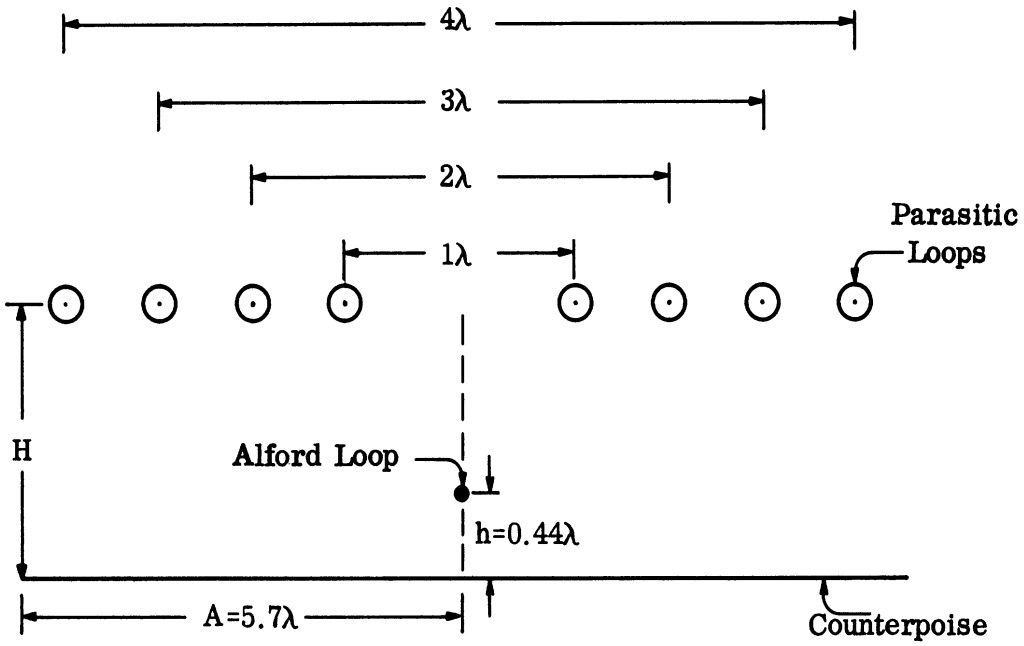

FIG. 6-1: MULTIPLE PARASITIC LOOP COUNTERPOISE ANTENNA.

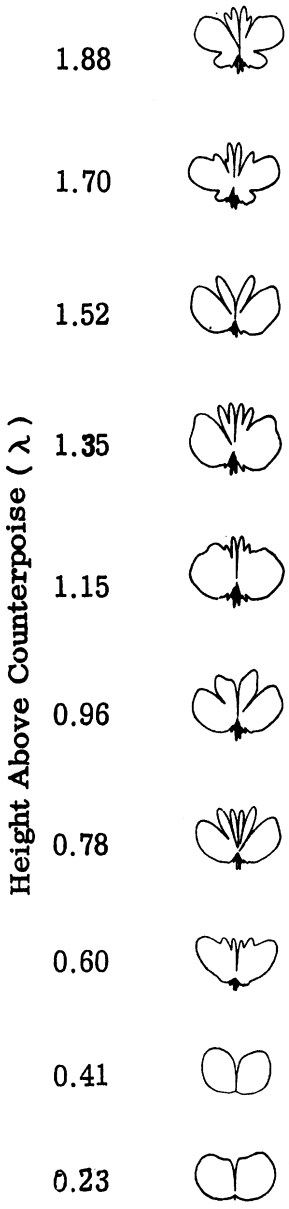

FIG. 6-2: MEASURED ELEVATION PATTERNS OF MULTIPLE PARASITIC LOOP COUNTERPOISE ANTENNA. $w_1=w_2=w_3=w_4=0.092\lambda$, f=1080 MHz, H variable.

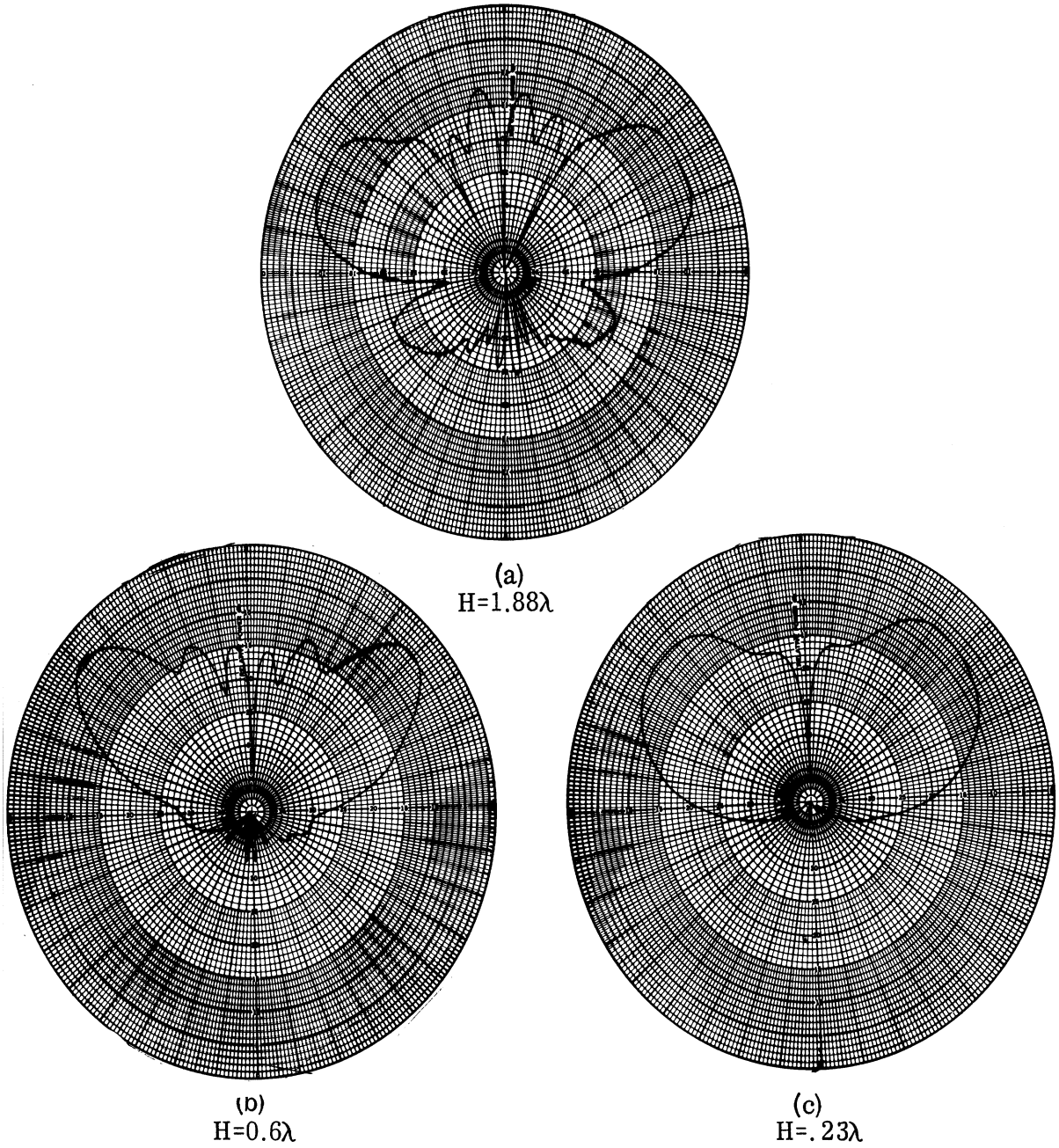

(a)
H=1.88λ

(b)
H=0.6λ

(c)
H=.23λ

FIG. 6-3: MEASURED ELEVATION PATTERNS OF MULTIPLE LOOP COUNTERPOISE ANTENNA. f=1080 MHz, $w_1=w_2=w_3=w_4=0.092\lambda$.

VII

PROPOSED VOR ANTENNA MODELS

7.1 Introduction

In the previous chapters we have discussed both theoretically and experimentally the radiation properties of parasitic loop counterpoise antennas. As mentioned in Chapter I, the purpose of the investigation has been to determine the feasibility of using parasitic loops to shape the patterns produced by the Alford loop counterpoise antenna. From the results given earlier it is evident that by suitably placing one or more parasitic loops it is possible to shape the Alford loop counterpoise antenna patterns in the regions of space which is of interest to the VOR systems.

In the present chapter we propose a few parasitic loop counterpoise antenna systems obtained on the basis of our investigation. All the proposed systems appear to be capable of improving the existing VOR antenna performances in one way or another. The choice of a particular system will depend on the specific VOR requirements. The antennas proposed here have omnidirectional patterns in azimuth. Hence, further study will be needed to establish their usefulness in the existing VOR systems which have figure-of-eight radiation patterns in azimuth.

7.2 VOR Antenna Requirements

The general requirements on the antenna radiation patterns for satisfactory operation of the VOR systems have been discussed in Chapter I. From the discussion given there it is found that the following criteria can be used for considering an antenna to be ideally suited for a VOR system.

i) the radiation pattern characteristics near the principal maximum should not be too different than that produced by an Alford loop above a counterpoise.

ii) the field gradient produced at the horizon should be as large as possible. An arbitrary limit is imposed such that $\alpha_g \geq 7$ db.

iii) the average level of the field produced in the directions $\theta > 90^o$ should be as small as possible. Arbitrarily we set the restriction such that the minimum value of the field ratio defined as

$$\rho = \left| \frac{E_\phi(\theta)}{E_\phi(90^o)} \right|$$

in the range $100^o \leq \theta \leq 120^o$ is -10 db or less.

iv) the field reduction factor α_F should be as small as possible. α_F for an Alford loop above a 5.7λ diameter counterpoise is about 10 db.

Almost any parasitic loop counterpoise antenna satisfies condition (i). Condition (iii) can be satisfied by placing single and double parasitic loops of proper diameters near the plane of the Alford loop. Condition (ii) is the most important and also the most difficult to achieve. As expected, it is very difficult, if not impossible, to satisfy all the four conditions simultaneously. In a practical system a compromise must be made.

7.3 Proposed Parasitic Loop Counterpoise Systems

On the basis of the criteria discussed in Section 7.2 we propose three parasitic loop counterpoise antennas which may be found useful in a VOR system. Because of their improved pattern characteristics, all three models appear to be capable of reducing the siting errors in the bearing indications of the present-day VOR system. Each of the three systems proposed uses a standard Alford loop antenna above a 5.7λ diameter counterpoise. All the dimensions are at first given for a full scale frequency 108 MHz. The normalized dimensions are then given so that their design at any frequency may be facilitated.

7.3.1 Basic Alford Loop Counterpoise Antenna

The radiation characteristics of the standard Alford loop counterpoise antenna have been discussed in Chapter II. The important design parameters of the antenna are A=52', h=4' at the full scale frequency, 108 MHz; the corresponding normalized values for these parameters are kA=17.92 and kh=2.75. The far field elevation pattern produced by the 1/10th scale model of the antenna at the frequenc 1080 MHz is shown in Fig. 2-4. The measured pattern shown in Fig. 2-4 has the following average characteristics: α_g= 3.09 db/6^o, α_F = 10.38 db and ρ = -6.15 db.

Antenna System No. 1. It consists of a single parasitic loop placed above and parallel to a counterpoise. The design parameters of the antenna are:

Full Scale Freq. 108 MHz	Normalized Values
A = 52'	kA=17.92
h = 4'	kh = 2.75
2B = 27' 3"	kB = 3π
H = 17' 1"	kH = 11.78
W = 10"	kb = 0.15

The far field pattern produced by the 1/10th scale model of the antenna at the frequency 1080 MHz is as shown in Fig. 3-10. The measured pattern produced by the model has the following average characteristics; α_g=7 db/6°, α_F=13.00 db and ρ = -8.5 db. This model appears to satisfy all the conditions reasonably well. However, it is desirable that α_g and ρ should be improved. Further study is needed to determine whether better values for α_g and ρ can be obtained from this antenna. The performance of the antenna over the frequency band of the VOR system should also be investigated.

Antenna System No. 2. It consists of a single parasitic loop placed above and parallel to a counterpoise. The design parameters are:

Full Scale Freq. 108 MHz	Normalized Values
A=52'	kA=17.92
h=4'	kh=2.75
2B=22' 9"	kB=2.5π
H=5' 10"	kH=4.02
W=1' 8"	kb=0.287

The far field elevation pattern produced by the 1/10th scale model of the antenna at 1080 MHz is given by Fig. 3-9 and was also discussed in our Quarterly Report[7]. The measured pattern shown in Fig. 3-9 has the following average characteristics; α_g=8.5 db/6°, α_F=29.7 db and ρ = -8 db. The main disadvantage of this antenna is that there is 10 db minimum in the pattern in the direction θ=30°. This may not be serious in some practical situations. The field along the horizon is considerably reduced. However, the pattern in the directions $\theta > 90°$ does not have any strong minor lobe. The field gradient obtained here is the same as that of the previous antenna.

Antenna System No. 3. It consists of two parasitic loops placed above and parallel to a counterpoise. This has been repeated by us elsewhere[8]. The design parameters of the double parasitic loop antenna are:

Full Scale Freq. 108 MHz	Normalized Values
A=52'	kA=17.92
h=4'	kh=2.75
$2B_1$=36' 3"	$kB_1=4\pi$
H_1=5' 5"	kH_1=3.73
W_1= 10"	kb_1= 0.15
$2B_2$=29' 10"	kB_2=10.26
H_2= 15' 5"	kH_2= 10.62
W_2= 10"	kb_2= 0.15

The measured far field radiation pattern produced by the 1/10th scale model of the double parasitic loop antenna system is given in Fig. 5-3. The pattern shown in Fig. 5-3 has the following average characteristics; α_g=2ldb/5^o.5, α_F= 23 db and ρ = +2.6 db. This system is highly frequency sensitive. The antenna produces the largest field gradient at the horizon at a considerable sacrifice of α_F and ρ . However, as mentioned in Section 5.5, both α_F and ρ can be improved by designing the system so that α_g is less than the optimum value (see Fig. 5-4 and Table V-1).

7.4 Comparison Between the Basic and Proposed Antenna Systems

The measured far field elevation patterns produced by the VOR parasitic loop counterpoise antenna systems proposed in the previous section are shown in Figs. 7-1, 7-2 and 7-3. The measured pattern, produced by a basic VOR Alford loop counterpoise antenna, is superposed on each of the above figures for comparison. The two patterns in each of the Figs. 7-1 through 7-3 are normalized so that they have the same response along the directions of their principal maxima in the patterns. In all these patterns the details in the region near the backward direction are omitted. It can be seen from these figures that each of the proposed parasitic loop counterpoise antennas are capable of superior performance when compared with the basic VOR Alford loop counterpoise system.

7.5 Discussion

We have proposed the above three antenna systems, each of which is capable of improving the existing VOR system performance. From viewpoint of the field gradient characteristics, Antenna System No. 3 seems to be the best. We do not give here our preference for any one of the three systems. Depending on the particular system requirements, and from mechanical considerations, any one of them may be found advantageous in a practical situation.

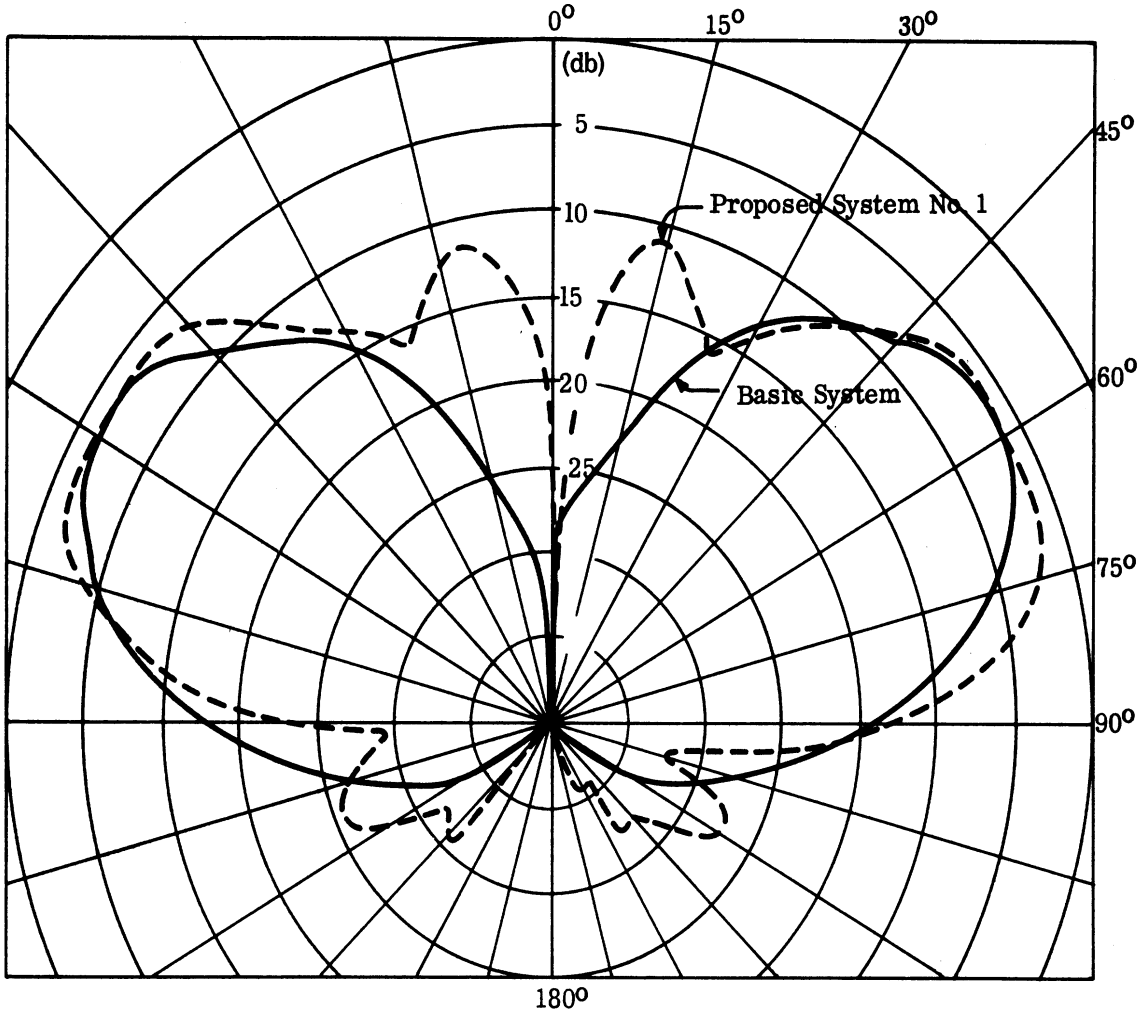

FIG. 7-1: MEASURED FAR FIELD ELEVATION PATTERNS OF VOR ANTENNAS AT 1080 MHz (—) Basic Alford Loop Counterpoise Antenna (--) Parasitic Loop Counterpoise Antenna System No. 1.

Average Performance Characteristics

Basic System	Proposed System No. 1
α_g=3.09 db/6°	α_g=7 db/6°
α_F=10.38 db	α_F=13.00 db
ρ_{min}= -6.2 db	ρ_{min}= -8.5 db

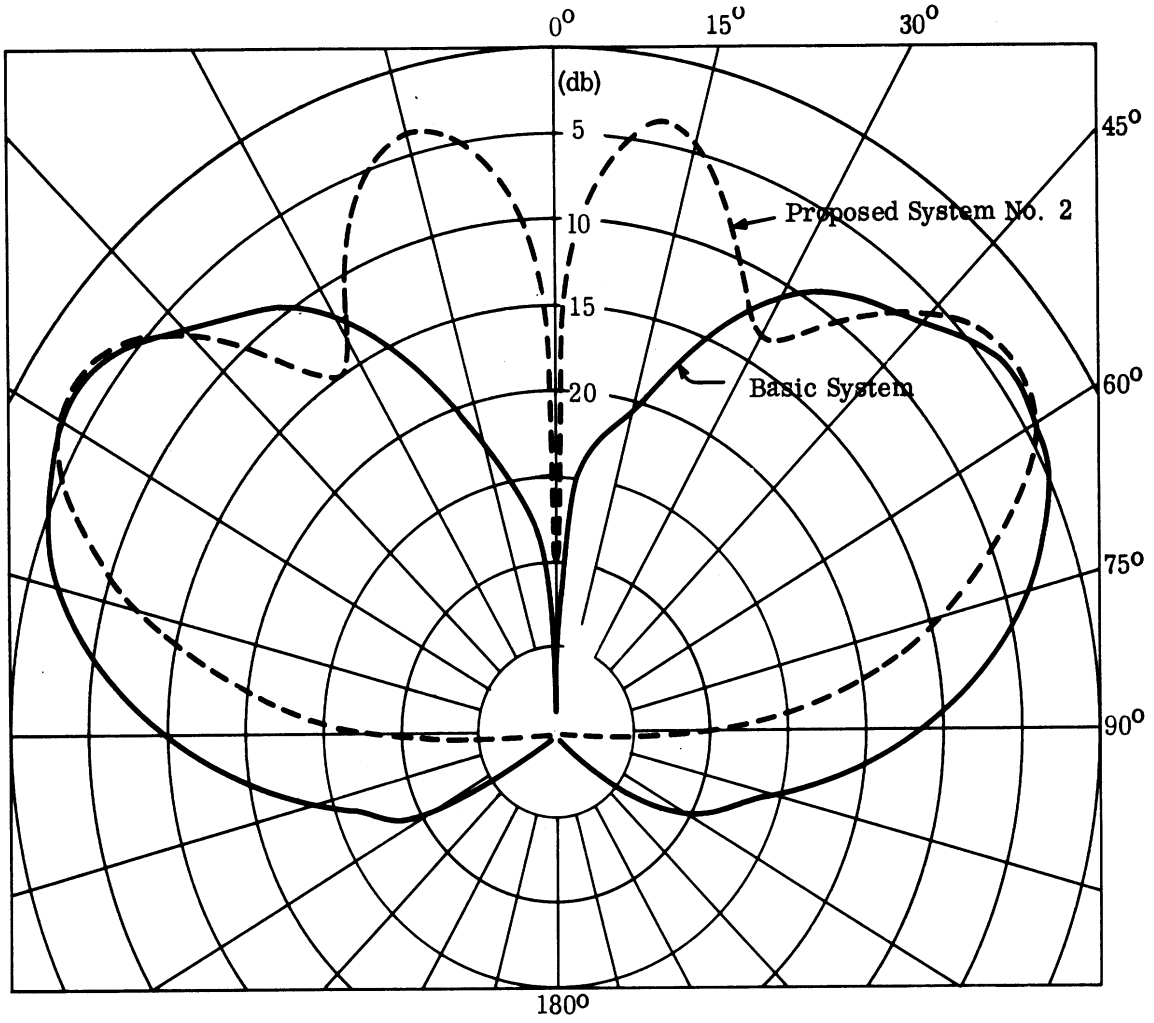

IG. 7-2: MEASURED FAR FIELD ELEVATION PATTERNS OF VOR ANTENNAS AT 1080 MHz(—) Basic Alford Loop Counterpoise Antenna (--) Parasitic Loop Counterpoise Antenna System No. 2.

Average Performance Characteristics

Basic System	Proposed System No. 2
α_g=3.09 db/6°	α_g=8.5 db/6°
α_F=10.38 db	α_F= 29.7 db
ρ_{min}= -6.2 db	ρ_{min}= -8 db

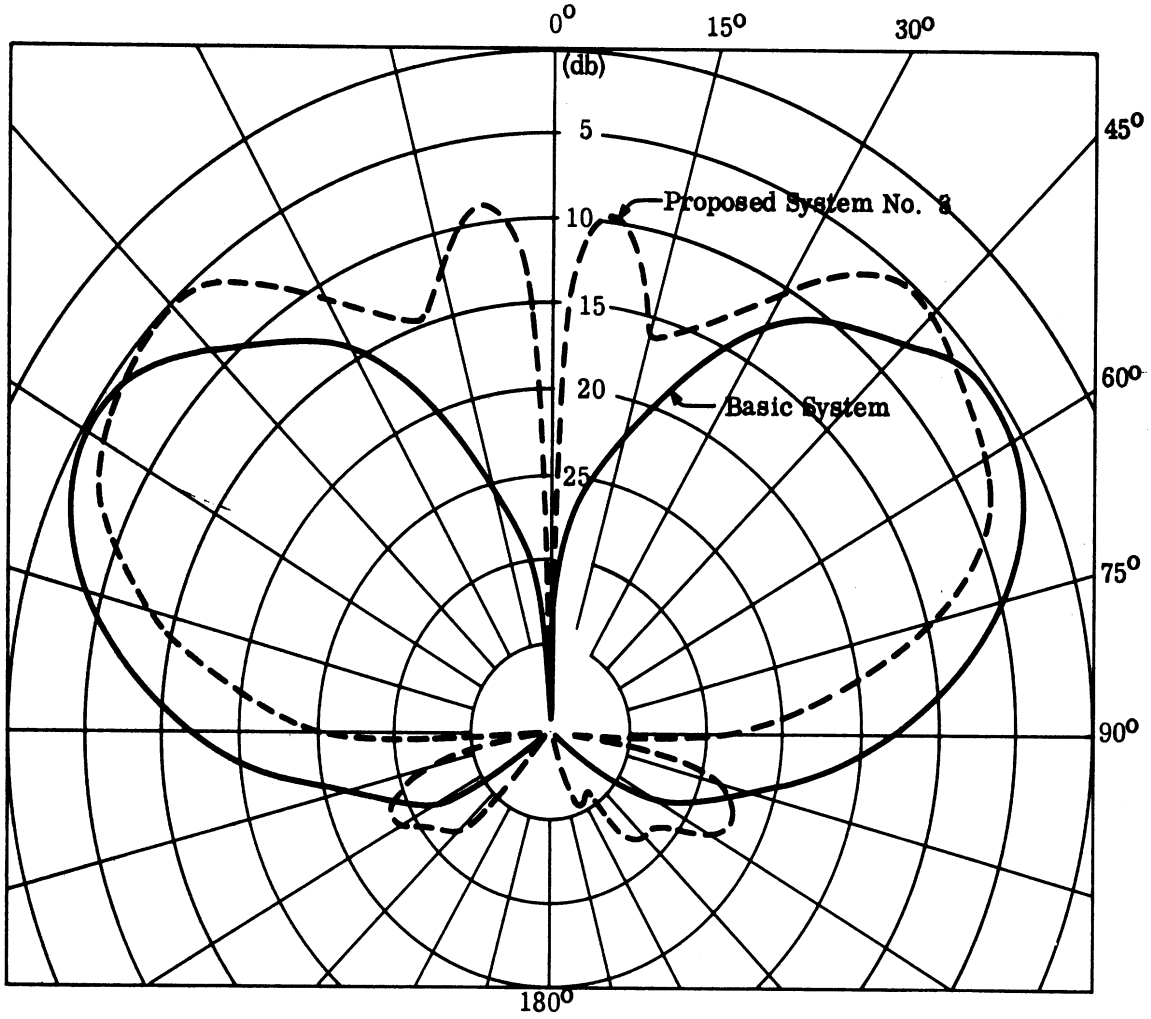

FIG. 7-3: MEASURED FAR FIELD ELEVATION PATTERNS OF VOR ANTENNAS AT 1080 MHz (—) Basic Alford Loop Counterpoise Antenna (--) Parasitic Loop Counterpoise Antenna System No. 3.

Average Performance Characteristics

Basic System	Proposed System No. 3
α_g=3.09 db/6°	α_g=21 db/5°.5
α_F= 10.38 db	α_F= 23 db
ρ_{min}= -6.2 db	ρ_{min}= +2.6 db

VIII

CONCLUSIONS AND RECOMMENDATIONS

8.1 Conclusions

The radiation field produced by a single parasitic loop counterpoise antenna has been investigated both theoretically and experimentally. Theoretical expressions for the radiation patterns produced by a single parasitic loop counterpoise antenna have been obtained by applying geometrical theory of diffraction. Within the range of approximation the agreement between theory and experiment has been found to be very good. The present investigation demonstrates an excellent application of geometrical theory of diffraction to antenna problems.

In a multiple parasitic loop counterpoise antenna system where the mutual coupling between the parasitic loop is negligible, the present theory can be extended to analyze the radiation field produced. For a double parasitic loop counterpoise antenna we have obtained good correlation between theory and experiment.

In general, it has been found that by introducing one or more parasitic loops the counterpoise edge diffraction effects in the patterns can be reduced considerably. The behavior of the pattern near the principal maximum is not appreciably changed compared to that produced by an Alford loop only above the counterpoise. Parasitic loops in general increase the response of the antenna in regions of space near $\theta=0^{o}$.

Extensive numerical and experimental investigations of various aspects of the parasitic loop counterpoise antenna have been carried out. These results being out the detailed effects of the different parameters of the system on the radiation patterns. As expected the antenna is found to be essentially narrow band.

The parasitic loop concept has been found to be capable of shaping the patterns produced by an Alford loop above a counterpoise in the regions of space below the plane of the counterpoise. In particular a double parasitic antenna system yielded a field gradient of 21 db/$5^{o}.5$ at the horizon. We thus conclude that the primary purpose of the present investigation has been fulfilled.

On the basis of our investigation we arrived at the conclusion that when suitably designed, the parasitic loop counterpoise antenna is potentially capable of minimizing the siting errors inherent in the existing VOR systems.

We have proposed three antenna systems which may find possible application in VOR systems. All three of the antennas appear to be capable of yielding improved performance compared to the present day VOR antenna. One or all of these proposed antennas should be investigated more carefully with the specific VOR application as the goal.

8.2 Recommendations for Further Work

Although we have discussed in detail the radiation characteristics of parasitic loop counterpoise antennas, we feel that further work is necessary before it can be established that such antennas will bring out superior performances from the existing VOR systems. Therefore, we recommend that further work be done along the following lines:

i) study the performance of the single parasitic system over the full frequency band 108 - 118 MHz. Investigate the possibility of steering the minimum below the horizon by adjusting the pertinent parameters.

ii) investigate the possibility of improving the field ratio ρ and the field reduction α_F but retaining the high value of the field gradient α_g of the double parasitic loop system.

iii) investigate the performance of the parasitic loop counterpoise antenna when the azimuthal pattern is a figure-of-eight instead of omnidirectional.

iv) study the possibility of obtaining a specified performance from the antenna with smaller counterpoise and possibly establish a minimum size for the counterpoise that can be useful.

ACKNOWLEDGEMENT

We wish to acknowledge the work of Mr. Peter H. Wilcox of this Laboratory who prepared the programming for this report.

REFERENCES

1 Anderson, S. R. (1965), "VHF Omnirange Accuracy Improvements," IEEE Trans., AME-12, No. 1, pp. 26-35.

2 Weston, V. H., J. E. Clark and F. M. Penar (1964), "New VOR Counterpoise System for Reduction of Siting Errors," Conductron Corporation Final Report No. RD-64-47, FAA Contract FA-WA-4665.

3 Van Bladel, J. (1964), Electromagnetic Fields, McGraw-Hill Book Co., New York, pp. 376-382.

4 Sommerfeld, A. (1954), Optics, Academic Press, Inc., pp. 247-265.

5 Kraus, J. D. (1950), Antennas, McGraw-Hill Book Co., New York, p. 238

6 Sengupta, D. L. and J. E. Ferris (1968), "Effects of Large Parasitic Loops on Alford Loop Counterpoise Radiation Patterns," IEE Electronic Letters (London), 4, No. 11, pp. 223-224.

7 Sengupta, D. L. and J. E. Ferris (1968), "VOR Parasitic Loop Counterpoise System," The University of Michigan Radiation Laboratory Report No. 8905-2-Q, FAA Contract FA67WA-1753, pp. 24-25.

8 Sengupta, D. L. and V. H. Weston (1968), "A new VOR Antenna System," Accepted for publication in the Proceedings of the IEEE.

9 Keller, J. B. (1962), "Geometrical Theory of Diffraction," J. Opt. Soc. Am., 52, No. 2, pp. 116-130.

APPENDIX A

FAR FIELD OF A LARGE CIRCULAR LOOP ABOVE A COUNTERPOISE

It was mentioned in Section 3.2.5 that the far field produced by a large circular loop carrying constant amplitude current and placed above and parallel to a counterpoise can be obtained by generalizing the method used by Weston et al[2] to obtain the far field produced by a small current loop above a counterpoise. We will not discuss the method in detail here. Only the key mathematical steps involved in the derivation of the far field expressions will be outlined.

Let the large circular loop of radius B be placed at a height H above the counterpoise of radius B (Fig. 3-5). It is assumed that the loop is carrying a current of the form $\vec{I}_p = \hat{\phi} I_{p_o} e^{-i\omega t}$,

where I_{p_o} is a constant. Because of the physical symmetry and the nature of the assumed current in the loop, the far field produced will be independent of ϕ and polarized along the ϕ-direction.

In obtaining the far field in the high frequency limit it is convenient to separate the entire space into the following three distinct regions:

i) Region I, known as the illuminated region defined as

$$0 \leq \theta \left(\frac{\pi}{2} - \phi_p \right)$$

ii) Region II, known as the transition region defined as

$$\left(\frac{\pi}{2} - \phi_p \right) \leq \theta \leq \left(\frac{\pi}{2} + \phi_p \right), \qquad \text{and}$$

iii) Region III, known as the shadow region defined as

$$\left(\frac{\pi}{2} + \phi_p \right) < \theta \leq \pi .$$

The parameter ϕ_p is defined in Fig. 3-5.

If the field point $P(\pi, \theta)$ lies in the illuminated region, then the far field at P may be written formally as:

$$E_\phi(P) = E^i_\phi(P) + E^r_\phi(P) + E^d_{\phi_d}(P) + E^d_{\phi_2}(P) , \qquad (A.1)$$

where

$E^{i}_{\phi}(P)$ is the direct field produced by the loop at the point P,

$E^{r}_{\phi}(P)$ is the reflected field produced by the loop at the point P,

$E^{d}_{\phi_1}(P)$ is the field produced at p due to the diffraction of the incident field by the near edge of the counterpoise,

$E^{d}_{\phi_2}(P)$ is the field produced at p due to the diffraction of the incident field by the far edge of the counterpoise.

For a point P(R, θ) within the transition region the field may be well approximated by that due to the near edge diffraction effects. Thus we can write

$$E_{\phi}(P) \simeq E^{d}_{\phi_1}(P) \ . \tag{A.2}$$

Equation (A.2) is a good approximation if ϕ_p is very small, i. e. $(H/A) \ll 1$, otherwise the contribution due to the far edge diffraction should be added to (A.2).

For a point P(R, θ) within the shadow region the far field can be written as

$$E_{\phi}(P)=E^{d}_{\phi_1}(P) + E^{d}_{\phi_2})P) \ , \tag{A.3}$$

i. e. the field consists of the near and far edge diffracted components only.

The proper expressions for the diffracted fields may be obtained by applying geometrical theory of diffraction[9] and the results of Sommerfeld's theory of diffraction by a conducting half-plane. Following a method discussed elsewhere[2] it can be shown that the following far field expressions may be obtained for Region I.

$$E^{i}_{\phi}(P)+E^{r}_{\phi}(p)= \eta_o I_{p_o} (\frac{kB}{2}) J_1(kB\sin\theta) \frac{e^{ikR}}{R} \left[-2i \sin(kH\cos\theta)\right] , \ 0 \le \theta < (\frac{\pi}{2} - \phi_p), \tag{A.4}$$

$$E^{d}_{\phi_1}(P)=\eta_o I_{p_o} (\frac{kB}{2}) J_1(kB\cos\phi_p) \frac{e^{ik(R-A\sin\theta+r_p)}}{R} e^{i\pi/4}$$

$$\times \left[\frac{\cos^3\phi_p}{\pi k r_p \sin\theta(1-\sin\theta)}\right]^{1/2} \frac{\cos\theta \sin\frac{\phi_o}{2}}{\cos\phi_p - \sin\theta} \ , \ 0 < \theta < \frac{\pi}{2} - \phi_p \tag{A.5}$$

$$E^d_{\phi_2}(P) = -\eta_o I_{p_o} \left(\frac{kB}{2}\right) J_1(kB\cos\phi_p) \cdot \frac{e^{ik(R+A\sin\theta+r_p)}}{R} e^{-i\pi/4}$$

$$\times \left[\frac{\cos^3\phi_p}{\pi k r_p \sin\theta(1+\sin\theta)}\right]^{1/2} \frac{\cos\theta \sin\frac{\phi_p}{2}}{\cos\phi+\sin\theta}, \quad 0 < \theta < \frac{\pi}{2} - \phi_p \ . \tag{A.6}$$

In the transition region the far field is

$$E_\phi(P) \simeq E^d_{\phi_1}(p) = \eta_o I_{p_o} \left(\frac{kB}{2}\right) J_1(kB\cos\phi_p) \frac{\cos^{1/2}\phi_p}{\sin^{1/2}\theta}$$

$$\times \frac{e^{ik(R-A\sin\theta)}}{R} V(\theta), \quad \frac{\pi}{2} - \phi_p \leq \theta \leq \frac{\pi}{2} + \phi_p \ , \tag{A.7}$$

where

$$V(\theta) = \frac{1-i}{2}\left[e^{ikr_p\sin(\theta-\phi_p)} \int_{-\infty}^{p_5} e^{i\pi t^2/} \, dt \right.$$

$$\left. -e^{ikr_p\sin(\theta+\phi_p)} \int_{-\infty}^{p_6} e^{i\pi t^2/2} \, dt\right] \tag{A.8}$$

$$p_5 = 2\left(\frac{kr_p}{\pi}\right)^{1/2} \cos\left(\frac{\phi_p - \theta - \pi/2}{2}\right) \ , \tag{A.9}$$

$$p_6 = 2\left(\frac{kr_p}{\pi}\right)^{1/2} \cos\left(\frac{\phi_p + \theta + \pi/2}{2}\right) \ . \tag{A.10}$$

In the shadow region

$$\frac{\pi}{2} + \phi_p < \theta < \pi \ ,$$

Eq. (A.7) gives the correct field due to the near edge diffraction so it can be used for $E^d_{\phi_1}(P)$. The far edge diffraction contribution $E^d_{\phi_2}$ in this region can be shown to be

given by (A.6) without the negative sign in front.

Thus it is found that different expressions are used to obtain the far field, depending on the region of space where the field point P lies. For computational purposes it is convenient to develop a single expression for the far field which is valid in the region $0 < \theta < \pi$.

A single expression for the far field is obtained in the following manner:

(a) Modify (A.7) so that it gives the correct $E^i_\phi(P)+E^r_\phi(P)$ + the near edge diffracted far field in Region I and the correct near edge diffracted field $E^d_{\phi_1}(P)$ in Region III

(b) Add the far edge diffracted far field expression to the modified expression derived in (a) to obtain the final expression for the far field valid in the entire region of space.

If the point P is within the illuminated region, i.e. θ is sufficiently smaller than $(\frac{\pi}{2}-\phi_p)$ both p_5 and p_6 given by (A.9) and (A.10) become large compared to unity. Under this condition the integrals in (A.8) can be split into two parts and we can rewrite (A.7) as

$$E^d_{\phi_1}(P)=\eta_o I_{p_o}(\frac{kB}{2})J_1(kB\cos\phi_p)\frac{\cos^{1/2}\phi_p}{\sin^{1/2}\theta}\frac{e^{ik(R-A\sin\theta)}}{R}\times\left[V_1(\theta)+V_2(\theta)\right] , \quad (A.11)$$

where

$$V_1(\theta)=\frac{1-i}{2}\left[e^{ikr_p\sin(\theta-\phi_p)}-e^{ikr_p\sin(\theta+\phi_p)}\right]\int_{-\infty}^{\infty}e^{i\pi t^2/2}\,dt , \quad (A.12)$$

$$V_2(\theta)=-\frac{1-i}{2}\left[e^{ikr_p\sin(\theta-\phi_p)}\int_{p_5}^{\infty}e^{i\pi t^2/2}\,dt-e^{ikr_p\sin(\theta+\phi_p)}\int_{p_6}^{\infty}e^{i\pi t^2/2}\,dt\right] . \quad (A.13)$$

After evaluating the integral in (A.12) and introducing $V_1(\theta)$ in (A.11) we obtain the following as the contribution to the far field due to $V_1(\theta)$:

$$E^t_{\phi_1}(P)=\eta_o I_{p_o}(\frac{kB}{2})J_1(kB\cos\phi_p)\frac{e^{ikR}}{R}\frac{\cos^{1/2}\phi_o}{\sin^{1/2}\theta}\times\left[-2i\sin(kH\cos\theta)\right] . \quad (A.14)$$

We now demand that $V_1(\theta)$ should contribute the correct incident and reflected field as given in (A. 4). After comparing (A.14) and (A.4) we see that (A.7) should be multiplied by the factor

$$\frac{J_1(kB\sin\theta)}{J_1(kB\cos\phi_p)}\left(\frac{\sin\theta}{\sin\phi_p}\right)^{1/2}$$

so that the contribution due to $V_1(\theta)$ in (A.11) yields the correct field given by (A.4). Hence the modified (A.7) yielding the correct incident and reflected field is:

$$E'_\phi(P)=\eta_o I_{p_o}\left(\frac{kB}{2}\right)J_1(kB\sin\theta)\frac{e^{ik(R-A\sin\theta)}}{R}V(\theta), \qquad (A.15)$$

where $V(\theta)=V_1(\theta)+V_2(\theta)$ as before.

Now consider the contribution due to $V_2(\theta)$. In evaluating the integrals in (A.13), we make the following approximation[4]

$$\int_p^\infty e^{i\pi t^2/2}\,dt \simeq \frac{e^{i\pi p^2/2}}{i\pi p}, \quad \text{for } p \gg 1. \qquad (A.16)$$

Using (A.16), $V_2(\theta)$ given by (A.13) may be expressed as follows;

$$V_2(\theta)=\frac{e^{ikr_p}}{\sqrt{\pi kr_p}}e^{i\pi/4}\,\frac{\cos\theta\sin\frac{\phi_p}{2}}{(1-\sin\theta)^{1/2}(\cos\phi_p-\sin\theta)}. \qquad (A.17)$$

After introducing (A.17) into (A.15) we obtain the following as the contribution to the far field at $P(R,\theta)$ due to $V_2(\theta)$:

$$E'_{\phi_1}(P)=\eta_o I_{p_o}\left(\frac{kB}{2}\right)J_1(kB\sin\theta)\frac{e^{ik(R-A\sin\theta+r_p)}}{R\sqrt{\pi kr_p}}e^{i\pi/4}\times\frac{\cos\theta\sin\frac{\phi_p}{2}}{(1-\sin\theta)^{1/2}(\cos\phi_p-\sin\theta)}. \qquad (A.18)$$

After comparing (A.18) with (A.5) we find that in order to obtain the correct near edge diffracted field from the contribution of $V_2(\theta)$ in (A.15), we must add the following to (A.15):

$$E_{\phi}^{c}(P)=\eta_o I_{p_o}\left(\frac{kB}{2}\right)\frac{e^{ik(R-A\sin\theta+r_p)}}{R\sqrt{\pi kr_p}}\,e^{i\pi/4}\,\frac{\cos\theta\sin\frac{\phi_p}{2}}{(\cos\phi_p-\sin\theta)}$$

$$\frac{\left[\cos^{1/2}\phi_p J_1(kB\cos\phi_p)-\sin^{1/2}\theta\, J_1(kB\sin\theta)\right]}{(1-\sin\theta)^{1/2}\,(\sin\theta)^{1/2}}\,. \qquad (A.19)$$

The composite expression obtained by adding (A.15) and (A.19) will give the correct near edge diffraction field in the shadow region if $\cos\theta$ in (A.19) is replaced by $|\cos\theta|$. The far edge diffracted field given by (A.6) will give the corresponding field in the shadow region if $\cos\theta$ is replaced by $|\cos\theta|$. With this in mind we now add (A.15), (A.19) and (A.6), and after some rearrangement of the terms obtain the following for the far field valid in the region $0 < \theta < \pi$, for $kA \gg 1$, $kB \gg 1$ and $kA > kB$:

$$E_{\phi}(P)=\eta_o I_{p_o}\left(\frac{kB}{2}\right)\frac{e^{i(kR-\pi/4)}}{R}\,F(\theta)\,, \qquad (A.20)$$

where

$$F(\theta)=\frac{J_1(kB\sin\theta)}{\sqrt{2}}F^{p}(\theta)e^{ikA\sin\theta}+\frac{|\cos\theta|\,\sin\left(\frac{\phi_p}{2}\right)}{\sqrt{\pi kr_p\sin\theta}}\,e^{ikr_p}\,L^{p}(\theta)\,, \qquad (A.21)$$

$$L^{p}(\theta)=\frac{e^{i\left(\frac{\pi}{2}-kA\sin\theta\right)}}{\sqrt{1-\sin\theta}}\left[\frac{\cos^{1/2}\phi_p J_1(kB\cos\phi_p)-\sin^{1/2}\theta J_1(kB\sin\theta)}{\cos\phi_p-\sin\theta}\right]$$

$$-\frac{e^{ikA\sin\theta}}{\sqrt{1+\sin\theta}}\left[\frac{J_1(kB\cos\phi_p)\cos^{1/2}\phi_p}{\cos\phi_p+\sin\theta}\right]\,, \qquad (A.22)$$

$$F^{p}(\theta)=e^{ikr_p\sin(\theta-\phi_p)}\int_{-\infty}^{p_5}e^{i\pi t^2/2}\,dt-e^{ikr_p\sin(\theta+\phi_p)}\int_{-\infty}^{p_6}e^{i\pi t^2/2}\,dt\,, \qquad (A.23)$$

$$p_5=2\left(\frac{kr_p}{\pi}\right)^{1/2}\cos\left(\frac{\phi_p-\theta-\pi/2}{2}\right)\,, \qquad (A.24)$$

$$p_6=2\left(\frac{kr_p}{\pi}\right)^{1/2}\cos\left(\frac{\phi_p+\theta+\pi/4}{2}\right) , \tag{A.25}$$

$$r_p^2=A^2+H^2 , \tag{A.26}$$

$$\tan\phi_p=\frac{H}{A} . \tag{A.27}$$

Equation (A.20) was quoted without derivation as Eq. (3.28) in Section 3.2.5. It should be noted that with proper definitions of the parameters r_p, p_5, p_6, H and ϕ_p Eq. (A.20) reduces to (2.1) provided we make the small argument approximation for the Bessel function $J_1(\rho)\simeq \rho/2$.

If the field is desired only within the illuminated region, for computational advantages it is better to use Eqs. (A.4) - (A.6) for the far field expression. By adding (A.4), (A.5) and (A.6) it can be shown that the far field in the illuminated region $0<\theta<\frac{\pi}{2}-\phi_p$ is given by the following expression:

$$E_\phi=\eta_o I_{p_o}\left(\frac{kB}{2}\right)\frac{e^{ikR}}{R}\left[-2i\sin(kH\cos\theta)J_1(kB\sin\theta)\right.$$

$$\left.+J_1(kB\cos\phi_p)\cos\theta\sin\left(\frac{\phi_p}{2}\right)\left(\frac{\cos\phi_p}{\pi kr_p\sin\theta}\right)^{1/2}e^{i(kr_p+\pi/4)}\,G(\theta)\right], \tag{A.28}$$

where

$$G(\theta)=\frac{e^{-ikA\sin\theta}}{(\cos\phi_p-\sin\theta)(1-\sin\theta)^{1/2}}+i\,\frac{e^{ikA\sin\theta}}{(\cos\phi_p+\sin\theta)(1+\sin\theta)^{1/2}} . \tag{A.29}$$

In some practical cases the field in the direction $\theta=\pi/2$ may be of special interest. It can be shown that for a point $P(R,\frac{\pi}{2})$ lying in the direction $\theta=\pi/2$, (A.20) - (A.25) reduce to the following:

$$E(R,\tfrac{\pi}{2})=\eta_o I_{p_o}\left(\frac{kB}{2}\right)\frac{e^{i(kR-\pi/4)}}{R}\times\left[\sqrt{2}\,J_1(kB)\int_0^p e^{i\pi t^2/2}dt\right.$$

$$\left.+\frac{2\sin\frac{\phi_p}{2}}{\pi kr_p}e^{i(\frac{\pi}{2}-kA)}\times\frac{\cos^{1/2}\phi_p J_1(kB\cos\phi_p)-J_1(kB)}{\cos\phi_p-1}\right], \tag{A.30}$$

where

$$p=2\left(\frac{kr_p}{\pi}\right)^{1/2}\sin\frac{\phi_p}{2} . \tag{A.31}$$

APPENDIX B

COMPUTER PROGRAM FOR EVALUATING $S^{A}(\theta)$, $S(\theta)$ WITH IBM-360, MODEL-67.

```
0001          IMPLICIT REAL*8(A,B,D-H,K,O-Z),COMPLEX*16(C)
0002          REAL*8 CDABS
0003          COMPLEX*16 DCMPLX
0004          CEIX(XX) = DCMPLX(DCOS(XX),DSIN(XX))
0005          LOGICAL TERM/.FALSE./
0006          DATA SQ2/1.4142135623731/, PI/3.141592653589 79/
0007          DATA POT/1.5707963267949/, EGAM/.577215664901533/
0008          DATA RCON/.01745329251992/, POF/.785398163397448/
0009          DATA KH/2.758D0/,KCBPI/0.D0/,NTL/3/,ITS/1/
0010          DATA KA/17.92D0/,KCB/12.56637D0/,KCH/3.75D0/,KB/.15D0/
0011          REAL*8 TH1(10)/5.D0,82.D0,115.D0,7*0.D0/,TH2(10)/80.D0,110.D0,
             & 170.D0,7*0.D0/, THS(10)/5.D0,2.D0,5.D0,7*0.D0/
0012          CALL FCVTHB(1)
0013    10    WRITE (6,999)
0014    999   FORMAT ('1')
0015          NAMELIST /IN/ TH1,TH2,THS,KH,KA,KB,KCB,KCH,TERM,KCBPI,NTL,ITS
0016          READ (1,IN,END=500)
0017          IF (KCBPI.NE.0.D0) KCB = KCBPI*PI
0018          KCBPI = 0.D0
0019          WRITE (6,1000) KH,KB,KA,KCH,KCB
0020    1000  FORMAT ('  KH = 'G15.7'  KB = 'G15.7'  KA = 'G15.7/
             &' KCH = 'G15.7' KCB = 'G15.7/1X)
0021          IF (.NOT.TERM) WRITE (6,2000)
0022    2000  FORMAT ('-'4X'THETA'5X'RE(SP+SP2)'5X'IM(SP+SP2)'4X'ARG(SP+SP2)'4X
             &' |SP+SP2|  '7X'RE(S)'10X'IM(S)'10X'SQ |S|'9X'|S| DB'/1X)
0023          CPLKB = DCMPLX(POT,EGAM+DLOG(KB*.5D0))
0024          DO 100 IT=ITS,NTL
0025          THSIT = THS(IT)
0026          IF (THSIT) 75,76,75
0027    75    NRT = (TH2(IT)-TH1(IT))/THSIT + 1.5
0028          GO TO 77
0029    76    NRT = 1
0030    77    THL = TH1(IT)-THSIT
0031          DO 100 I=1,NRT
0032          TH = (THL+I*THSIT)*RCON
0033          CALL FCAL(KH,KA,TH,PHZ,KRZ,CFZ)
0034          CALL FCAL(KCH,KA,TH,PHP,KRP,CFP)
0035          TS = DSIN(TH)
0036          TC = DCOS(TH)
0037          CALL LFAC(TS,TC,KA,CF1,CF2,CTA)
0038          TS1 = DSQRT(TS)
0039          PC = DCOS(PHP)
0040          PC1 = DSQRT(PC)
0041          BSL1 = DJONE(KCB*PC)
0042          BSL2 = DJONE(KCB*TS)
0043          T1 = (PC1*BSL1-TS1*BSL2)/(PC-TS)
0044          T2 = PC1*BSL1/(PC+TS)
0045          CLP = CF1*T1 - CF2*T2
0046          PC = DCOS(PHZ)
0047          PC1 = DSQRT(PC*PC*PC)
0048          TS1 = TS1*TS1*TS1
0049          T1 = (PC1-TS1)/(PC-TS)
0050          T2 = PC1 / (PC+TS)
0051          CLZ = CF1*T1 - CF2*T2
0052          T1 = DSIN(PHZ*.5D0)/DSQRT(PI*KRZ*TS)
```

```
0053                CXZ = CEIX(KRZ)
0054                CSA = (TS/SQ2)*CFZ*CTA + T1*CXZ*CLZ
0055                T1 = KCB*KCB
0056                T2 = PI*T1
0057                KR1S = T1 + (KCH-KH)**2
0058                CX1 = CEIX(DSQRT(KR1S))/KR1S
0059                KR2S = T1 + (KCH+KH)**2
0060                CT3 = CEIX(DSQRT(KR2S))/KR2S
0061                CT1 = (T2/CPLKB)*(CX1-CT3)
0062                CT2 = (BSL2/SQ2)*CFP*CTA
0063                T1 = DSIN(PHP*.5D0)/DSQRT(PI*KRP*TS)
0064                CT2 = CT2 + T1*CLP*CFIX(KRP)
0065                CSP = CT1 * CT2
0066                T1 = PI*KCB
0067                T1 = DSQRT(T1*T1*T1)
0068                CT1 = CEIX(KCB+KCB+POF) - DSQRT(KCB/KCH)*CEIX(KCB+KCB-POF)
0069                CT1 = CT1 * CX1 * T1
0070                CT1 = CT1 / (-2.D0*CPLKB*CPLKB)
0071                CSP2 = CT1*CT2
0072                ASA = CDABS(CSA)**2
0073                DBCSA = 10.D0*DLOG10(ASA)
0074                CSUM = CSP+CSP2
0075                ASUM = CDABS(CSUM)
0076                ARCSUM = ARGC(CSUM)/RCON
0077                IF (ARCSUM .LT. 0.) ARCSUM = ARCSUM + 360.
0078                DASUM = 10.D0*DLOG10(ASUM)
0079                CS = CSA+CSP+CSP2
0080                ACS = CDABS(CS)**2
0081                DBSUM = 10.D0*DLOG10(ACS)
0082                TH = TH/RCON
0083                IF (TERM) GO TO 79
0084                WRITE (6,2001) TH,CSUM,ARCSUM,ASUM,CS,ACS,DBSUM
0085          2001  FORMAT (F12.4,8G15.7)
0086                GO TO 100
0087          79    WRITE (6,1001) TH,CSA,CSUM,CS,ACS,DBSUM
0088          1001  FORMAT ('0TH = 'G15.7' SA = '2G15.7/' SP+SP2 = '2G15.7/
                   &' S = '2G15.7/' /S/ SQ = 'G15.7' /S/ DB = 'G15.7)
0089          100   CONTINUE
0090                GO TO 10
0091          500   CALL SYSTEM
0092                END
```

SUBROUTINE

FORTRAN IV G COMPILER LFAC

```
0001            SUBROUTINE LFAC(TS,TC,KA,CF1,CF2,CTA)
0002            IMPLICIT REAL*8(A,B,D-H,K,O-Z),COMPLEX*16(C)
0003            COMPLEX*16 DCMPLX
0004            DATA SQRT2/1.414213562373 1/
0005            T2 = KA*TS
0006            T1 = DCOS(T2)
0007            T2 = DSIN(T2)
0008            CTA = DCMPLX(T1,-T2)
0009            ATC = DABS(TC)
0010            IF (ATC.LT.1.D-8) GO TO 60
0011            T = ATC/DSQRT(1.D0-TS)
0012            CF1 = T*DCMPLX(T2,T1)
0013            T = ATC/DSQRT(1.D0+TS)
0014            CF2 = T*DCMPLX(T1,T2)
0015            RETURN
0016         60 CF1 = SQRT2*DCMPLX(T2,T1)
0017            CF2 = 0.D0
0018            RETURN
0019            END
```

SUBROUTINE

```
FORTRAN IV G COMPILER        FCAL          04-26-68        18:13:38

0001                 SUBROUTINE FCAL(KH,KA,TH,PHI,KR,CFZZ)
0002                 IMPLICIT REAL*8 (A,B,D-H,K,O-Z),COMPLEX*16(C)
0003                 COMPLEX*16 DCMPLX
0004                 CEIX(XX) = DCMPLX(DCOS(XX),DSIN(XX))
0005                 DATA SQ2/1.41421356237321/, PI/3.14159265358979/
0006                 DATA POT/1.57079632679349/
0007                 PHI = DATAN2(KH,KA)
0008                 KR = DSQRT(KA*KA+KH*KH)
0009                 P2 = 2.DO*DSQRT(KR/PI)
0010                 P1 = P2*DCOS((PHI-TH-POT)/2.DO)
0011                 P2 = P2*DCOS((PHI+TH+POT)/2.DO)
0012                 CALL FRNL(A,B,P1)
0013                 CF1 = DCMPLX(A,B)
0014                 CALL FRNL(A,B,P2)
0015                 CF2 = DCMPLX(A,B)
0016                 CA = CEIX(KR*DSIN(TH-PHI))
0017                 CB = CEIX(KR*DSIN(TH+PHI))
0018                 CFZZ = CA-CB
0019                 CFZZ = CFZZ*(.5DO,.5DO)
0020                 CA = CA*CF1
0021                 CB = CB*CF2
0022                 CFZZ = CFZZ+CA-CB
0023                 RETURN
0024                 END
```

SUBROUTINE

```
0001          SUBROUTINE FRNL(C,S,XX)
0002          IMPLICIT REAL*8 (A-H,O-Z)
0003          ZZ = XX*1.2533141373155
0004          Z = ZZ*ZZ
0005          GO TO 3
0006          ENTRY CS(C,S,X)
0007          Z = DABS(X)
0008          ZZ = DSQRT(Z)
0009    3     IF (Z.GT.4.D0) GO TO 4
0010          C = ZZ
0011          S = Z*C
0012          Z = Z*Z
0013          C = C*(((((((.50998348D-10*Z-.10140729D-7)*Z+.11605284D-5)*Z
              & -.85224622D-4)*Z+.36938586D-2)*Z-.079788405)*Z+.79788455)
0014          S = S*(((((-.66777447D-9*Z+.11225331D-6)*Z-.10525853D-4)*Z
              & +.60435371D-3)*Z-.18997110D-1)*Z+.26596149)
0015          RETURN
              C
0016    4     D = DCOS(Z)
0017          S = DSIN(Z)
0018          Z = 4.D0/Z
0019          A = (((((((.87682583D-3*Z-.41692894D-2)*Z+.79709430D-2)*Z
              & -.67928011D-2)*Z-.30953412D-3)*Z+.59721508D-2)*Z-.16064281D-4)*Z
              & -.024933215)*Z-.44440909D-8
0020          B = ((((((-.66339256D-3*Z+.34014090D-2)*Z-.72716901D-2)*Z
              & +.74282459D-2)*Z-.40271450D-3)*Z-.93149105D-2)*Z-.12079984D-5)*Z
              & +.19947115
0021          Z = DSIGN(.5D0,ZZ)
0022          ZZ = 2.D0/ZZ
0023          C = Z + ZZ*(D*A+S*B)
0024          S = Z + ZZ*(S*A-D*B)
0025          RETURN
0026          END
```

SUBROUTINE

```
0001          FUNCTION DJONE(X)
0002          IMPLICIT REAL*8 (A-Z)
0003          REAL*8 CJ1(7)/.5D0,-.56249985,.21093573,-.3954289D-1,.443319D-2,
             & -.31761D-3,.1109D-4/
0004          REAL*8 CY1(7)/-.6366198D0,.2212091D0,2.1682709,-1.3164827,
             & .3123951D0,-.400976D-1,.27873D-2/
0005          REAL*8 CF1(7)/.79788456,.156D-5,.1659667D-1,.17105D-3,-.249511D-2,
             & .113653D-2,-.20033D-3/
0006          REAL*8 CT1(7)/-2.35619449,.12499612,.565D-4,-.637879D-2,.74348D-3,
             & .79824D-3,-.29166D-3/
0007          ENTRY JONE(X)
0008          IF (DABS(X) .LE. 3.D0) GO TO 600
0009          TOX = 3.D0 / X
0010          F1 = P(TOX,CF1,7)
0011          T1 = X + P(TOX,CT1,7)
0012          JONE = F1*DCOS(T1)/DSQRT(DABS(X))
0013    98    DJONE = JONE
0014    99     RETURN
0015    600   TOX = X*X/9.D0
0016    9     JONE = X*P(TOX,CJ1,7)
0017          GO TO 98
0018          ENTRY YONE(X)
0019          IF (X .LE. 3.D0) GO TO 700
0020          TOX = 3.D0 / X
0021          F1 = P(TOX,CF1,7)
0022          T1 = X + P(TOX,CT1,7)
0023          YONE = F1*DSIN(T1)/DSQRT(X)
0024          RETURN
0025    700   TOX = X*X/9.D0
0026          F1 = .6366197723676*X*DLOG(X/2.D0)*P(TOX,CJ1,7)
0027          YONE = F1 + P(TOX,CY1,7)/X
0028          RETURN
0029          END
```

APPENDIX C

THEORETICAL ELEVATION PATTERNS OF ALFORD LOOP COUNTERPOISE ANTENNA

The far field produced by an Alford loop above a counterpoise is given by the following expression:

$$E_{\phi}^{A} \sim \eta_o I_o \left(\frac{ka}{2}\right)^2 \frac{e^{i(kR-\pi/4)}}{R} S^{A}(\theta) \quad , \tag{C.1}$$

where the various notations are as explained in Section 2.2. The term $S^{A}(\theta)$ is identified with the complex far field elevation pattern produced by the Alford loop counterpoise antenna. The complete expression for $S^{A}(\theta)$ is given by Eqs. (2.2) - (2.8). $S^{A}(\theta)$ has been computed in the range $0 < \theta < \pi$ for different values of the counterpoise radius A and a fixed value of h. The results of the computation are given in Tables C-1 - C-6. The following explanatory notes will be helpful in using the tables.

The elevation pattern $S^{A}(\theta)$ is expressed in the complex form as follows:

$$S^{A}(\theta) = \text{Re } S^{A}(\theta) + i \text{ Im } S^{A}(\theta) \tag{C.2}$$

where Re $S^{A}(\theta)$, Im $S^{A}(\theta)$ represent the real and imaginary parts respectively of $S^{A}(\theta)$. In all the tables the different columns represent:

Column 1	gives the elevation angle θ
Column 2	gives the real part of $S^{A}(\theta)$
Column 3	gives the imaginary part of $S^{A}(\theta)$
Column 4	gives $\lvert S^{A}(\theta) \rvert^2$ which is the power pattern
Column 5	gives $20 \log_{10} \lvert S^{A}(\theta) \rvert$.

The phase of the far field can be easily obtained from Columns 2 and 3.

TABLE C-4: kB = 2.750000, kA = 4.993000

THETA	RE(SA)	IM(SA)	SQ |SA|	|SA| DB
5.0000	-0.7318962D-02	-0.3183489D-01	0.1067028D-02	-29.71824
10.0000	0.1602480	-0.3396091D-01	0.2683277D-01	-15.71335
15.0000	0.2908073	-0.9376230D-01	0.9836027D-01	-10.29838
20.0000	0.4013844	-0.2099433	0.2051857	-6.878530
25.0000	0.4949663	-0.3728095	0.3839785	-4.156931
30.0000	0.5739326	-0.5624557	0.6457550	-1.899322
35.0000	0.6425416	-0.7532826	0.9802945	-0.8643447
40.0000	0.7066404	-0.9194650	1.344756	1.286436
45.0000	0.7719207	-1.039299	1.676004	2.242750
50.0000	0.8416416	-1.097692	1.913289	2.817806
55.0000	0.9147507	-1.087020	2.018382	3.050034
60.0000	0.9851334	-1.006992	1.984521	2.976556
65.0000	1.042304	-0.8641043	1.833075	2.631802
70.0000	1.073422	-0.6709173	1.602366	2.047616
75.0000	1.066138	-0.4450558	1.334724	1.253914
80.0000	1.011600	-0.2077204	1.066482	0.2795335
82.0000	0.9756674	-0.1146591	0.9650736	-0.1543958
84.0000	0.9317655	-0.2483765D-01	0.8688038	-0.6107828
86.0000	0.8802273	0.6036622D-01	0.7784443	-1.087725
88.0000	0.8215809	0.1396625	0.6945008	-1.583273
90.0000	0.7565400	0.2116777	0.6172450	-2.095424
92.0000	0.6861445	0.2750989	0.5464737	-2.624307
94.0000	0.6112559	0.3293376	0.4820971	-3.168655
96.0000	0.5330169	0.3739109	0.4239164	-3.727198
98.0000	0.4526682	0.4083400	0.3716501	-4.298658
100.0000	0.3715168	0.4323625	0.3249620	-4.881674
102.0000	0.2909021	0.4459386	0.2834852	-5.474695
104.0000	0.2121611	0.4492528	0.2468404	-6.075837
106.0000	0.1365943	0.4427094	0.2146496	-6.682699
108.0000	0.6543182D-01	0.4269227	0.1865443	-7.292179
110.0000	-0.1978014D-03	0.4027028	0.1621696	-7.900305
115.0000	-0.1338972	0.3120972	0.1153331	-9.380459
120.0000	-0.2162103	0.1943518	0.8451954D-01	-10.73043
125.0000	-0.2436805	0.7141073D-01	0.6447968D-01	-11.90577
130.0000	-0.2207825	-0.3526830D-01	0.4998877D-01	-13.01128
135.0000	-0.1590450	-0.1083331	0.3703137D-01	-14.31430
140.0000	-0.7499427D-01	-0.1378303	0.2462134D-01	-16.08688
145.0000	0.1276187D-01	-0.1235029	0.1541583D-01	-18.12033
150.0000	0.8677987D-01	-0.7530295D-01	0.1320128D-01	-18.79384
155.0000	0.1336217	-0.1146494D-01	0.1798621D-01	-17.45060
160.0000	0.1455060	0.4598506D-01	0.2328203D-01	-16.32979
165.0000	0.1200672	0.7697785D-01	0.2034172D-01	-16.91612
170.0000	0.5712274D-01	0.6916435D-01	0.8046715D-02	-20.94381

TABLE C-2: kh = 2.750000, kA = 10.34000

THETA	RE(SA)	IM(SA)	SQ |SA|	|SA| DB
5.0000	0.4189484D-01	-0.7404572D-01	0.7237947D-02	-21.40385
10.0000	0.2730642D-01	-0.1599882	0.2634185D-01	-15.79354
15.0000	0.8549802D-01	-0.2014075	0.4787490D-01	-13.19892
20.0000	0.2087572	-0.2338198	0.9825124D-01	-10.07662
25.0000	0.3770130	-0.3020758	0.2333886	-6.319204
30.0000	0.5583464	-0.4346914	0.5007073	-3.004161
35.0000	0.7209331	-0.6267114	0.9125118	-0.3976153
40.0000	0.8447479	-0.8428692	1.424028	1.535184
45.0000	0.9262730	-1.035155	1.929528	2.854512
50.0000	0.9747592	-1.161908	2.300186	3.617629
55.0000	1.003601	-1.199112	2.445084	3.882938
60.0000	1.022094	-1.142226	2.349357	3.709490
65.0000	1.031216	-1.002050	2.067511	3.154479
70.0000	1.024110	-0.7990158	1.687228	2.271737
75.0000	0.9898519	-0.5584590	1.291683	1.111560
80.0000	0.9183464	-0.3073693	0.9378359	-0.2787315
82.0000	0.8779513	-0.2099402	0.8148733	-0.8890989
84.0000	0.8307134	-0.1166388	0.7036894	-1.526190
86.0000	0.7768561	-0.2894614D-01	0.6043433	-2.187163
88.0000	0.7168235	0.5177928D-01	0.5165171	-2.869153
90.0000	0.6512765	0.1243257	0.4396179	-3.569246
92.0000	0.5813872	0.1872157	0.3730607	-4.282205
94.0000	0.5078847	0.2400253	0.3155590	-5.009195
96.0000	0.4319648	0.2821098	0.2661795	-5.748253
98.0000	0.3549521	0.3130590	0.2239969	-6.497579
100.0000	0.2782635	0.3327136	0.1881289	-7.255445
102.0000	0.2033686	0.3411766	0.1577602	-8.020025
104.0000	0.1317465	0.3388207	0.1321566	-8.789112
106.0000	0.6484046D-01	0.3262901	0.1106695	-9.559719
108.0000	0.4011359D-02	0.3044959	0.9273384D-01	-10.32762
110.0000	-0.4951012D-01	0.2746044	0.7785881D-01	-11.08692
115.0000	-0.1449854	0.1741515	0.5134950D-01	-12.89464
120.0000	-0.1792495	0.5911774D-01	0.3562528D-01	-14.48242
125.0000	-0.1548307	-0.4068102D-01	0.2562748D-01	-15.91294
130.0000	-0.8766487D-01	-0.9948389D-01	0.1758217D-01	-17.54927
135.0000	-0.4692763D-02	-0.1041897	0.1087752D-01	-19.63470
140.0000	0.6311326D-01	-0.6123456D-01	0.7732955D-02	-21.11655
145.0000	0.9115336D-01	0.3068307D-02	0.8318349D-02	-20.79963
150.0000	0.7119369D-01	0.5246132D-01	0.7820731D-02	-21.06753
155.0000	0.1566850D-01	0.5926876D-01	0.3758287D-02	-24.25010
160.0000	-0.4712124D-01	0.2205863D-01	0.2706995D-02	-25.67513
165.0000	-0.8524213D-01	-0.3066737D-01	0.8206709D-02	-20.85831
170.0000	-0.7581885D-01	-0.5686289D-01	0.8981886D-02	-20.46632

TABLE C-3: $kh = 2.750000$, $kA = 13.74000$

THETA	RE(SA)	IM(SA)	SQ |SA|	|SA| DB
5.0000	0.7280129D-01	-0.1382008D-01	0.5491022D-02	-22.60347
10.0000	0.1618747	-0.5873657D-01	0.2965340D-01	-15.27925
15.0000	0.2023407	-0.1751153	0.7160711D-01	-11.45044
20.0000	0.2345164	-0.2977389	0.1436464	-8.427052
25.0000	0.3098724	-0.3851576	0.2443673	-6.119570
30.0000	0.4555382	-0.4599595	0.4190778	-3.777053
35.0000	0.6520306	-0.5757697	0.7566547	-1.211023
40.0000	0.8471082	-0.7559703	1.289083	1.102810
45.0000	0.9917176	-0.9683712	1.921247	2.835831
50.0000	1.066722	-1.148646	2.457282	3.904550
55.0000	1.083632	-1.240139	2.712203	4.333222
60.0000	1.066923	-1.217735	2.621204	4.185009
65.0000	1.035493	-1.088460	2.256992	3.535301
70.0000	0.9943259	-0.8794556	1.762126	2.460370
75.0000	0.9367064	-0.6253981	1.268542	1.033047
80.0000	0.8516547	-0.3606924	0.8554148	-0.6782323
82.0000	0.8079739	-0.2588571	0.7198288	-1.427708
84.0000	0.7583916	-0.1620185	0.6014078	-2.208309
86.0000	0.7029780	-0.7176752D-01	0.4993286	-3.016136
88.0000	0.6420606	0.1046715D-01	0.4123513	-3.847326
90.0000	0.5762265	0.8342555D-01	0.3389985	-4.698023
92.0000	0.5066242	0.1459035	0.2779559	-5.560241
94.0000	0.4340065	0.1972039	0.2272511	-6.434941
96.0000	0.3596431	0.2367301	0.1853843	-7.319271
98.0000	0.2849748	0.2641421	0.1509817	-8.210758
100.0000	0.2115719	0.2793904	0.1228217	-9.107250
102.0000	0.1410846	0.2827378	0.9984550D-01	-10.00672
104.0000	0.7518591D-01	0.2747780	0.8115588D-01	-10.90680
106.0000	0.1550809D-01	0.2564498	0.6600648D-01	-11.80413
108.0000	-0.3642882D-01	0.2290358	0.5378444D-01	-12.69343
110.0000	-0.7929426D-01	0.1941646	0.4398746D-01	-13.56671
115.0000	-0.1407081	0.8774142D-01	0.2749732D-01	-15.60710
120.0000	-0.1344202	-0.1639135D-01	0.1833748D-01	-17.36660
125.0000	-0.7479925D-01	-0.8170780D-01	0.1227109D-01	-19.11117
130.0000	0.4297534D-02	-0.8622149D-01	0.7452615D-02	-21.27691
135.0000	0.6075191D-01	-0.3740554D-01	0.5089968D-02	-22.93285
140.0000	0.6547357D-01	0.2566434D-01	0.4945447D-02	-23.05794
145.0000	0.2225091D-01	0.5401007D-01	0.3412190D-02	-24.66967
150.0000	-0.3161448D-01	0.2719318D-01	0.1738944D-02	-27.59714
155.0000	-0.5147214D-01	-0.2381307D-01	0.3216443D-02	-24.92624
160.0000	-0.2136197D-01	-0.4186052D-01	0.2208637D-02	-26.55876
165.0000	0.3160051D-01	-0.4375142D-02	0.1017734D-02	-29.92366
170.0000	0.5874944D-01	0.4438870D-01	0.5421853D-02	-22.65852

TABLE C-4: kh = 2.750000, kA = 17.92000

THETA	RE(SA)	IM(SA)	SQ |SA|	|SA| DB
5.0000	0.5772935D-01	-0.9584591D-01	0.1251912D-01	-19.02426
10.0000	0.9646671D-01	-0.1399903	0.2890312D-01	-15.39055
15.0000	0.1567395	-0.1430116	0.4501959D-01	-13.46598
20.0000	0.2660704	-0.2228759	0.1204671	-9.191314
25.0000	0.3827133	-0.3804236	0.2911916	-5.358212
30.0000	0.4790196	-0.5262772	0.5064275	-2.954828
35.0000	0.5966636	-0.6258072	0.7476421	-1.263063
40.0000	0.7730752	-0.7339938	1.136392	0.5552823
45.0000	0.9708266	-0.8999007	1.752326	2.436148
50.0000	1.113462	-1.094396	2.437501	3.869448
55.0000	1.160419	-1.236835	2.876329	4.588385
60.0000	1.128228	-1.262251	2.866176	4.573029
65.0000	1.057740	-1.156383	2.456036	3.902348
70.0000	0.9776063	-0.9472533	1.853003	2.678761
75.0000	0.8927447	-0.6805042	1.260079	1.003978
80.0000	0.7929542	-0.4010644	0.7896290	-1.025769
82.0000	0.7460390	-0.2943213	0.6431992	-1.916545
84.0000	0.6943121	-0.1935248	0.5195212	-2.843967
86.0000	0.6375998	-0.1004144	0.4166165	-3.802635
88.0000	0.5760426	-0.1651285D-01	0.3320977	-4.787341
90.0000	0.5101075	0.5687626D-01	0.2634446	-5.793107
92.0000	0.4406062	0.1189235	0.2082766	-6.813595
94.0000	0.3686284	0.1685570	0.1642983	-7.843669
96.0000	0.2955636	0.2052238	0.1294746	-8.878153
98.0000	0.2230398	0.2286779	0.1020403	-9.912281
100.0000	0.1528713	0.2390184	0.8049945D-01	-10.94207
102.0000	0.8699212D-01	0.2367301	0.6360875D-01	-11.96483
104.0000	0.2737189D-01	0.2227221	0.5035434D-01	-12.97963
106.0000	-0.2408717D-01	0.1983591	0.3992651D-01	-13.98739
108.0000	-0.6567446D-01	0.1654760	0.3169545D-01	-14.99003
110.0000	-0.9601380D-01	0.1263669	0.2518723D-01	-15.98820
115.0000	-0.1184617	0.1981810D-01	0.1442593D-01	-18.40856
120.0000	-0.7311594D-01	-0.6090763D-01	0.9055679D-02	-20.43079
125.0000	0.1986353D-02	-0.7840347D-01	0.6151050D-02	-22.11051
130.0000	0.5103820D-01	-0.3197182D-01	0.3627095D-02	-24.40441
135.0000	0.3986087D-01	0.3106498D-01	0.2553922D-02	-25.92792
140.0000	-0.8559417D-02	0.4764090D-01	0.2342919D-02	-26.30243
145.0000	-0.3311611D-01	0.3972581D-02	0.1112458D-02	-29.53716
150.0000	-0.8133113D-02	-0.3912449D-01	0.1596873D-02	-27.96730
155.0000	0.2136876D-01	-0.1907910D-01	0.8206361D-03	-30.85849
160.0000	0.1019201D-01	0.3300252D-01	0.1193043D-02	-29.23344
165.0000	-0.1400064D-01	0.2772855D-01	0.9648901D-03	-30.15522
170.0000	-0.6658552D-02	-0.3686506D-01	0.1403369D-02	-28.52828

TABLE C-5: kh = 2.750000, kA = 34.47000

THETA	RE(SA)	IM(SA)	SQ |SA|	|SA| DB
5.0000	0.3463960D-01	-0.3235859D-01	0.2246980D-02	-26.48401
10.0000	0.1136654	-0.1164559	0.2648182D-01	-15.77052
15.0000	0.1605864	-0.1585087	0.5091300D-01	-12.93171
20.0000	0.2668658	-0.2666901	0.1423410	-8.466700
25.0000	0.3489614	-0.3534914	0.2467302	-6.077777
30.0000	0.5002848	-0.4892249	0.4896259	-3.101356
35.0000	0.6190433	-0.6367660	0.7886855	-1.030962
40.0000	0.7833957	-0.7653307	1.199440	0.7897848
45.0000	0.9448698	-0.9473152	1.790185	2.528979
50.0000	1.038925	-1.066157	2.216055	3.455805
55.0000	1.160583	-1.128156	2.619688	4.182496
60.0000	1.239838	-1.210420	3.002314	4.774561
65.0000	1.170540	-1.228707	2.879883	4.593749
70.0000	1.001446	-1.085881	2.182030	3.388607
75.0000	0.8267790	-0.8079897	1.336411	1.259400
80.0000	0.6767148	-0.4855049	0.6936580	-1.588546
82.0000	0.6197454	-0.3622031	0.5152755	-2.879605
84.0000	0.5618642	-0.2475894	0.3769919	-4.236680
86.0000	0.5017048	-0.1441876	0.2724977	-5.646371
88.0000	0.4384842	-0.5393756D-01	0.1951776	-7.095699
90.0000	0.3720962	0.2166574D-01	0.1389250	-8.572197
92.0000	0.3030478	0.8149881D-01	0.9848004D-01	-10.06652
94.0000	0.2327333	0.1247838	0.6973582D-01	-11.56544
96.0000	0.1631157	0.1511592	0.4945582D-01	-13.05783
98.0000	0.9674628D-01	0.1607960	0.3521521D-01	-14.53270
100.0000	0.3663201D-01	0.1545780	0.2523625D-01	-15.97975
102.0000	-0.1398973D-01	0.1343081	0.1823438D-01	-17.39109
104.0000	-0.5200158D-01	0.1028950	0.1329154D-01	-18.76425
106.0000	-0.7490144D-01	0.6443890D-01	0.9762597D-02	-20.10435
108.0000	-0.8142076D-01	0.2411452D-01	0.7210850D-02	-21.42014
110.0000	-0.7217459D-01	-0.1226049D-01	0.5359491D-02	-22.70876
115.0000	-0.5662059D-02	-0.5250539D-01	0.2788875D-02	-25.54571
120.0000	0.3849437D-01	-0.9075873D-02	0.1564188D-02	-28.05711
125.0000	0.2151852D-02	0.3027551D-01	0.9212371D-03	-30.35629
130.0000	-0.2349915D-01	-0.3732400D-02	0.5661408D-03	-32.47076
135.0000	0.1390410D-01	-0.1634953D-01	0.4606313D-03	-33.36647
140.0000	0.1761058D-02	0.1630400D-01	0.2689217D-03	-35.70374
145.0000	-0.1073647D-01	-0.6986221D-02	0.1640792D-03	-37.84947
150.0000	0.1313206D-01	-0.2072241D-02	0.1767453D-03	-37.52652
155.0000	-0.1238309D-01	0.7853155D-02	0.2150130D-03	-36.67535
160.0000	0.1098739D-01	-0.1081173D-01	0.2376162D-03	-36.24124
165.0000	-0.1015373D-01	0.1223146D-01	0.2527068D-03	-35.97383
170.0000	0.1054016D-01	-0.1333068D-01	0.2888019D-03	-35.39400

TABLE C-6: $\bar{kh}$ = 2.750000, kA = 51.69000

THETA	RE(SA)	IM(SA)	SQ |SA|	|SA| DB
5.0000	0.4334707D-01	-0.5450189D-01	0.4849424D-02	-23.14310
10.0000	0.1111561	-0.9738241D-01	0.2183900D-01	-16.60767
15.0000	0.1687257	-0.1679923	0.5668977D-01	-12.46495
20.0000	0.2509335	-0.2621242	0.1316767	-8.804910
25.0000	0.3683215	-0.3592847	0.2647462	-5.771702
30.0000	0.4829869	-0.4830643	0.4666275	-3.310297
35.0000	0.6294426	-0.6375197	0.8026294	-0.9548493
40.0000	0.7857858	-0.7727548	1.214609	0.8443662
45.0000	0.9244501	-0.9405928	1.739323	2.403802
50.0000	1.069255	-1.050380	2.246604	3.515265
55.0000	1.155923	-1.175124	2.717075	4.341016
60.0000	1.190003	-1.182866	2.815280	4.495216
65.0000	1.206597	-1.176753	2.840623	4.534135
70.0000	1.060788	-1.115374	2.369331	3.746257
75.0000	0.8276108	-0.8765387	1.453260	1.623432
80.0000	0.6286561	-0.5341049	0.6804765	-1.671869
82.0000	0.5619137	-0.3983814	0.4744547	-3.238053
84.0000	0.4985242	-0.2727317	0.3229090	-4.909199
86.0000	0.4356622	-0.1609342	0.2157013	-6.661472
88.0000	0.3713172	-0.6550988D-01	0.1421680	-8.471980
90.0000	0.3045959	0.1183805D-01	0.9291878D-01	-10.31896
92.0000	0.2358809	0.6992649D-01	0.6052950D-01	-12.18033
94.0000	0.1666908	0.1080373	0.3945786D-01	-14.03866
96.0000	0.9977563D-01	0.1260159	0.2583542D-01	-15.87784
98.0000	0.3891449D-01	0.1246178	0.1704394D-01	-17.68430
100.0000	-0.1142675D-01	0.1059780	0.1136190D-01	-19.44549
102.0000	-0.4675114D-01	0.7412596D-01	0.7680327D-02	-21.14620
104.0000	-0.6359234D-01	0.3526969D-01	0.5287937D-02	-22.76714
106.0000	-0.6092455D-01	-0.2499314D-02	0.3718048D-02	-24.29685
108.0000	-0.4156531D-01	-0.3047863D-01	0.2656622D-02	-25.75670
110.0000	-0.1283209D-01	-0.4175404D-01	0.1908062D-02	-27.19407
115.0000	0.3039496D-01	-0.5513260D-03	0.9241577D-03	-30.34254
120.0000	-0.1134052D-01	0.1847758D-01	0.4700284D-03	-33.27876
125.0000	-0.2508414D-02	-0.1669323D-01	0.2849560D-03	-35.45222
130.0000	0.6831151D-02	0.1204460D-01	0.1917370D-03	-37.17294
135.0000	-0.6515654D-02	-0.9627118D-02	0.1351351D-03	-38.69232
140.0000	0.4151156D-02	0.8879832D-02	0.9603851D-04	-40.17351
145.0000	-0.3371105D-03	-0.7739976D-02	0.6002088D-04	-42.21698
150.0000	-0.4165824D-02	0.4088371D-02	0.3406887D-04	-44.67642
155.0000	0.6977022D-02	0.2059827D-02	0.5292172D-04	-42.76366
160.0000	-0.4944922D-02	-0.6246794D-02	0.6346219D-04	-41.97485
165.0000	-0.2014430D-02	0.2747869D-02	0.1160871D-04	-49.35216
170.0000	0.8030793D-02	0.5742860D-02	0.9747408D-04	-40.11111

APPENDIX D

RADIATION CHARACTERISTICS OF A SINGLE PARASITIC LOOP COUNTERPOISE ANTENNA NEAR THE HORIZON

We give here the theoretical values for the complex far field produced by a single parasitic loop counterpoise antenna in the vicinity and below the horizon. The antenna has the following constant parameters; kh=2.75, kA=17.92 and kb=0.15. The normalized height kH and the normalized radius kB of the parasitic loop are varied over some selected values. Note that

$$S(\theta) = S^{A}(\theta) + S^{p}_{12}(\theta) + S^{p}_{56}(\theta)$$

in Tables D-1 through D-3.

The Tables D-4 through D-6 give the complex far field $S^{p}(\theta)$, produced by the parasitic current only above the counterpoise. The normalized height kH and the normalized radius kB of the parasitic loop are varied over some selected values. Note that

$$S^{p}(\theta) = S^{p}_{12}(\theta) + S^{p}_{56}(\theta)$$

for Tables D-4 through D-6.

The results given in these tables may be found useful for the design of a double parasitic loop counterpoise antenna whose far field radiation pattern is required to have a sharp minimum in a direction just below the horizon. Controlling the amplitude of this minimum, the field gradient at the horizon can also be controlled if desired. The complete pattern produced by the antenna can be obtained from the theoretical expressions given before.

TABLE D-1: S(θ) vs θ, kH = 3.7

θ (°)	kB = 3.8π		kB = 4.0 π		kB = 4.2 π	
	Re(S(θ)	ImS(θ)	ReS(θ)	ImS(θ)	Re S(θ)	ImS(θ)
90	0.25629	0.15064	0.30112	0.02619	0.42019	0.04460
92	0.20481	0.16701	0.26132	0.07261	0.35525	0.10574
94	0.15453	0.175496	0.21683	0.10835	0.28746	0.15067
96	0.10679	0.17598	0.17009	0.13289	0.21967	0.17984
98	0.16305	0.16881	0.12359	0.14640	0.15459	0.19428
100	0.02479	0.15485	0.07965	0.14971	0.09462	0.19557
102	-0.00676	0.13543	0.04025	0.14425	0.04172	0.18573
104	-0.03077	0.11230	0.00682	0.13187	-0.00271	0.16708
106	-0.04694	0.08743	-0.01987	0.11463	-0.03788	0.14211
108	-0.05561	0.06283	-0.06971	0.09456	-0.06364	0.11323
110	-0.05774	0.04024	-0.05318	0.07345	-0.08039	0.08263

TABLE D-2: S(θ) vs θ, kH = 3.8

90	0.24392	0.14453	0.29360	0.01797	0.41644	0.04044
92	0.19444	0.15971	0.25540	0.06442	0.35178	0.10163
94	0.14631	0.16727	0.21248	0.10025	0.28438	0.14644
96	0.10080	0.16715	0.16730	0.12497	0.21715	0.17542
98	0.05935	0.15975	0.12235	0.13881	0.15282	0.18968
100	0.02335	0.14598	0.07994	0.14266	0.09375	0.19090
102	-0.00606	0.12719	0.04196	0.13780	0.04185	0.18120
104	-0.02815	0.10514	0.00978	0.12669	-0.00157	0.16297
106	-0.04276	0.08177	-0.01595	0.11079	-0.03584	0.13870
108	-0.05037	0.05899	-0.03522	0.09227	-0.06093	0.11077
110	-0.05202	0.03840	-0.04859	0.07279	-0.07736	0.08128

TABLE D-3: S(θ) vs θ, kH = 4.0

90	0.21969	0.12918	0.27975	-0.00077	0.40959	0.03080
92	0.17455	0.14228	0.24483	0.04603	0.34548	0.09215
94	0.13102	0.14833	0.20516	0.08232	0.27894	0.13679
96	0.09029	0.14739	0.16321	0.10771	0.21295	0.16546
98	0.05367	0.13997	0.12146	0.12254	0.15023	0.17951
100	0.02237	0.12706	0.08215	0.12784	0.09310	0.18082
102	-0.00267	0.11006	0.04703	0.12515	0.04329	0.17166
104	-0.02098	0.09070	0.01725	0.11639	0.00192	0.15455
106	-0.03265	0.07083	-0.00672	0.10355	-0.03061	0.13199
108	-0.03841	0.05212	-0.02511	0.08845	-0.05452	0.10625
110	-0.03950	0.03589	-0.03864	0.07247	-0.07052	0.07922

TABLE D-4: $S^p(\theta)$ vs θ, kH = 11.6

	kB = 2.8π		kB = 3 π		kB = 3.2 π	
$\theta(^o)$	Re $S^p(\theta)$	Im $S^p(\theta)$	Re $S^p(\theta)$	Im $S^p(\theta)$	Re $S^p(\theta)$	Im $S^p(\theta)$
90	-0.08413	0.19023	-0.17060	0.10947	-0.08789	-0.05092
92	-0.15008	0.14954	-0.20894	0.05432	-0.08962	-0.06495
94	-0.19537	0.08620	-0.22496	-0.01294	-0.08766	-0.08270
96	-0.21284	0.00992	-0.21554	-0.08417	-0.07919	-0.10458
98	-0.19956	-0.06743	-0.18012	-0.15013	-0.06055	-0.12848
100	-0.15746	-0.13365	-0.12138	-0.20126	-0.02914	-0.14941
102	-0.09322	-0.17807	-0.04569	-0.22890	0.01471	-0.16032
104	-0.01745	-0.19350	0.03707	-0.22695	0.06650	-0.15411
106	0.05702	-0.17769	0.11452	-0.19352	0.11767	-0.12609
108	0.11740	-0.13400	0.17375	-0.13220	0.15715	-0.07634
110	0.15339	-0.07100	0.20388	-0.05219	0.17422	-0.01089

TABLE D-5: $S^p(\theta)$ vs θ, kH = 11.8

90	-0.10690	0.16762	-0.17484	0.07650	-0.06946	-0.06429
92	-0.16481	0.11797	-0.20405	0.01708	-0.06907	-0.07820
94	-0119864	0.04925	-0.20911	-0.05085	-0.06427	-0.09497
96	-0.20281	-0.02760	-0.18817	-0.11844	-0.05227	-0.11449
98	-0.17643	-0.10014	-0.14230	-0.17625	-0.02989	-0.13399
100	-0.12366	-0.15648	-0.07599	-0.21511	0.00446	-0.14804
102	-0.05319	-0.18721	0.00270	-0.22752	0.04904	-0.14974
104	0.02219	-0.15681	0.08263	-0.20927	0.09795	-0.13293
106	0.09163	-0.10200	0.15102	-0.61602	0.14168	-0.09477
108	0.14070	-0.03351	0.19568	-0.08901	0.16925	-0.03767
110	0.16181	0.03527	0.20772	-0.00478	0.17128	0.02999

TABLE D-6: $S^p(\theta)$ vs θ, kH = 12.00

90	-0.12523	0.14323	-0.17361	0.04558	-0.04954	-0.07242
92	-0.17388	0.08606	-0.19322	-0.01668	-0.04710	-0.08587
94	-0.19564	0.01392	-0.18744	-0.08349	-0.03974	-0.10123
96	-0.18675	-0.06122	-0.15589	-0.14558	-0.02479	-0.11783
98	-0.14849	-0.12677	-0.10131	-0.19359	0.00033	-0.13240
100	-0.08719	-0.17154	-0.02993	-0.21908	0.03613	-0.13920
102	-0.01332	-0.18778	0.04869	-0.21606	0.07949	-0.13181
104	0.06016	-0.17273	0.12256	-0.18251	0.12330	-0.10533
106	0.12011	-0.12940	0.17899	-0.12169	0.15755	-0.05893
108	0.15583	-0.06625	0.20711	-0.04241	0.17181	0.00264
110	0.16131	0.04290	0.20055	0.04195	0.15860	0.06904

The University of Michigan Radiation Laboratory, Ann Arbor, Michigan
THEORETICAL AND EXPERIMENTAL INVESTIGATION OF PARASITIC LOOP COUNTERPOISE ANTENNAS, by D. L. Sengupta, J. E. Ferris and V. H. Weston, September 1968, Final Report (June 1967-June 1968), 112 pp., incl. illus., 9 refs.
(Contract FA67WA-1753, Project 330-004-05N, Report No. RD-68-50)

Unclassified Report

The radiation field produced by a single parasitic loop counterpoise antenna has been investigated both theoretically and experimentally. Geometrical theory of diffraction is applied to obtain theoretical expressions for the far field produced by such an antenna. Within the range of approximation the agreement between theory and experiment has been found to be very good. In the absence of mutual coupling between the parasitic elements, the present theory can be applied to double- and multiple-parasitic loop counterpoise antennas.

The parasitic loops in general reduce the counterpoise edge diffraction effects on the far field patterns. The behavior of the parasitic loop counterpoise antenna pattern near the principal maximum is not appreciably different than the Alford loop counterpoise pattern near its maximum. Parasitic loops increase the response of the antenna in regions of space near the zenith $\theta=0^{o}$.

Detailed results of numerical and experimental investigations of various aspects of the parasitic loop counterpoise antenna have been given. These results bring out the effects of the different parameters of this new antenna system on the radiation patterns.

The parasitic loop concept has been found to be capable of shaping the pattern produced by an Alford loop counterpoise antenna pattern in regions of space below the plane of the counterpoise.

On the basis of our investigation we conclude that when suitably designed, the parasitic loop counterpoise antenna is potentially capable of minimizing the siting errors associated with existing VOR systems. We have proposed three new antenna systems which may find possible application in a VOR system.

UNCLASSIFIED

I. Sengupta, D. L. ,
Ferris, J. E.
Weston, V. H.
II. Contract FA67WA-1753
III. Project 330-004-05N
IV. Report No. RD-68-50

Descriptors

Parasitic Loop Counterpoise Antennas
VOR Antennas
Geometrical Theory of Diffraction
Pattern Shaping
Reduction of Edge Diffraction Effects

The University of Michigan Radiation Laboratory, Ann Arbor, Michigan
THEORETICAL AND EXPERIMENTAL INVESTIGATION OF PARASITIC LOOP COUNTERPOISE ANTENNAS, by D. L. Sengupta, J. E. Ferris and V. H. Weston, September 1968, Final Report (June 1967-June 1968), 112 pp., incl. illus., 9 refs.
(Contract FA67WA-1753, Project 330-004-05N, Report No. RD-68-50)

Unclassified Report

The radiation field produced by a single parasitic loop counterpoise antenna has been investigated both theoretically and experimentally. Geometrical theory of diffraction is applied to obtain theoretical expressions for the far field produced by such an antenna. Within the range of approximation the agreement between theory and experiment has been found to be very good. In the absence of mutual coupling between the parasitic elements, the present theory can be applied to double- and multiple-parasitic loop counterpoise antennas.

The parasitic loops in general reduce the counterpoise edge diffraction effects on the far field patterns. The behavior of the parasitic loop counterpoise antenna pattern near the principal maximum is not appreciably different than the Alford loop counterpoise pattern near its maximum. Parasitic loops increase the response of the antenna in regions of space near the zenith $\theta=0^{o}$.

Detailed results of numerical and experimental investigations of various aspects of the parasitic loop counterpoise antenna have been given. These results bring out the effects of the different parameters of this new antenna system on the radiation patterns.

The parasitic loop concept has been found to be capable of shaping the pattern produced by an Alford loop counterpoise antenna pattern in regions of space below the plane of the counterpoise.

On the basis of our investigation we conclude that when suitably designed, the parasitic loop counterpoise antenna is potentially capable of minimizing the siting errors associated with existing VOR systems. We have proposed three new antenna systems which may find possible application in a VOR system.

UNCLASSIFIED

I. Sengupta, D. L. ,
Ferris, J. E.
Weston, V. H.
II. Contract FA67WA-1753
III. Project 330-004-05N
IV. Report No. RD-68-50

Descriptors

Parasitic Loop Counterpoise Antennas
VOR Antennas
Geometrical Theory of Diffraction
Pattern Shaping
Reduction of Edge Diffraction Effects

The University of Michigan Radiation Laboratory, Ann Arbor, Michigan
THEORETICAL AND EXPERIMENTAL INVESTIGATION OF PARASITIC LOOP COUNTERPOISE ANTENNAS, by D. L. Sengupta, J. E. Ferris and V. H. Weston, September 1968, Final Report (June 1967-June 1968), 112 pp., incl. illus., 9 refs.
(Contract FA67WA-1753, Project 330-004-05N, Report No. RD-68-50)

Unclassified Report

The radiation field produced by a single parasitic loop counterpoise antenna has been investigated both theoretically and experimentally. Geometrical theory of diffraction is applied to obtain theoretical expressions for the far field produced by such an antenna. Within the range of approximation the agreement between theory and experiment has been found to be very good. In the absence of mutual coupling between the parasitic elements, the present theory can be applied to double- and multiple-parasitic loop counterpoise antennas.

The parasitic loops in general reduce the counterpoise edge diffraction effects on the far field patterns. The behavior of the parasitic loop counterpoise antenna pattern near the principal maximum is not appreciably different than the Alford loop counterpoise pattern near its maximum. Parasitic loops increase the response of the antenna in regions of space near the zenith $\theta=0^{o}$.

Detailed results of numerical and experimental investigations of various aspects of the parasitic loop counterpoise antenna have been given. These results bring out the effects of the different parameters of this new antenna system on the radiation patterns.

The parasitic loop concept has been found to be capable of shaping the pattern produced by an Alford loop counterpoise antenna pattern in regions of space below the plane of the counterpoise.

On the basis of our investigation we conclude that when suitably designed, the parasitic loop counterpoise antenna is potentially capable of minimizing the siting errors associated with existing VOR systems. We have proposed three new antenna systems which may find possible application in a VOR system.

UNCLASSIFIED

I. Sengupta, D. L.
Ferris, J. E.
Weston, V. H.
II. Contract FA67WA-1753
III. Project 330-004-05N
IV. Report No. RD-68-50

Descriptors

Parasitic Loop Counterpoise Antennas
VOR Antennas
Geometrical Theory of Diffraction
Pattern Shaping
Reduction of Edge Diffraction Effects

The University of Michigan Radiation Laboratory, Ann Arbor, Michigan
THEORETICAL AND EXPERIMENTAL INVESTIGATION OF PARASITIC LOOP COUNTERPOISE ANTENNAS, by D. L. Sengupta, J. E. Ferris and V. H. Weston, September 1968, Final Report (June 1967-June 1968), 112 pp., incl. illus., 9 refs.
(Contract FA67WA-1753, Project 330-004-05N, Report No. RD-68-50)

Unclassified Report

The radiation field produced by a single parasitic loop counterpoise antenna has been investigated both theoretically and experimentally. Geometrical theory of diffraction is applied to obtain theoretical expressions for the far field produced by such an antenna. Within the range of approximation the agreement between theory and experiment has been found to be very good. In the absence of mutual coupling between the parasitic elements, the present theory can be applied to double- and multiple-parasitic loop counterpoise antennas.

The parasitic loops in general reduce the counterpoise edge diffraction effects on the far field patterns. The behavior of the parasitic loop counterpoise antenna pattern near the principal maximum is not appreciably different than the Alford loop counterpoise pattern near its maximum. Parasitic loops increase the response of the antenna in regions of space near the zenith $\theta=0^{o}$.

Detailed results of numerical and experimental investigations of various aspects of the parasitic loop counterpoise antenna have been given. These results bring out the effects of the different parameters of this new antenna system on the radiation patterns.

The parasitic loop concept has been found to be capable of shaping the pattern produced by an Alford loop counterpoise antenna pattern in regions of space below the plane of the counterpoise.

On the basis of our investigation we conclude that when suitably designed, the parasitic loop counterpoise antenna is potentially capable of minimizing the siting errors associated with existing VOR systems. We have proposed three new antenna systems which may find possible application in a VOR system.

UNCLASSIFIED

I. Sengupta, D. L. ,
Ferris, J. E.
Weston, V. H.
II. Contract FA67WA-1753
III. Project 330-004-05N
IV. Report No. RD-68-50

Descriptors

Parasitic Loop Counterpoise Antennas
VOR Antennas
Geometrical Theory of Diffraction
Pattern Shaping
Reduction of Edge Diffraction Effects